Transtensional rifting in the proto–Gulf of California near Bahía Kino, Sonora, México

Scott E.K. Bennett[1,2,†], Michael E. Oskin[2], and Alexander Iriondo[3,4]
[1]*Department of Geological Sciences, University of North Carolina, Chapel Hill, North Carolina 27599-3315, USA*
[2]*Department of Earth and Planetary Sciences, University of California–Davis, Davis, California 95616, USA*
[3]*Centro de Geociencias, Universidad Nacional Autónoma de México, Juriquilla, No. 3001, Querétaro 76230, México*
[4]*Department of Geological Sciences, The University of Texas at Austin, Austin, Texas 78712, USA*

ABSTRACT

Continental rifts require focused strain to rupture and form an ocean basin. In oblique rifts, such as the Gulf of California, focused transtensional strain associated with strike-slip faulting may serve as a catalyst for rupture. To test this hypothesis, we analyzed structural mapping, geochronology, paleomagnetism, and fault kinematics of pre- and synrift rocks exposed in an ~200 km^2 coastal mountain belt flanking the eastern rift margin of the northern Gulf of California. This coastal Sonora region hosts the onshore portion of the transform boundary between the Upper Tiburón and Adair-Tepoca marine basins—two early-formed oblique rift segments. Extension commenced here between 11.5 Ma and 7 Ma, resulting in 25°–40° of E-NE tilting, initiation of clockwise vertical-axis rotation of fault-bounded blocks, and minor basin sedimentation. Rates of deformation prior to 7 Ma are unconstrained due to a lack of exposed syntectonic deposits. Deformation after 7 Ma was associated with rapid tilting and the majority of observed clockwise vertical-axis rotation and strike-slip faulting. Nonmarine sedimentary basins accumulated coarse sediments above an unconformity eroded across older, tilted strata. By 5–6 Ma, deformation in coastal Sonora must have largely ceased and migrated westward into the Upper Tiburón marine basin. We document up to 120% total extension and total clockwise block rotations up to 53°. In portions of the study area, extension and rotation were supplanted by strike-slip faulting as deformation proceeded. We develop a tectonic model for this Coastal Sonora fault zone, which is bounded by major NW-striking transform faults with >10 km of displacement. Internal to the Coastal Sonora fault zone, the majority of an estimated 6.2 ± 1.1 km of dextral deformation, associated with up to 5.7 km of WNW-directed extension, occurred over the final 1–2 m.y. of its life span, at a strain rate approaching 10^{-14} s^{-1}. This activity occurred as the plate boundary localized along nascent pull-apart basins in the northern Gulf of California, consistent with the hypothesis that late proto–Gulf of California dextral shear zones, such as the Coastal Sonora fault zone, acted to focus lithospheric-scale strain and promoted continental rupture in the wide-rift setting of the Mexican Basin and Range.

INTRODUCTION AND MOTIVATION

Because continental crust tends to stretch rather than break (McKenzie, 1978; Lavier and Manatschal, 2006), strain localization across the lithospheric column must somehow occur in order for a continent to rupture and form a new ocean basin (Buck, 1991). Factors controlling rifting style include the initial thermal state and crustal thickness (Buck, 1991), presence of lower-crustal flow (Buck, 1991; Hopper and Buck, 1996; Buck et al., 1999; Al-Zoubi and ten Brink, 2002), buoyancy contrasts (Lavier et al., 1999; Buck, 1991; Forsyth, 1992; Buck et al., 1999), strain rate (England, 1983; Kusznir and Park, 1987; Bassi, 1995; Huismans and Beaumont, 2003), sediment cover (Lavier and Steckler, 1997; Bialas and Buck, 2009), and intensity of rift magmatism (Buck et al., 1999; Kusznir and Park, 1987; Hopper and Buck, 1996). Many of these factors are intricately linked to one another. For example, a low strain rate that produces slow exhumation allows for conductive cooling of the lithosphere, which permits it to maintain strength. Alternatively, higher strain rates may locally weaken the lithosphere by outpacing conductive cooling. This strain softening may lead to a concentration of deformation into a narrower zone, which in turn fosters a further increase in extensional strain rate (England, 1983). Such positive feedbacks may allow for large amounts of localized thinning and increase the potential for crustal rupture (Kusznir and Park, 1987; Huismans and Beaumont, 2003).

A factor not considered by most rift models is the three-dimensional rift geometry. In particular, two-dimensional models cannot evaluate the role of rift obliquity (e.g., Buck, 1991; Lavier et al., 1999; Lavier and Manatschal, 2006), and three-dimensional models of oblique rifting are in early stages of development (e.g., Choi and Buck, 2011; Van Wijk et al., 2011; Brune et al., 2012). Rift obliquity is common to active rifts such as the Gulf of California (Umhoefer and Stone, 1996; Dorsey, 2010), Gulf of Aden (Tron and Brun, 1991; Bellahsen et al., 2006; Withjack and Jamison, 1986), the Malawi Rift (Chorowicz and Sorlien, 1992), and the northern Mid-Atlantic Ridge system (Applegate and Shor, 1994; Dauteuil and Brun, 1996), and also to ancient rifts as seen in the Triassic Hartford basin of eastern North America (deBoer and Clifton, 1988), the Jurassic High Atlas trough in Morocco (El Kochri and Chorowicz, 1996), and offshore Ghana in the Gulf of Guinea (Edwards et al., 1997). A fundamental distinction between oblique rifts and orthogonal rifts is the occurrence of significant shear accommodated along steep strike-slip faults. Orthogonal continental extension tends to be distributed because of buoyancy variations (Buck, 1991) and flexural forces on normal faults as slip accumulates (Forsyth, 1992). Because slip on a strike-slip fault does not by itself lead to lithospheric thinning or change fault dip, buoyancy and flexural forces do not hinder fault displacement and strain rate. Where extension is hosted within a strike-slip–dominated setting, the overall higher strain rates that may result could ultimately enhance the potential of a rift to proceed to rupture (Al-Zoubi and ten Brink, 2002).

†Current address: U.S. Geological Survey, Geologic Hazards Science Center, 1711 Illinois Street, Golden, Colorado 80401, USA; e-mail: sekbennett@usgs.gov

GSA Bulletin; November/December 2013; v. 125; no. 11/12; p. 1752–1782; doi: 10.1130/B30676.1; 16 figures; 5 tables; Data Repository item 2013354.

GULF OF CALIFORNIA OBLIQUE RIFT

The Gulf of California is a youthful rift in northwestern México well suited for study of the role of obliquity in continental rupture. The rift formed through NW-SE oblique divergence along the Pacific–North America plate boundary, immediately south of the restraining bend of the San Andreas fault system of southern California (Fig. 1; Hamilton, 1961). The Gulf of California is highly oblique, characterized by a small angle (0°–30°) between the overall rift trend and the direction of relative plate motion. For this magnitude of rift obliquity, analog experimental models predict combinations of NW-striking dextral faults, NE-striking sinistral faults, N-S–striking dip-slip faults, and variously oriented oblique-slip structures for the Gulf of California (Withjack and Jamison, 1986). Marine geophysical (e.g., Lonsdale, 1989; Fenby and Gastil, 1991; Aragón-Arreola et al., 2005; Aragón-Arreola and Martín-Barajas, 2007) and onshore geological studies (e.g., Gastil et al., 1975; Umhoefer and Stone, 1996; Seiler et al., 2010; Fletcher and Munguía, 2000; this study) in the Gulf of California have identified significant rift structures that corroborate these model predictions and together accommodate obliquely divergent relative plate motion.

A protracted history of diffuse extension across the Mexican Basin and Range preceded formation of the Gulf of California (Henry, 1989; Henry and Aranda-Gomez, 1992; Gans, 1997; Ferrari et al., 2012). Crustal stretching initiated in Oligocene time within the Sierra Madre Occidental volcanic plateau (Fig. 2). This region of backarc extension expanded westward during the early Miocene, behind (east of) the volcanic arc related to subduction of the Farallon plate and its successors beneath the North American plate (Figs. 2A and 2B; Ferrari et al., 2007). Between 16 and 12.5 Ma, the Rivera triple junction jumped the entire length of the Baja California Peninsula, lengthening the Pacific–North America plate boundary by over 1000 km (Atwater, 1989). As a result, the plate boundary in northwestern México evolved from subduction and backarc extension (Fig. 2B) to dextral transtension (Fig. 2C), setting the stage for the formation of the Gulf of California.

PACIFIC–NORTH AMERICA DEXTRAL-SLIP BUDGET

Early work in the Gulf of California divided its history into two rift stages: an early proto–Gulf of California stage (Moore and Buffington, 1968; Karig and Jensky, 1972), spanning from ca. 12.5 Ma to 6 Ma, and a later modern Gulf of California stage, spanning from ca. 6 Ma to present. Subsequent studies suggested that the dextral component of Pacific–North America relative motion during proto–Gulf of California time was accommodated beyond the Mexican Basin and Range Province, on strike-slip faults west of the tectonically stable Baja California Peninsula (Spencer and Normark, 1979; Hausback, 1984), while subsequent, modern Gulf of California dextral faulting was accommodated within the nascent plate boundary, east of Baja California (Stock and Hodges, 1989; Angelier et al., 1981). Assuming Pacific–North America displacements determined from a global plate circuit reconstruction (Atwater and Stock, 1998), this tectonic model for the evolution of the Gulf of California requires ~325 km of total dextral slip west of Baja California during proto–Gulf of California time, and ~300 km east of Baja California during modern Gulf of California time. Strain distribution during the modern gulf period is broadly well understood, as cumulative post–6 Ma offsets of geologic features (276 ± 13 km) across the Gulf of California (Oskin et al., 2001; Oskin and Stock, 2003a) corroborate the expected slip amount. Since 6 Ma, residual Pacific–North America strain of a few mm/yr was accommodated on faults west of Baja California (Michaud et al., 2004; Fletcher et al., 2007), at a rate likely similar to the modern-day strain budget determined from geodesy (Plattner et al., 2007).

The distribution of Pacific–North America strain during proto–Gulf of California time is less well understood. The plate-circuit reconstruction (Atwater and Stock, 1998) requires similarly large dextral slip, but shear zones that accommodate this slip are not fully documented. One locus of proto–Gulf of California strike-slip faulting is the Tosco-Abreojos fault system west of the Baja California Peninsula (Spencer and Normark, 1979). However, detrital zircon of the Magdalena fan offshore southern Baja California constrains total dextral offset on this system to 100 ± 50 km (Fletcher et al., 2007), suggesting that at least half of the necessary proto-gulf-age dextral slip (150 km) occurred east of Baja California. In the southern Gulf of California, this slip is likely embedded within the wider marine basin. Indeed, recently published interpretation of a multichannel seismic-reflection profile across the Alarcón marine basin at the mouth of the Gulf of California documents transtensional rifting throughout proto–Gulf of California time, and crustal thinning consistent with >400 km of NW-directed extension (e.g., Sutherland et al., 2012). The narrower northern Gulf of California marine basins largely opened after 6 Ma (Oskin et al., 2001). Thus, evidence of earlier transtensional deformation should be located largely within the onshore, exposed continental margins. Structural mapping and thermochronology in northeastern Baja California indicate that transtensional faulting initiated ca. 9–8 Ma (Seiler et al., 2010, 2011). Gans (1997) documented that the majority of NE-SW extension in the Mexican Basin and Range Province of central and eastern Sonora occurred from 27 Ma to 12 Ma, prior to proto–Gulf of California time. Dextral faulting of likely proto–Gulf of California age crosscuts earlier extensional faulting, with more intense dextral transtension associated with a zone of clockwise vertical-axis rotation in coastal Sonora (Herman and Gans, 2006; Gans et al., 2006; Herman, 2013). Though the record of proto–Gulf of California dextral slip is incomplete, the weight of evidence supports the interpretation that integrated transtensional deformation (oblique rifting) characterized the proto–Gulf of California stage (Fig. 2C) and occurred simultaneously both the east and west of the stable Baja California Peninsula (Fletcher et al., 2007; Seiler et al., 2010).

LOCALIZATION OF TRANSTENSIONAL STRAIN

In this paper, we explore the relationship of highly oblique proto–Gulf of California rifting to strain localization. Similar to Umhoefer (2011), we hypothesize that strike-slip faulting during proto–Gulf of California time became focused within an en-echelon set of dextral shear zones embedded within the western portion of the broader Mexican Basin and Range extensional province. These shear zones and intervening extensional pull-apart regions together formed a NNW-trending, narrow zone (~50–100 km-wide) of localized transtensional strain that coalesced during late proto–Gulf of California time (Fig. 2D). By 5–6 Ma, the plate boundary had localized in this transtensional corridor and subsequently led to the large amounts of thinning on kinematically linked, large-offset normal faults that formed the marine basins of the Gulf of California (Fig. 2E). Such a configuration and history of deformation would resemble how the dextral Walker Lane system (Pezzopane and Weldon, 1993; Unruh et al., 2003) has become embedded within the western portion of the broader Basin and Range extensional province of the United States (Henry and Faulds, 2006).

To test if strain localization in the Gulf of California was closely preceded in time and space by a zone of significant strike-slip faulting and focused transtensional deformation, we evaluate the timing and magnitude of dextral shear and extension along the eastern margin of the Gulf of California in central coastal Sonora (Fig. 1). Here, dextral faults are recognized

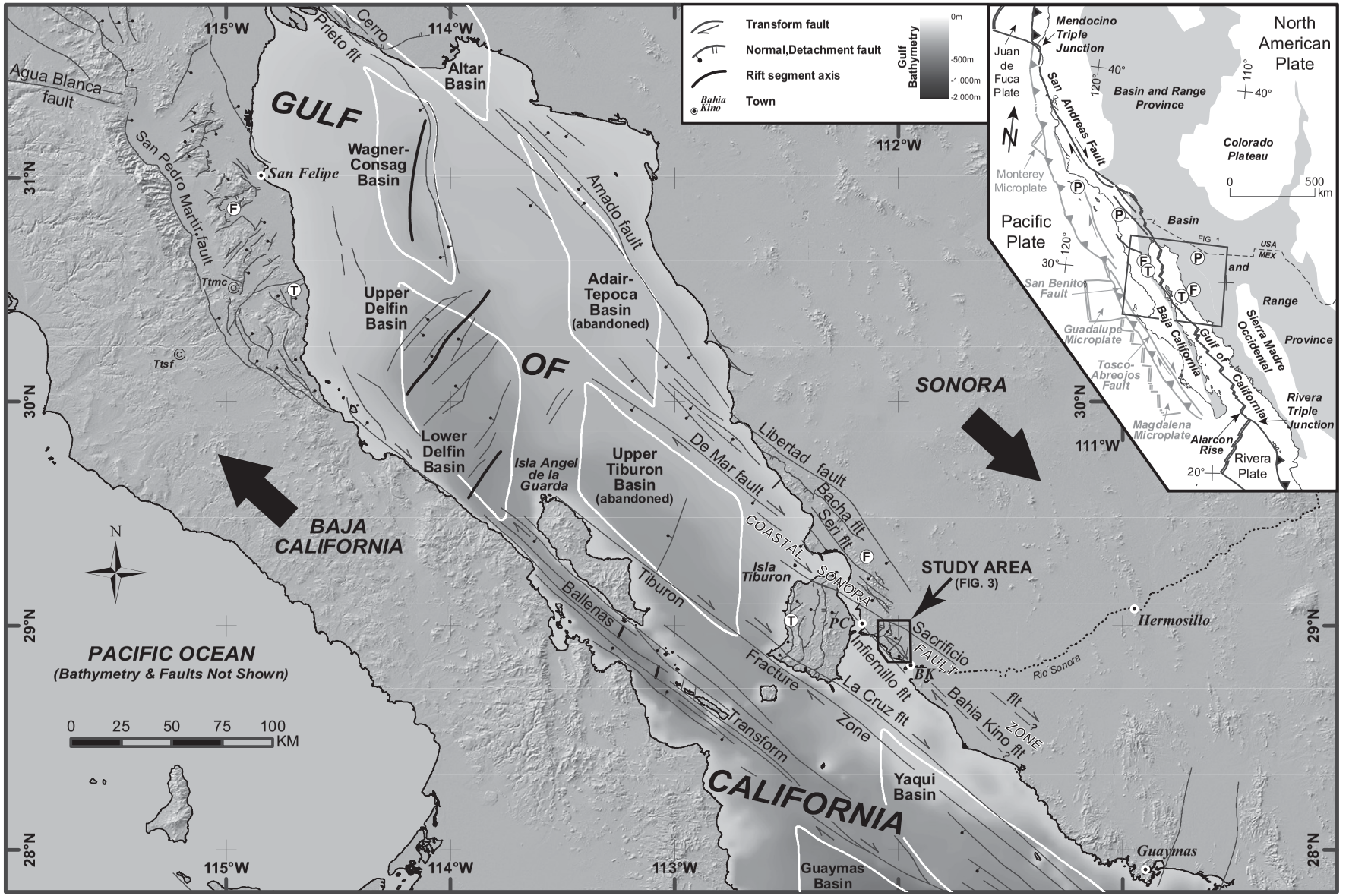

Figure 1. Hillshade and bathymetry of the northern Gulf of California. Structures related to oblique rifting shown (black lines) are from Fenby and Gastil (1991), Oskin (2002), Aragón-Arreola and Martín-Barajas (2007), Aragón-Arreola et al. (2005), Darin (2011), Seiler et al. (2010), Pacheco et al. (2006), and this study. Rhombochasm-shaped transtensional basins are from Aragón-Arreola and Martín-Barajas (2007). Coastal Sonora study area of 1:10,000 scale geologic mapping is indicated with a black rectangle. Paleomagnetic reference sites for marker tuffs in Baja California are shown as black donuts. BK—Bahía de Kino, PC—Punta Chueca. Inset: Regional tectonic map of western North America showing the diffuse boundary between the Pacific–North American lithospheric plates (after Oskin and Stock, 2003a). Active faults and spreading centers are in black; inactive offshore structures are in gray. Basin and Range extensional province is shown as gray region. Cross-gulf tie points (some also in main figure): P—Poway conglomerate (Abbott and Smith, 1989); F—fusulinid-rich clast conglomerate (Gastil et al., 1973); T—tuff sequence (Oskin et al., 2001; Oskin and Stock, 2003a).

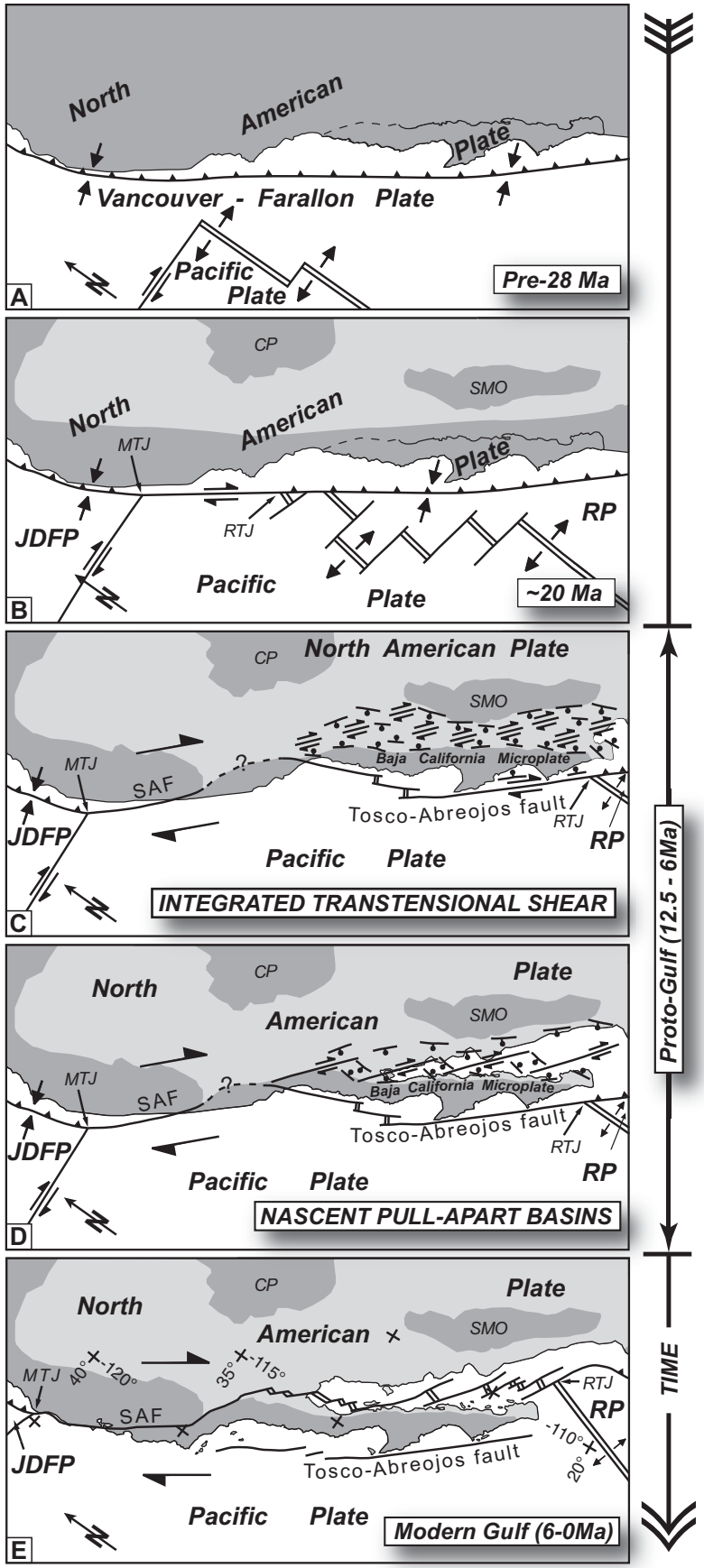

Figure 2. Modified integrated transtensional shear model for the tectonic evolution of the Gulf of California. North America plate fixed. (A) Prior to 28 Ma, the spreading center between Pacific and Vancouver-Farallon tectonic plates approached the subduction zone between North America and Vancouver-Farallon plates. (B) By ca. 20 Ma, contact between the Pacific and North America plates created early dextral transform relative plate motion. The Basin and Range extensional province (light gray) accommodated moderate extension throughout western North America. (C) The Rivera triple junction migrated the full length of the Baja California Peninsula by ca. 12.5 Ma, lengthening the Pacific–North American transform plate boundary. The proto–Gulf of California period commenced (ca. 12.5 Ma) with transtensional strain distributed across two distinct transtensional deformation belts, west and east of the stable Baja California microplate. (D) In late proto–Gulf of California time, shear deformation gradually localized within a narrow belt of focused en-echelon dextral shear zones embedded within the greater Mexican Basin and Range extensional province. These shear zones and intervening extensional regions both experienced high-magnitude strain. (E) By ca. 6 Ma, Pacific–North America plate boundary strain was localized and focused crustal thinning and subsidence in transtensional pull-apart basins that formed the Gulf of California. Faults shown represent primary structures active during Quaternary time. RP—Rivera plate, JDFP—Juan de Fuca plate, RTJ—Rivera triple junction, MTJ—Mendocino triple junction, SAF—San Andreas fault, CP—Colorado Plateau, SMO—Sierra Madre Occidental.

onshore (Gastil and Krummenacher, 1977a, 1977b; Oskin, 2002; Oskin and Stock, 2003a) that may be directly linked to the transform faults offshore (Aragón-Arreola and Martín-Barajas, 2007) that accommodated the initial oblique opening of the Upper Tiburón and Adair-Tepoca marine basins presently located in the northeastern Gulf of California. Previous reconnaissance mapping has documented well-exposed moderately to steeply dipping prerift and synrift volcanic and sedimentary rocks deformed within a NW-trending belt of strike-slip and dip-slip faults (Gastil and Krummenacher, 1977b; Oskin, 2002), thought to have been active 12–8 Ma (Gastil and Krummenacher, 1977b). This structural belt has been proposed to have accommodated up to ~150–250 km of dextral shear prior to the opening of the Gulf of California, during proto–Gulf of California time (Nicholson et al., 1994; Gans, 1997; Wilson et al., 2005; Fletcher et al., 2007; Seiler et al., 2010). We applied structural field mapping, paleomagnetism, geochronology, and fault kinematic analysis to characterize and quantify this deformation and refine its timing. We show that this Coastal Sonora fault zone played a significant role in plate boundary deformation leading up to the ca. 6 Ma strain localization event that culminated with formation of the northern Gulf of California marine basin.

GEOLOGIC MAPPING IN COASTAL SONORA

Geologic mapping (Fig. 3) was conducted at 1:10,000 scale using Quickbird satellite imagery with topographic contours derived from the 90 m Shuttle Radar Topography Mission digital elevation model. One infrared and three visible bands of Quickbird imagery were pan-sharpened to generate a 0.6-m-resolution false-color base map. Enlargements of 1:50,000 scale Instituto Nacional de Estadística y Geografía topographic maps aided our mapping.

Prerift Rocks

In coastal Sonora, Miocene volcanic and sedimentary units and the pre-Cenozoic basement units that they nonconformably overlie are well dated (Fig. 3; Table 1). These basement rocks consist of both the Late Cretaceous coastal Sonora batholith (Ramos-Velázquez et al., 2008) and their Mesozoic to Paleozoic host rocks (Gastil and Krummenacher, 1977a, 1977b; Gastil, 1993). Basement rocks are overlain by Neogene sedimentary and volcanic units typically deposited on an erosional surface that lacks significant paleorelief and occasionally displays a weathering horizon up to 3 m thick.

A package of andesitic volcanic and volcaniclastic rocks (Tvu), ranging from 200 to 1000 m thick, overlies basement rocks (Fig. 4A). These rocks were likely emplaced due to arc magmatism associated with subduction of the Farallon plate beneath North America (Gastil et al., 1979; Hausback, 1984). A distinctive package of epiclastic and pyroclastic strata (Tvs) caps this sequence. These strata vary from thin (0–30 m) deposits of recessive fluvial pebbly sandstone and conglomerate in the northeast to thick (220 m) deposits in the south (Figs. 4A and 4B) that consist of cliff-forming volcaniclastic sandstone and debris-flow deposits, ash-flow and pisolitic tuffs, and fluvial sandstone and conglomerate.

Tuff of San Felipe

The Tuff of San Felipe (Ttsf), a regional ca. 12.6 Ma Miocene ignimbrite (Figs. 4A, 4B, and 4D–4F) that blanketed >4000 km^2 of the Mexican Basin and Range (Stock et al., 1999; Oskin et al., 2001; Oskin and Stock, 2003a), can be found throughout the study area and acts as a key structural marker. In coastal Sonora, Ttsf lies disconformably on arc-related volcanic rocks (Figs. 4A and 4B) and gradually thickens from 135 m thick in the southern study area (Oskin, 2002) to ~500 m thick in the northwestern study area, where up to three cooling units are present (Figs. 4D and 4E). This trend is consistent with a source vent for Ttsf located just west of the northwestern edge of the study area, near Punta Chueca (Oskin, 2002; Oskin and Stock, 2003a; Stock et al., 2006), as also supported by our limited pumice lineation data (Fig. 3).

Deposits of the Tuff of San Felipe across northwestern México consistently have an unusual shallow (~5°) up-to-the-SW direction of paleomagnetic remanence (Lewis and Stock, 1998; Stock et al., 1999; Oskin et al., 2001; this study). Even taking into account magnetic secular variation, this remanence direction lies far from the expected Miocene magnetic field at this latitude and records an apparent geomagnetic field excursion or reversal (Stock et al., 1999). This unique magnetic signature strengthens the utility of the Tuff of San Felipe as a regional tectonic marker.

Geochronologic ages for Ttsf from northeastern Baja California (Gastil et al., 1979; Stock, 1989; Lewis, 1996; Nagy et al., 1999; Stock et al., 1999) and from central and coastal Sonora (Paz-Moreno, 1992; McDowell et al., 1997; Page et al., 2003; Vidal-Solano et al., 2005, 2007) display a significant range of calculated ages (9.1–16.7 Ma), with the spread mostly coming from earlier studies that used the K-Ar technique. Dates determined by ^{40}Ar/^{39}Ar are more clustered. Stock et al. (1999) suggested that a 12.6 Ma age corroborates best with its stratigraphic position. However, minor xenocrystic contamination may slightly influence calculated ages, and 12.35 Ma may be the most accurate eruption age (Stock et al., 2008). Nevertheless, we report a new ^{40}Ar/^{39}Ar age of 12.50 ± 0.08 Ma on multiple anorthoclase crystals from Ttsf (394500E, 3208670N, reported in Universal Transverse Mercator projection, zone 12N) in the study area (Fig. 5A; Table 2), consistent with single-crystal ages of 12.44 ± 0.05 Ma and 12.56 ± 0.08 Ma reported by Vidal-Solano et al. (2005) from samples near Hermosillo, and with a multicrystal aliquot ^{40}Ar/^{39}Ar age of 12.43 ± 0.14 Ma from the Santa Rosa basin of northeastern Baja California (Stock et al., 1999).

In the study area, the Tuff of San Felipe is locally overlain by discontinuous rhyolite flows, tuffs, and a basalt flow (see Table 1). Disparate packages of local, prerift volcanic units are exposed only in the southern (Tvls) and northern (Tvln) portions of the study area. Tvls and Tvln are not observed in contact with each other, and their relative age is unknown. We report a new ^{40}Ar/^{39}Ar age of 11.47 ± 0.05 Ma on volcanic matrix from the Basalt of Punta Chueca (Tbpc; Fig. 5B; Table 3), the youngest local volcanic deposit in the northern study area (394710E, 3208830N). These local volcanic units conformably overlie the Tuff of San Felipe which are tilted down to the east at 57° ± 15° (n = 25) and 61° ± 4° (n = 315), respectively (Fig. 6, inset).

Synrift Rocks

Two distinct sedimentary basins, Kino and Punta Chueca, formed above the hanging walls of normal faults (Fig. 6). Sedimentary and volcanic deposits within these basins have moderate to shallow dips (mean 21° ± 4°, n = 135; Fig. 6, inset) and record the synrift history of coastal Sonora. Across the study area, these basin deposits are commonly in 25°–40° angular unconformable contact with underlying volcanic rocks. Despite the proximity of the study area to the Gulf of California, all basin fill consists entirely of nonmarine deposits.

Basin Conglomerate

Synrift basin conglomerate (Tcg) consists of a fanning-dip section predominantly of gray, tan, and orangish-brown, massive to poorly- to well-stratified, matrix- and clast-supported sandy- to boulder-conglomerate and subordinate sandstone (Figs. 4C and 4I). Clast composition consists of basement units, Tvu, Ttsf, Tvls, Tvln, and interbedded tuffs coeval with basin deposits. Locally, clast composition patterns reveal higher concentrations of older, footwall units (e.g., basement) both up section

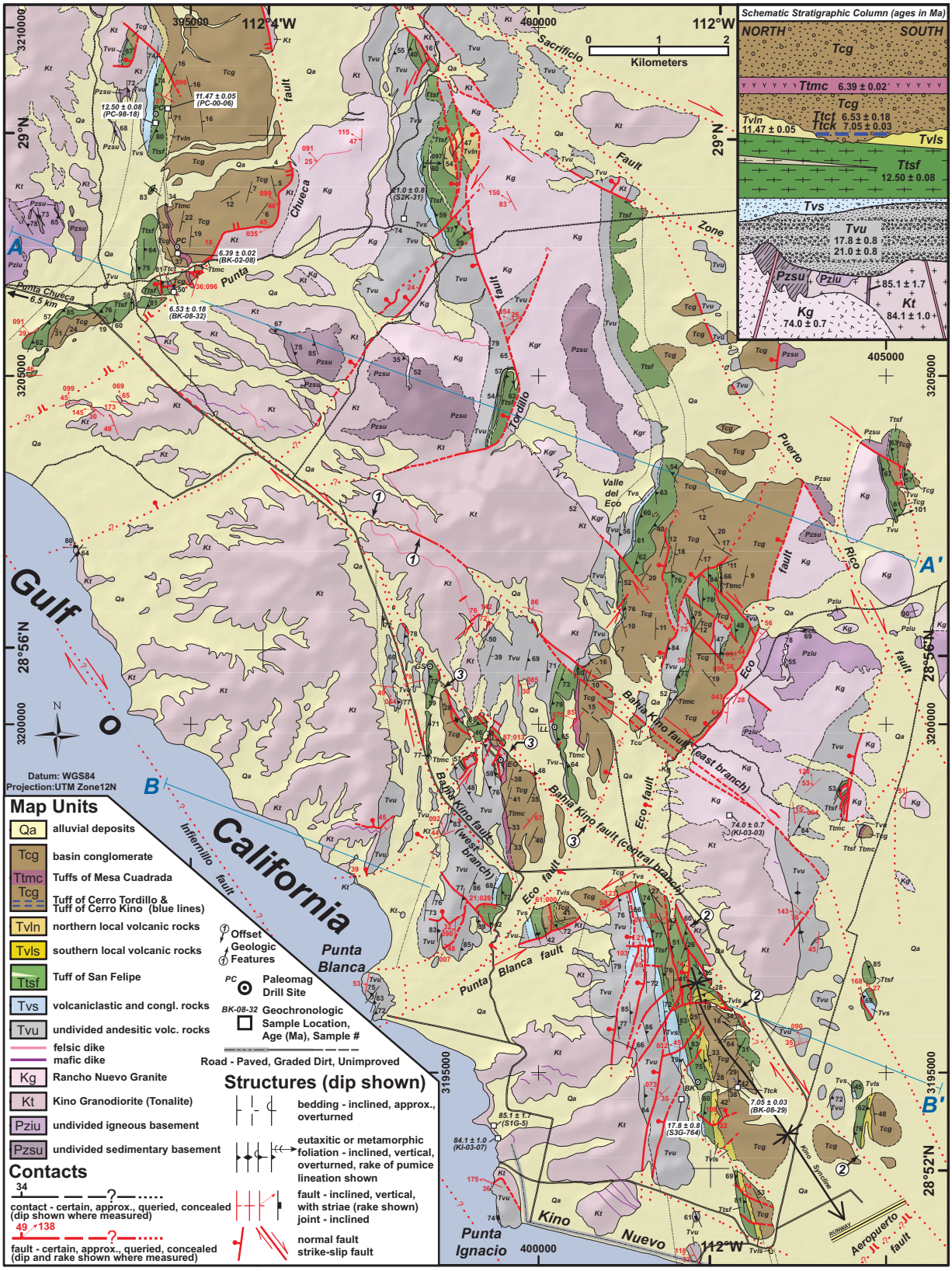

Figure 3. Simplified geologic map of the Coastal Sonora fault zone between the towns of Bahía Kino and Punta Chueca, Sonora, Mexico. Mapping was conducted at 1:10,000 scale. See Bennett (2009, plate 1) for detailed geologic map. Geologic markers used for dextral offset estimates across branches of the Bahía Kino fault are indicated by circled numbers. See text for details. Inset: Schematic stratigraphic column showing contact relationships and ages of mapped rock units. See Table 1 for detailed rock descriptions and geochronology.

TABLE 1. FIELD DESCRIPTIONS AND SUMMARY OF GEOCHRONOLOGIC AGES OF LITHOLOGIC MAP UNITS

Lithologic group	Map unit	Unit name	Dominant lithologies	Rock description	Unit thickness	Age (Ma)	Dating technique/ material	Published sample number	Reference	Previous published names
Basement	Pzsu	Undifferentiated sedimentary basement	Quartzite, slate, limestone, carbonate-cemented sandstone	Gray to black quartzite and slate; meta-limestones and meta-carbonate-cemented sandstones that form 0.5–5-cm-thick alternating bands of gray, white, and orangish-red	–	Paleozoic(?)	–	–	Gastil and Krummenacher (1977a); Gastil (1993)	–
	Pziu	Undifferentiated igneous basement	Meta-basalt, meta-gabbro	Meta-basalt or meta-gabbro with multiple crosscutting felsic dikes	–	Paleozoic(?)	–	–	Gastil and Krummenacher (1977a); Gastil (1993)	–
	Kt	Kino tonalite	Tonalite	Plagioclase (long axis up to 0.5 cm) >> hornblende (long axis up to 1.0 cm) >> quartz (locally up to 1.0 cm in diameter) > biotite	–	84.1 ± 1.0	U/Pb zircon	KI-03-07	Ramos-Velázquez et al. (2008)	Kino Granodiorite
					–	85.1 ± 1.7	K-Ar on hornblende-rich mafic dike	S1G-5	Gastil and Krummenacher (1977a)	–
	Kg	Rancho Nuevo granite	Granite	Abundant alkali-feldspar megacrysts up to 2 cm in length > quartz >> plagioclase-feldspar >> biotite >> amphibole	–	74.0 ± 0.7	U/Pb zircon	KI-03-03	Ramos-Velázquez et al. (2008)	–
Arc-related rocks	Tvu	Undifferentiated arc-related volcanic rocks	Andesite, pyroclastic breccia, basaltic andesite, conglomerate	Local basal unit of conglomerate, purplish-gray to maroon matrix, moderately to well-stratified fine-grained sandstone to pebbly sandstones to cobble conglomerates with clast compositions dominated by andesite and less common clasts of all basement units; maroon monolithologic andesitic pyroclastic breccia with rare tonalite blocks; very resistant ridge- and cliff-forming stacked andesitic flows, with 1–3-cm-spaced foliation, purplish-gray, massive, porphyritic with centimeter-scale hornblende (locally twinned) >> subcentimeter plagioclase and olivine phenocrysts, and few xenolith boulders of Kt up to 60 cm in diameter; polylithologic pyroclastic breccia and tuff breccia deposits containing 30%–80% subangular lithic fragments of dacite, andesite, rhyolite, and rare tonalite (Kt) up to 1 m in diameter, 10%–30% andesitic pumice up to 0.5 cm in diameter, and 40%–60% tan and pink nonwelded ash matrix. Individual pyroclastic beds range from 0.5 to 2 m thick; moderately resistant basaltic andesite flow consisting of a 1–2-m-thick basal and upper breccia of dark-gray and pink scoria fragments with olivine and hornblende phenocrysts, and a 5-m-thick core of dark purplish-gray, poorly foliated basaltic andesite with <10% phenocrysts of olivine (1–3 mm) and oxidized hornblende (1–5 mm). Tvu was further subdivided into map units by Bennett (2009).	200–1000 m	21.0 ± 0.8 17.8 ± 0.8 20.8 ± 5.7	K-Ar hornblende K-Ar hornblende K-Ar biotite	S2K-31 S3G-764 S3G-764	Gastil and Krummenacher (1977a)	–
	Tvs	Volcaniclastic sedimentary rocks	Volcaniclastic sandstone and conglomerate, lapilli tuff, pisolitic tuff, fluvial sandstone and conglomerate	Southern study area—Fine- to medium-grained orange volcaniclastic sandstone beds up to 10 cm thick; reversely sorted orange and pink volcaniclastic debris-flow deposits consisting of 50%–90% ash matrix, 0%–5% pumice, and 10%–45% lithic fragments of andesite, basaltic-andesite, and tonalite; multiple welded ash-flow lapilli tuffs typically consisting of 70% ash and plagioclase phenocryst matrix, 5% flattened and devitrified pumice with plagioclase and hornblende phenocrysts, and 25% lithic fragments of andesite, basaltic-andesite, and tonalite; multiple 2–3-m-thick pisolitic tuffs composed of spherical accretionary lapilli up to 5 cm diameter; welded ash-flow lapilli tuff; ~10 m of 10–50-cm-thick fluvial volcaniclastic beds of medium-grained sandstone and coarse-gravel conglomerate. Northern study area—Fluvial pebbly sandstone with subrounded to rounded Tvu clasts; poorly stratified burgundy-red clast-supported pebble-cobble conglomerate with angular to subrounded clasts of rhyolite, andesite, and rare crystalline basement; poorly stratified clast-supported sandy cobble-boulder conglomerate and cross-bedded pebbly sandstone with subrounded pebbles and cobbles of andesite.	Up to 220 m	–	–	–	–	–

(*continued*)

TABLE 1. FIELD DESCRIPTIONS AND SUMMARY OF GEOCHRONOLOGIC AGES OF LITHOLOGIC MAP UNITS (*continued*)

Lithologic group	Map unit	Unit name	Dominant lithologies	Rock description	Unit thickness	Age (Ma)	Dating technique/ material	Published sample number	Reference	Previous published names
Tuff of San Felipe	Ttsf	Tuff of San Felipe	Densely welded ash-flow tuff	A typical section of the Tuff of San Felipe consists of (1) a basal nonwelded yellow air-fall tuff, typically <1 m thick, overlain by (2) black glassy vitrophyre, typically 0.5 to 2 m thick, with occasional subcentimeter oxidized spherulites. The vitrophyre grades upward into (3) a densely welded spherulite-rich zone of pumice-poor brick-red tuff up to 5 m thick. The spherulitic zone grades upward into (4) a >100-m-thick densely welded zone of pumice-fiamme–rich burgundy lapilli tuff with a distinctive eutaxitic foliation of pumice-fiamme. Large pumices are flattened to 0.1–2 cm thick and stretched up to 1 m in length measured in the lineation direction. Pumice concentration increases higher in the unit, as does the degree of vapor-phase alteration. Segregation pipes oriented orthogonal to eutaxitic foliation are observed in the upper few meters. Local internal rheomorphic flow deformation is observed as strong folding and/or brecciation of foliated pumice-fiamme. Within fiamme-rich horizons, rare to uncommon pods of distinctive black trachyte inclusions that contain alkali-feldspar, plagioclase, and fayalite phenocrysts (Oskin and Stock, 2003a) are observed. These inclusions were deformed plastically during rheomorphism. Near the probable vent location, Ttsf consists of up to three cooling units, described by Bennett (2009).	135–>500 m	12.50 ± 0.08	Ar/Ar on multiple individual anorthoclase crystals	PC-98-18	This study	Tmr1 (Baja California—Bryant, 1986) Tuff of Hermosillo (central Sonora—Paz-Moreno et al., 2000)
Northern prerift local volcanic rocks	Tvln	Tuff of Punta Chueca (Ttpc)	Nonwelded ash-flow tuff	Recessive, nonwelded, pumice-rich ash-flow tuff; consists of two distinct units: (1) a lower nonwelded lithic-poor, 20-m-thick pyroclastic flow deposit with 1–3% centimeter-scale volcanic lithics, 3%–10% pumice up to 20 cm, which locally displays a black basal vitrophyre 1–3 m thick, and (2) an upper nonwelded lithic-rich, 70-m-thick pyroclastic flow deposit with up to 10% volcanic lithics up to 2 cm and 3%–10% pumice up to 5 cm, and sedimentary structures (e.g., trough cross-bedding) that indicate the upper 1–2 m may be fluvially reworked.	90 m	–	–	–	–	–
		Basalt of Punta Chueca (Tbpc)	Basalt	Aphanitic, locally vesicular basalt flow; outcrops typically consist of resistant, yet unstable, ridgelines of unorganized piles of large basalt boulders, limiting exposures for obtaining reliable structural information; vague 1–15 cm-spaced foliations are measured within this unit within the limited extent of intact outcrops; where the basal contact of Tbpc is exposed, the lower 1 m is brecciated and in sharp planar contact with the underlying Ttpc.	5–10 m	11.47 ± 0.05	Ar/Ar on volcanic matrix	PC-00-06	This study	–
Southern prerift local volcanic rocks	Tvls	Tuff of Hast Eucla (The)	Poorly welded air-fall tuff	Light lime green on fresh surfaces, but weathers to orangish-yellow and contains common to abundant andesitic lithic fragments up to 0.5 cm in diameter.	1–4 m	–	–	–	–	–
		Ryholite of Hast Eucla (Trhe)	Rhyolite	Rhyolite, burgundy w/ common 1–5-cm-spaced flow foliation.	Up to 90 m	–	–	–	–	–
Synrift rocks	Tcg	Basin conglomerate	Nonmarine conglomerate and sandstone	Gray, tan, and orange, massive to poorly- to well-stratified, poorly- to well-sorted, fine-grained sandstone with centimeter-scale beds, pebbly sandstone, and clast-supported and matrix-supported sandy- to boulder-conglomerate, with individual stratified beds up to 2 m thick. Tcg also contains few discontinuous and undulatory white air-fall ash beds, 5–15 cm thick, between cobble-conglomerate beds. Within early Tcg deposits in the Punta Chueca basin, a 15-m-thick package of fine- to medium-grained light-pink to buff sandstone with abundant cross-beds up to 5 cm thick is observed. Clast composition of Tcg consists of basement units, Tvu, Ttsf, Tvln, Tvls, and interbedded tuffs coeval with basin fill.	≥480 m (top not exposed)	Ca. 7–~5 Ma	–	–	This study	T3 and Qf (Gastil and Krummenacher, 1977b)

(*continued*)

TABLE 1. FIELD DESCRIPTIONS AND SUMMARY OF GEOCHRONOLOGIC AGES OF LITHOLOGIC MAP UNITS (*continued*)

Lithologic group	Map unit	Unit name	Dominant lithologies	Rock description	Unit thickness	Age (Ma)	Dating technique/ material	Published sample number	Reference	Previous published names
Interbedded tuffs	Ttck	Tuff of Cerro Kino	Air-fall tuff	Moderately- to well-laminated, white to light-brownish-gray, air-fall tuff with 3%–5% phenocrysts of alkali-feldspar ≈ quartz > amphibole > zircon, contains angular lithics of rhyolite, andesite, and Ttsf up to 1.0 cm in diameter (typically 2–5 mm), contains 1%–3% silicified white, gray pumice.	14 cm	7.05 ± 0.03	Ar/Ar on multiple sanidines	BK-08-29	This study	-
	Ttct	Tuff of Cerro Tordillo	Air-fall tuff	Slightly welded to nonwelded, light-gray to light-yellowish-gray tuff with 5%–15% phenocrysts of amphibole > alkali-feldspar > quartz, contains angular lithics of rhyolite, andesite, and Kt up to 0.5 cm (typically 1–2 mm), contains 1–3% yellow, white, and orange pumice; unit displays vague centimeter-scale sorted beds.	2 m	6.53 ± 0.18	U/Pb on multiple zircons	BK-08-32	This study	-
	Ttmc	Tuffs of Mesa Cuadrada	Poorly welded to nonwelded ash-flow tuff	Poorly welded to nonwelded salmon-colored ash-flow tuff with 5%–10% phenocrysts of alkali-feldspar >> quartz >> hornblende >> zircon >> sphene >> pyroxene, 5% poorly welded to nonwelded pumice with similar phenocrysts as matrix, 5%–10% very angular lithic fragments of dark-brown to purple aphanitic andesite and rhyolite, typically 0.5–2 cm in diameter. Accidental lithic fragments of Tvu and Ttsf are common within the lowest 1–2 m of this deposit. Both the matrix and pumice weather to light orange. Welding in Ttmc increases up section. Tabular, lithic-rich segregation pipes 8–15 cm thick are locally observed in Ttmc perpendicular to, or at high angles to, outcrop strike.	Up to 30 m	6.39 ± 0.02	Ar/Ar on multiple sanidines	BK-02-08	This study	Tmr3 (Oskin and Stock, 2003a) Tmr3b (Lewis and Stock, 1998)

and toward basin-bounding faults. Boulder-sized basement clasts occur in the youngest Tcg deposits adjacent to the Punta Chueca fault. The thickest exposure of Tcg is found in the Punta Chueca basin above the hanging wall of the Punta Chueca fault (395350E, 3207000N), where it is ≥480 m thick (Dorsey et al., 2008). In the Kino basin, Dorsey et al. (2008) reported Tcg measured sections of 180 m (399700E, 3198900N) and 250 m (402550E, 3195300N). These are minimum basin thicknesses because the top of the basin is eroded, and up to ~300 m of additional Tcg may lie at deeper structural levels in the hanging wall of normal faults that were active early in the formation of the Punta Chueca and Kino basins. In the southwestern corner of the Punta Chueca basin, a package of Tcg appears to have been deposited in an ~1-km-wide paleovalley with steep buttress contacts against Ttsf. No minimum age constraints exist for Tcg, but its deposition likely spanned to near the Miocene-Pliocene boundary.

Tcg overlies older volcanic units (e.g., Ttsf, Tvln, Tvls) above a time-transgressive unconformity surface that grades laterally from a disconformity in the downdip direction to an angular unconformity in the updip direction. Up section, another important, internal unconformity exists within basin conglomerate deposits, forming the most common contact between basin fill and older volcanic units. This feature also grades laterally from a subtle disconformity in the downdip direction, as observed in the Punta Chueca basin (Fig. 3), to a sharp, 25°–40° angular unconformity atop older volcanic units (e.g., Tvu, Ttsf, Tvln, Tvls) in the updip direction. This extensive unconformity commonly cuts the older unconformity and is observed across the entire study area (Fig. 3).

Interbedded Tuffs

Tuff of Cerro Kino. The Tuff of Cerro Kino (Ttck) is a 14-cm-thick, moderately- to well-laminated, white to light brownish-gray air-fall tuff exposed only in the southern portion of the Kino basin, interbedded ~200 m above the angular unconformable contact at the base of the basin conglomerate (402870E, 3194820N). Ttck contains 3%–5% phenocrysts of alkali-feldspar ≈ quartz > amphibole > zircon, angular lithics of rhyolite, andesite, and Ttsf up to 1.0 cm in diameter, and 1%– 3% silicified white to gray pumice. We report a new $^{40}Ar/^{39}Ar$ age of 7.05 ± 0.03 Ma on multiple sanidines from Ttck (Fig. 5C; Table 2). We also report results from sensitive high-resolution ion microprobe-reverse geometry (SHRIMP-RG) $^{206}Pb/^{238}U$ analyses of zircons from Ttck, which include 6.75 ± 0.15 Ma and 7.13 ± 0.16 Ma grains (1σ) (Fig. 7; Table 4), consistent with the $^{40}Ar/^{39}Ar$ results. Both geo-

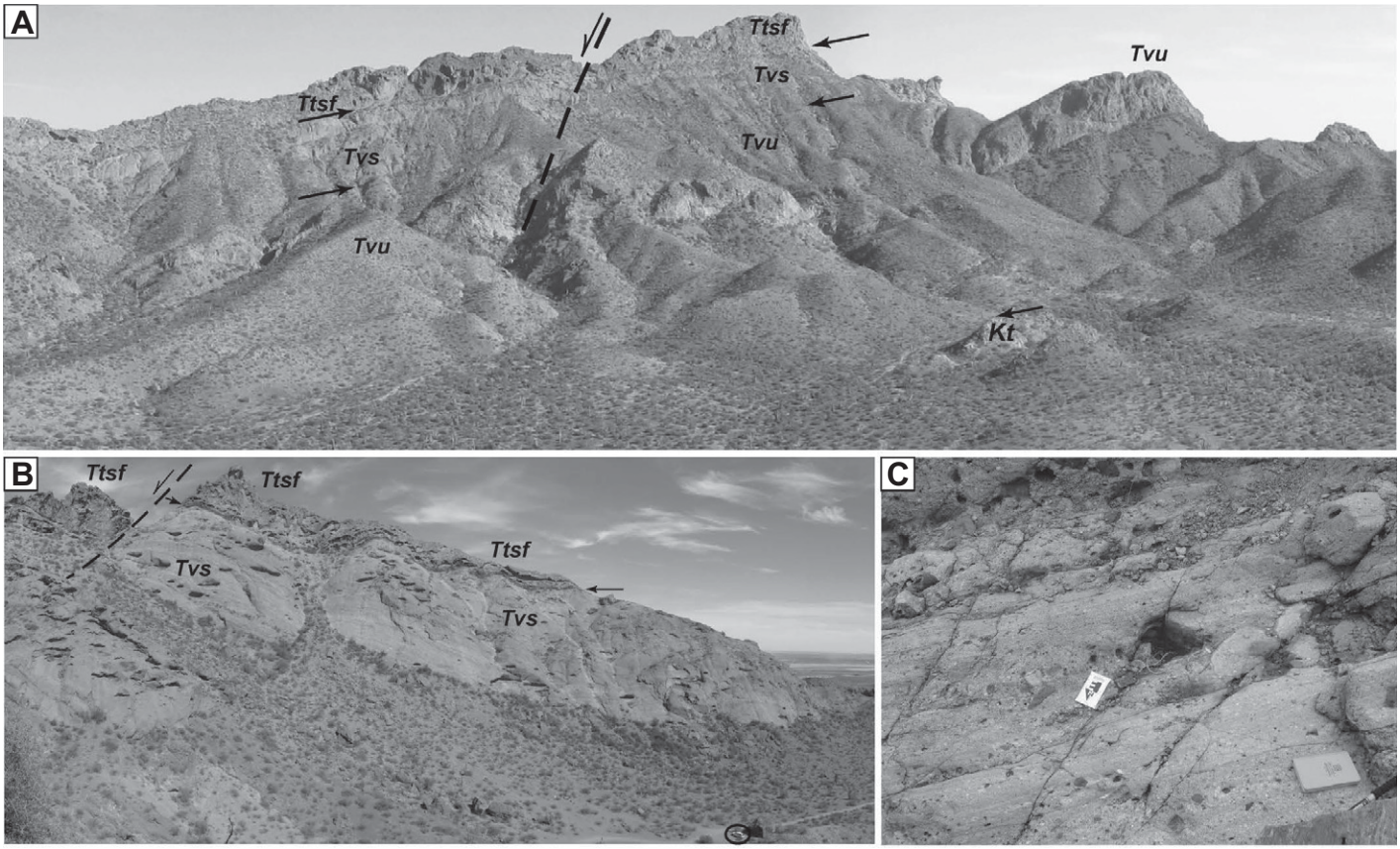

Figure 4 (*on this and following two pages*). Field photographs displaying contact relationships and layering of map units. Contacts between units are indicated with arrows. (A) Looking southeast at the Cerro Kino ridgeline, which is a resistant ridge in the southeastern study area consisting of steeply dipping Tuff of San Felipe (Ttsf). Moderately resistant volcaniclastic (Tvs) and andesitic (Tvu) units underlie the Tuff of San Felipe in the foreground. Relief from high peak to alluvial flat in foreground is ~270 m. Total field of view is ~1.6 km long. (B) Looking east at the southern portion of the Cerro Kino ridgeline. The very resistant Tuff of San Felipe (darker unit capping ridgeline) overlies unvegetated outcrops of volcaniclastic sandstone (Tvs). A ~5-m-long Dodge Durango is at toe of slope (circled). (C) Outcrop of well-stratified basin conglomerate (Tcg) displaying 1–30-cm-scale beds of pebbly sandstone and cobble conglomerate. Arrow on card is 10 cm.

chronologic techniques involve the analysis of multiple, single-crystals and reveal populations of older, inherited crystals, which group into ages consistent with the older rocks found in the study area. For example, eight zircons and 19 sanidines are ca. 10–12 Ma, similar to the age of local volcanic rocks and the Tuff of San Felipe, eight zircons are ca. 14–19 Ma, similar to the age of the arc-related andesitic and volcaniclastic rocks in the study area, and three zircons are >90 Ma, similar to the age of the regional basement rocks.

Tuff of Cerro Tordillo. The Tuff of Cerro Tordillo (Ttct) is a 2-m-thick, light-gray to yellowish-gray air-fall tuff exposed only in the Punta Chueca basin (394750E, 3206330N), interbedded 65 m above the exposed base of basin conglomerate (Tcg). Ttct contains 5%–15% phenocrysts of amphibole > alkali-feldspar > quartz, angular lithics of rhyolite, andesite, and Kt up to 0.5 cm, and 1%–3% yellow, white, and orange pumice lapilli. This tuff is slightly welded to nonwelded and displays vague centimeter-scale sorted beds. We report a new SHRIMP-RG $^{206}Pb/^{238}U$ weighted mean age of 6.53 ± 0.18 Ma (n = 14; mean square of weighted deviates [MSWD] = 1.3) on zircons separated from Ttct (Fig. 8; Table 4).

Tuffs of Mesa Cuadrada. The Tuffs of Mesa Cuadrada (Ttmc) represent another regionally extensive ignimbrite that blanketed >2100 km^2 of present-day northeastern Baja California (Stock, 1989; Lewis, 1996; Nagy et al., 1999), Isla Tiburón (Oskin et al., 2001; Oskin and Stock, 2003a, 2003b), and coastal Sonora (Oskin and Martín-Barajas, 2003; this study). Only the Tmr3 cooling unit of the Tuffs of Mesa Cuadrada of Oskin and Stock (2003a) is present within the study area (Fig. 4G). Deposits of Ttmc, up to 30 m thick, are observed near or at the base of both the Punta Chueca and Kino basins. In the Kino basin, Ttmc is in angular unconformable contact with underlying volcanic rocks (e.g., Tvu, Ttsf) that have steeper dips. In the Punta Chueca basin, Ttmc is interbedded with basin deposits of Tcg. We report a new $^{40}Ar/^{39}Ar$ age of 6.39 ± 0.02 Ma on multiple sanidines from Ttmc (394810E, 3206860N) in the Punta Chueca basin (Fig. 5D; Table 2), consistent with isotopic ages from this unit in northeastern Baja California (Stock, 1989; Lewis, 1996; Nagy et al., 1999) and Isla Tiburón (Gastil et al., 1979; Oskin, 2002).

The Tuffs of Mesa Cuadrada have a typical normal polarity (down 50°–60° to the N to NE) direction of paleomagnetic remanence (Lewis and Stock, 1998; Nagy, 2000; Oskin et al., 2001; this study). This direction was determined on the Tmr3b unit of Lewis and Stock (1998) from northeastern Baja California, and it is close to the expected Miocene magnetic field at this latitude.

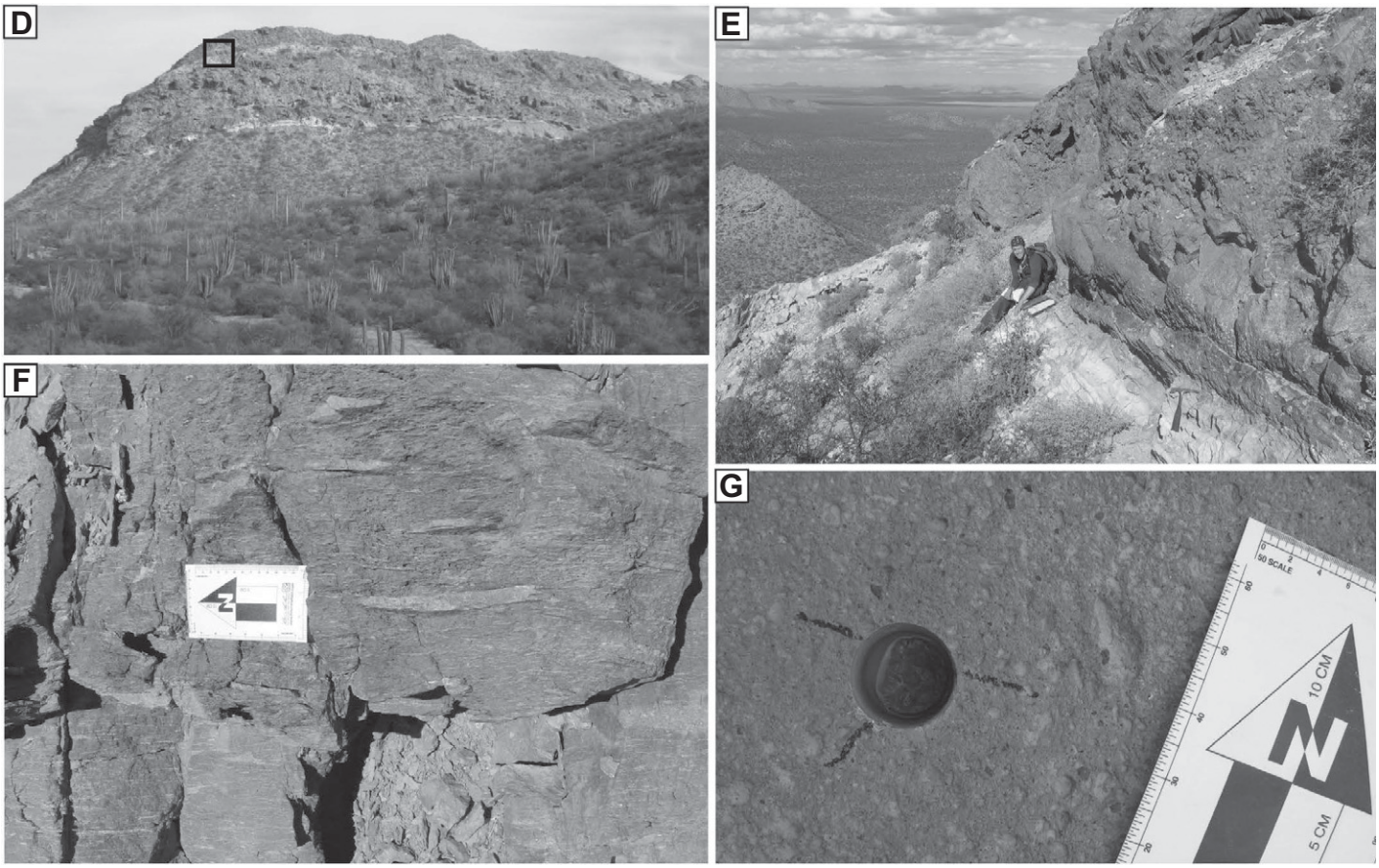

Figure 4 (*continued*). Field photographs display regional ignimbrites exposed in coastal Sonora study area. (D) Looking east at three cooling units of the Tuff of San Felipe (Ttsf) in the central study area. The lower and upper cooling units each overlie ~5 m of light-colored air-fall ash deposits. (E) Looking northeast at contact between second and third cooling units of the Tuff of San Felipe (Ttsf). Black basal vitrophyre of third cooling unit overlies laminated and cross-bedded ash beds of surge deposit. 28-cm-long hammer is in foreground. Area of photo is black box in photo D. (F) Typical outcrop of densely welded Tuff of San Felipe (Ttsf) with strongly flattened pumice fiamme. Arrow on card is 10 cm. (G) Typical outcrop of the Tuffs of Mesa Cuadrada (Ttmc) with occasional volcanic lithics (dark angular fragments) and nonwelded pumice (lighter than matrix). Outcrop is wet from drilling 1-in.-diameter (2.54 cm) paleomagnetic cores.

RIFT STRUCTURES

The coastal Sonora region is dissected by normal, dextral, oblique-normal, and sinistral faults (Fig. 3) associated with the Neogene opening of the northern Gulf of California oblique rift. These structures created and later deformed the east-tilted Kino and Punta Chueca tectonic basins (Fig. 6). Fault kinematic data, collected primarily from small-offset faults found throughout the study area, are highly variable and do not show a consistent relationship between the rake of striae and either fault strike or fault dip (Fig. DR1[1]). This suggests that many faults have been rotated since their formation, complicating kinematic analysis. Overall, the fault kinematic data (Table DR1 [see footnote 1]) are consistent with transtensional deformation of the area (Fig. DR2 [see footnote 1]).

Normal Faults

The Punta Chueca fault is an undulatory low-angle normal fault that juxtaposes the Tuff of San Felipe and sediments of the Punta Chueca basin against basement rocks. The Punta Chueca fault varies from N-striking in the north to NE-striking along its southwestern portion. Local fault dip measurements range from 18° to 49° toward the northwest, with W-directed slip indicators (Fig. 3). We interpret that the steeper dips reflect local structural complexity, such as a tear fault, within an overall low-angle fault zone. Where sufficient exposures permit, we used three-point fits to resolve dips that range from ~5° west to ~10° back-tilted to the southeast.

Three additional significant normal faults are recognized and named (Fig. 3). The Eco fault (Fig. 4H) and Tordillo fault are WNW-dipping, moderate-angle (45°–60°) normal faults. These faults juxtapose prerift volcanic rocks and synrift basin conglomerate of the Kino basin against basement rocks. Additional subparallel, small-offset normal faults within the hanging wall of the Eco and Tordillo faults contribute to the dilation of this part of the study area. The Aeropuerto fault is a low-angle(?) normal fault that is inferred to exist in the southeastern part of the study area (Fig. 3). This fault is inferred because prerift rocks (e.g., Ttsf) are steeply tilted, up to ~80°, similar to rocks in the hanging wall of the Punta Chueca fault. This geometry requires a significant normal fault to exist beneath the

[1]GSA Data Repository item 2013354, fault kinematic data from coastal Sonora, is available at http://www.geosociety.org/pubs/ft2013.htm or by request to editing@geosociety.org.

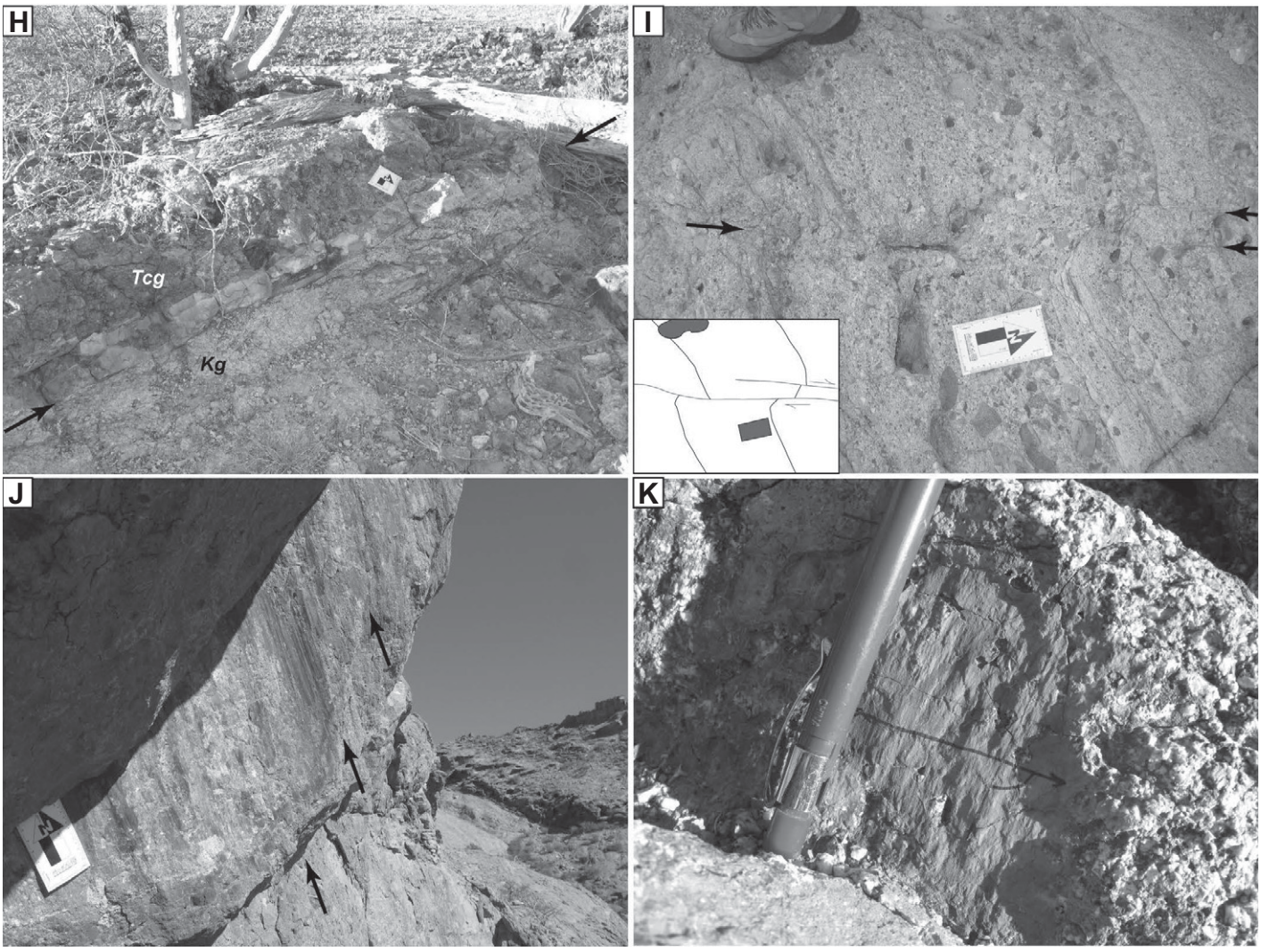

Figure 4 (*continued*). Field photographs display rift-related brittle structures. (H) Looking north at NW-dipping Eco fault in east-central study area. Sharp fault contact (arrows) juxtaposes basin conglomerate (Tcg) in hanging wall against granite basement (Kg) in footwall of moderately dipping normal fault. Arrow on card is 10 cm. (I) Outcrop of deformed ~35-cm-thick cobble conglomerate bed in basin conglomerate (Tcg). Bed is offset and slightly folded across pair of dextral faults, as interpreted in inset. Arrows point to brittle faults shown in inset interpretation. Arrow on card is 10 cm. (J) Fault slickenlines preserved on strongly polished brittle fault surface in volcaniclastic sandstone (Tvs). Arrows point parallel to slickenlines. Arrow on card is 10 cm. (K) Fault slickenlines preserved in clay gouge on brittle fault surface in tonalite basement (Kt). Strike line is drawn with fine black marker. Pencil is parallel to slickenlines and ~8 mm in diameter.

younger alluvium southeast of the Kino basin. The location and dip of the Aeropuerto fault are not constrained, and it could lie well southeast of its inferred, buried map trace (Fig. 3).

Strike-Slip Faults

Several strike-slip faults with hundreds of meters to several kilometers of slip occur within the study area (Fig. 3). The dextral Bahía Kino fault consists of three NW-striking branches that truncate all pre-Quaternary map units in the central and southern parts of the study area. These branches are the best exposed strike-slip faults in the study area, and their orientations (310°–320°) are subparallel to offshore dextral structures within both the active (Fenby and Gastil, 1991) and abandoned (Aragón-Arreola and Martín-Barajas, 2007; Mar-Hernández et al., 2012) rift basins (e.g., De Mar fault; Fig. 1). The Puerto Rico fault is a poorly exposed NW-striking dextral fault in the east. The Punta Blanca fault is a NE-striking sinistral structure in the south-central part of the study area. Due to poor fault exposure, the dips of these two latter faults are not well constrained.

The Sacrificio fault zone first appeared on maps by Gastil and Krummenacher (1977a, 1977b) and was named by Oskin (2002). In the northeastern part of the study area, the Sacrificio fault zone consists of multiple subparallel NW-striking strike-slip faults (Fig. 3) with a possible down-to-the-W dip-slip component (Gastil and Krummenacher, 1977a). The Infiernillo fault first appeared on maps by Gastil and Krummenacher (1977a, 1977b) as an inferred, unnamed structure that separated coastal Sonora from Isla Tiburón. Its location, strike, and dip are neither observed nor constrained. Both the Infiernillo

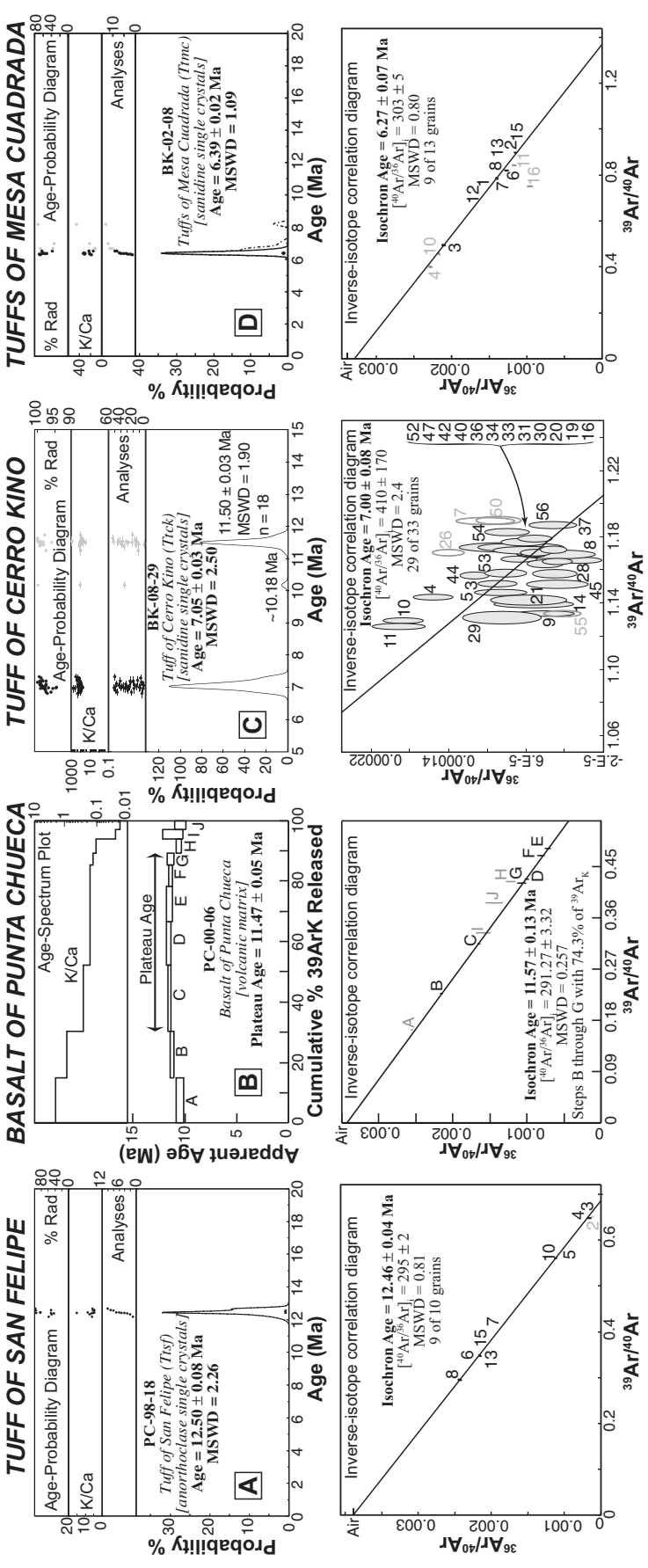

Figure 5. $^{40}Ar/^{39}Ar$ geochronological ages calculated for volcanic rocks from coastal Sonora. (A) Age-probability diagram and inverse-isotope correlation diagram for the Tuff of San Felipe (Ttsf). (B) Age spectrum plot and inverse-isotope correlation diagram for sample from Basalt of Punta Chueca (Tbpc), the youngest subunit of prerift volcanic units in northern part of study area (Tvln). (C) Age-probability diagram and inverse-isotope correlation diagram for the Tuff of Cerro Kino (Ttck). (D) Age-probability diagram and inverse-isotope correlation diagram for the Tuffs of Mesa Cuadrada (Ttmc). See Tables 2 and 3 for data table. MSWD—mean square of weighted deviates.

and Sacrificio faults continue northwest of the study area and likely trend into other NW-striking structures on northeastern Isla Tiburón (Bennett et al., 2012) and beneath the Gulf of California (Mar-Hernández et al., 2012), and also to the southeast, parallel to the shoreline, and concealed by the Rio Sonora delta plain (Fig. 1).

PALEOMAGNETISM

Field and Laboratory Methods

Either Ttmc or Ttsf was sampled for paleomagnetic analysis at four sites between the towns of Bahía de Kino and Punta Chueca in coastal Sonora (Fig. 9). These sites were selected to quantify clockwise vertical-axis rotations of fault blocks attributed to distributed dextral deformation. Such documentation of dextral deformation has proven successful on the conjugate rift margin in northeastern Baja California (e.g., Lewis and Stock, 1998). The isotopic age determined here for Ttmc (6.39 ± 0.02 Ma) indicates that it likely erupted during normal polarity subchron C3An.2n (6.436–6.733 Ma; Lourens et al., 2004), although within error the age is ~26 k.y. younger than the upper limit (6.436 Ma) of this normal chron. This may indicate a minor calibration issue with the latest published astronomical time scale of Lourens et al. (2004), which is always being reevaluated and revised. The isotopic age determined here for Ttsf (12.50 ± 0.08 Ma) indicates that it likely erupted during reversed polarity subchron C5Ar.1r (12.415–12.730 Ma). In total, 57 samples (cores) were collected from these paleomagnetic drill sites (e.g., Fig. 4G), and 1-cm-tall specimens were prepared from these samples for demagnetization experiments. Multiple randomly oriented samples were collected at each paleomagnetic site ($n > 10$) to adequately quantify the error in site directions and resulting block rotation values.

All specimens were subjected to progressive alternating field (AF) demagnetization, typically including 13 steps to a magnetic field strength of 80 mT. AF partial demagnetization steps gradually demagnetize the secondary low-stability component and isolate the primary high-stability component of natural remanent magnetization (NRM) of a specimen. This primary NRM, typically a thermoremanent magnetism, is representative of Earth's magnetic field at the time the sampled rock cooled below the Curie temperature (Butler, 1992). Because ignimbrites cool much faster than significant changes in the secular variation of Earth's magnetic field, the NRM directions determined from multiple specimens collected from the same ignimbrite

cooling unit should agree within uncertainty (Lewis and Stock, 1998). NRM and low-temperature measurement steps preceded all AF steps. All experiments were conducted using an automated 2G Enterprises superconducting rock magnetometer in a magnetically shielded μ-metal room at the Paleomagnetics Laboratory of the California Institute of Technology, as described by Kirschvink et al. (2008). No thermal demagnetization steps were performed.

Paleomagnetic data were analyzed using PaleoMag v3.1b1 (Jones, 2002) to estimate the best fit of lines and planes for demagnetization paths for each specimen (Fig. 10), following the technique of Kirschvink (1980). Typically, directions resolved from higher AF steps were utilized to obtain best-fit lines, while NRM, low-temperature, and low AF steps revealed inconsistent vector directions, indicative of variable magnitudes of a secondary NRM component.

Results

To quantify vertical-axis block rotation in coastal Sonora, data from paleomagnetic remanence directions measured on ignimbrites were compared to their respective reference locations in stable Baja California. Because these reference locations have remained more or less tectonically stable since at least middle Miocene time, the paleomagnetic vectors of the same ignimbrite measured there are good estimates of the magnetic field at the time each ignimbrite cooled below the Curie temperature. Two additional Tuff of San Felipe paleomagnetic sites within the study area from Oskin et al. (2001) were reevaluated and are included in this analysis. These comparisons indicate vertical-axis rotations that range from ~1° counterclockwise to ~53° clockwise. Representative examples of paleomagnetic measurements from each coastal Sonora drill site are shown in Figure 10, and their relative declination and inclination anomalies (magnitudes of rotation and flattening) are summarized in Figure 9 and Table 5. Three additional Tuffs of Mesa Cuadrada sites in the central part of the study area were sampled for paleomagnetism. However, due to largely unstable demagnetization paths, no reliable site-mean directions could be determined for samples collected from these sites, and are not reported here. For all Ttsf paleomagnetic sites, rotation values were calculated with respect to Ttsf deposits at the high-precision reference site of Bennett and Oskin (2008) near El Metate in north-central Baja California (Fig. 1). For the Ttmc paleomagnetic site, rotation values were calculated with respect to the Tmr3b unit reference site of Lewis and Stock (1998) from Mesa Cuadrada in northeastern Baja California (Fig. 1).

TABLE 2. $^{40}Ar/^{39}Ar$ LASER TOTAL FUSION DATA OF SINGLE-CRYSTAL SANIDINES

Hole number	$^{39}Ar_k$ (moles)	Radiogenic yield (%)	$^{40}Ar^*/^{39}Ar_k$	K/Ca	K/Cl	Age (Ma)		Error (Ma)
Tuff of San Felipe (PC-98-18)								
7	7.33E–15	57.5	1.427	5.9	164	12.21	±	0.18
6	1.56E–14	49.1	1.444	7.4	216	12.35	±	0.13
8	8.33E–15	42.9	1.450	6.3	157	12.41	±	0.18
4	2.19E–14	94.7	1.453	14.9	211	12.43	±	0.04
13	1.69E–14	50.4	1.454	5.1	189	12.44	±	0.12
10	1.02E–14	81.8	1.455	4.5	152	12.45	±	0.09
5	1.79E–14	82.6	1.456	8.5	198	12.46	±	0.06
3	6.65E–15	95.4	1.471	5.4	270	12.59	±	0.09
15	1.38E–14	51.3	1.472	4.4	158	12.60	±	0.13
2	*1.41E–14*	*96.6*	*1.482*	*5.6*	*192*	*12.68*	±	*0.05*
J = 0.004760 ± 0.25% #7KD31					**Weighted mean age =**	**12.50**	±	**0.08**
Tuff of Mesa Cuadrada (BK-02-08)								
2	2.24E–14	66.1	0.735	18.0	285	6.31	±	0.05
13	4.10E–14	63.9	0.737	19.5	22	6.33	±	0.07
15	1.98E–14	67.8	0.737	29.5	12	6.33	±	0.10
8	3.82E–14	60.9	0.742	32.0	56	6.38	±	0.07
1	2.36E–14	54.8	0.745	28.6	271	6.40	±	0.06
12	5.06E–14	50.0	0.745	21.4	13	6.40	±	0.08
7	7.32E–14	58.9	0.750	31.6	19	6.44	±	0.06
6	2.89E–14	62.6	0.761	14.6	20	6.54	±	0.08
3	3.47E–14	37.8	0.761	21.9	298	6.54	±	0.12
11	*2.82E–14*	*65.6*	*0.778*	*10.7*	*19*	*6.68*	±	*0.08*
10	*3.70E–14*	*35.9*	*0.780*	*12.7*	*62*	*6.70*	±	*0.11*
4	*2.32-14*	*32.7*	*0.813*	*21.6*	*32*	*6.98*	±	*0.17*
16	*1.99E–14*	*71.8*	*0.954*	*44.1*	*4*	*8.20*	±	*0.10*
J = 0.004771 ± 0.25% #8KD31					**Weighted mean age =**	**6.39**	±	**0.02**
Tuff of Cerro Kino (BK-08-29)								
7	*4.67E–15*	*97.0*	*0.815*	*213.2*	*10,000*	*6.82*	±	*0.06*
50	*3.43E–15*	*97.4*	*0.819*	*113.4*	*11,111*	*6.85*	±	*0.05*
26	*8.88E–15*	*95.9*	*0.819*	*137.7*	*10,000*	*6.85*	±	*0.04*
54	3.97E–15	97.7	0.825	144.9	12,500	6.90	±	0.05
33	3.50E–15	97.6	0.832	83.6	*	6.96	±	0.06
20	2.50E–15	97.8	0.833	114.5	8333	6.97	±	0.12
34	4.58E–15	98.2	0.834	357.1	*	6.98	±	0.05
4	6.96E–15	95.4	0.834	84.4	16,667	6.98	±	0.05
37	4.74E–15	99.1	0.835	591.7	*	6.98	±	0.05
44	5.22E–15	96.7	0.836	61.2	7143	6.99	±	0.03
56	5.06E–15	98.5	0.836	150.2	25,000	6.99	±	0.04
31	4.89E–15	98.1	0.837	135.9	4348	7.00	±	0.05
10	6.83E–15	94.5	0.837	94.0	4545	7.00	±	0.05
11	5.63E–15	94.4	0.838	92.6	10,000	7.01	±	0.06

(*continued*)

DISCUSSION

Coastal Sonora Fault Zone

This study documents a NW-trending, transtensional fault zone, herein named the Coastal Sonora fault zone. The entire study area is contained within the core of the 10–15-km-wide Coastal Sonora fault zone, which hosts several crosscutting systems of normal and dextral faults, each with several kilometers of slip, and is bracketed by the Sacrificio and Infiernillo strike-slip faults. Formation of the nonmarine Kino and Punta Chueca basins was synchronous with fault activity, and all pre-Quaternary map units are cut by faults (Fig. 3). Here, we synthesize estimates of fault displacement, crosscutting relationships, and timing of fault activity that support the interpretation that the Coastal Sonora fault zone may have hosted a significant proportion of Pacific–North American dextral plate motion just prior to the localization of rifting in the axis of the Gulf of California.

Normal Faults

Generally, two classes of normal faults are observed: (1) NE-striking normal faults, many of which dip at low to moderate angle, with larger magnitudes of slip, and (2) N-striking and WNW-striking, high-angle, normal faults with smaller magnitudes of slip. Blocks bracketed by normal faults have been variably rotated in a clockwise sense about a vertical axis, and tilted down to the east up to 90° by slip and rotation of low-angle (5°–15°) and moderate-angle (40°–60°) normal faults (Fig. 11). Hanging-wall cutoff angles >90° are common and require a complex polystage history of tilting on at least two generations of normal faults (e.g., Proffett, 1977; Gans, 1997; Brady et al., 2000).

We calculated estimates of slip magnitudes on normal faults and total horizontal extension from restoration of cross-section A (Figs. 11A and 11B). Cross sections were drawn perpendicular to the structural grain of tilted fault blocks and normal faults, approximately parallel to the ~WNW tectonic transport direction

TABLE 2. $^{40}Ar/^{39}Ar$ LASER TOTAL FUSION DATA OF SINGLE-CRYSTAL SANIDINES (*continued*)

Hole number	$^{39}Ar_k$ (moles)	Radiogenic yield (%)	$^{40}Ar^*/^{39}Ar_k$	K/Ca	K/Cl	Age (Ma)		Error (Ma)
Tuff of Cerro Kino (BK-08-29) (*continued*)								
40	2.76E–15	98.3	0.839	56.9	7692	7.02	±	0.08
16	7.81E–15	98.0	0.840	95.7	*	7.03	±	0.04
30	6.40E–15	98.4	0.841	194.6	100,000	7.04	±	0.04
42	5.93E–15	98.5	0.842	79.5	16,667	7.04	±	0.04
53	3.83E–15	97.6	0.843	69.5	8333	7.05	±	0.05
47	5.88E–15	99.1	0.845	79.4	12,500	7.07	±	0.03
3	8.53E–15	97.4	0.845	157.0	10,000	7.07	±	0.05
19	3.82E–15	99.2	0.848	100.4	25,000	7.10	±	0.08
36	5.47E–15	98.8	0.849	132.5	25,000	7.10	±	0.04
5	6.04E–15	97.5	0.850	135.9	20,000	7.11	±	0.06
52	5.79E–15	99.2	0.851	121.1	12,500	7.12	±	0.03
28	6.74E–15	99.1	0.856	89.1	33,333	7.16	±	0.05
8	6.91E–15	99.9	0.857	122.2	*	7.17	±	0.05
21	6.00E–15	98.3	0.861	154.3	4000	7.20	±	0.09
45	2.32E–15	99.2	0.862	109.2	9091	7.21	±	0.07
29	2.78E–15	97.5	0.862	129.4	9091	7.21	±	0.09
14	4.44E–15	98.5	0.864	228.8	7692	7.23	±	0.09
9	4.74E–15	98.8	0.872	167.2	10,000	7.29	±	0.07
55	4.34E–15	99.4	0.876	296.7	7692	7.33	±	0.04
38	*3.64E–15*	*99.8*	*1.218*	*107.0*	*5000*	*10.18*	±	*0.06*
13	*4.15E–15*	*97.3*	*1.348*	*90.3*	*6667*	*11.26*	±	*0.09*
39	*4.76E–15*	*99.2*	*1.365*	*118.3*	*	*11.40*	±	*0.06*
2	*8.02E–15*	*98.2*	*1.368*	*101.2*	*9091*	*11.43*	±	*0.04*
12	*5.14E–15*	*98.8*	*1.371*	*95.4*	*8333*	*11.45*	±	*0.07*
17	*6.47E–15*	*99.3*	*1.372*	*100.5*	*50,000*	*11.46*	±	*0.05*
43	*5.80E–15*	*98.7*	*1.372*	*89.0*	*8333*	*11.46*	±	*0.03*
1	*6.38E–15*	*98.3*	*1.374*	*113.8*	*5263*	*11.47*	±	*0.07*
32	*7.55E–15*	*98.9*	*1.377*	*102.5*	*6667*	*11.50*	±	*0.03*
49	*4.37E–15*	*99.0*	*1.377*	*27.7*	*16,667*	*11.50*	±	*0.04*
24	*6.67E–15*	*95.8*	*1.379*	*50.8*	*5882*	*11.52*	±	*0.05*
57	*5.20E–15*	*99.8*	*1.379*	*105.7*	*33,333*	*11.52*	±	*0.04*
35	*6.83E–15*	*99.6*	*1.379*	*50.3*	*100,000*	*11.52*	±	*0.04*
15	*3.90E–15*	*98.4*	*1.380*	*98.1*	*5882*	*11.52*	±	*0.11*
41	*2.24E–15*	*99.8*	*1.382*	*757.6*	*4545*	*11.55*	±	*0.09*
46	*4.85E–15*	*99.7*	*1.383*	*95.8*	*6250*	*11.55*	±	*0.04*
48	*5.24E–15*	*99.3*	*1.383*	*55.9*	*	*11.55*	±	*0.04*
18	*4.18E–15*	*99.9*	*1.387*	*50.2*	*4545*	*11.59*	±	*0.08*
58	*4.15E–15*	*100.0*	*1.395*	*79.4*	*7143*	*11.65*	±	*0.05*
23	*7.54E–15*	*97.8*	*1.407*	*98.7*	*12,500*	*11.75*	±	*0.05*
J = 0.004645 ± 0.25% #159KD53					**Weighted mean age =**	**7.05**	±	**0.03**

Note: Analyses in gray italics were not used to calculate the weighted mean age.
*K/Cl not calculated.

determined from offset metamorphic basement rocks and facies trends in the Tuff of San Felipe (Fig. 3). Additionally, slickenline orientations measured on the Punta Chueca fault (uncorrected for clockwise vertical-axis rotation) reflect dip-slip motion toward the northwest (Fig. 3). Fault dips were constrained by direct field measurements or three-point fits. A total of 9.1 km of post–12.5 Ma dip-slip displacement has occurred on normal faults along cross-section A (Fig. 11A). Total dip-slip displacement of the base of the 12.5 Ma Tuff of San Felipe across the Eco, Tordillo, and Punta Chueca faults is 2.4 km, 2.1 km, and 4.6 km, respectively. Note that slip on the Eco fault is less well constrained due to dextral displacement across the Puerto Rico fault. In map view, the Punta Chueca fault displays an apparent gradient of slip along strike. The basement nonconformity shows ~4 km of map-view separation in the northeast and ~6 km in the southwest (Fig. 3). Along cross-section A, a total of 5.7 km (120%) horizontal extension occurred along the Punta Chueca fault, Tordillo fault, Eco fault, and smaller intervening synthetic faults (Fig. 11B). The pin line for this calculation is the basal contact of the Tuff of San Felipe, in the footwall of the Eco fault to the southeast, and in hanging wall of the Punta Chueca fault to the northwest. Figure 12 illustrates the interpreted evolution of normal faulting and syntectonic accumulation of basin conglomerate and interbedded tuffs along cross-section A. Large strike-slip fault displacements through cross-section B (Fig. 11C) complicate restoration, and thus measurement of extension was not attempted. Based on the steep dips of prerift volcanic rocks here, extension along cross-section B likely also exceeds 100% (Wernicke and Burchfiel, 1982).

Strike-Slip Faults

NW-striking dextral faults and NNE-striking sinistral faults cut map units and extensional structures in the central, southern, and eastern parts of the study area (Fig. 3). The Sacrificio and Infiernillo strike-slip faults are the primary, bounding structures of the Coastal Sonora fault zone (Figs. 1 and 3) and have accommodated significant dextral deformation. In addition to these discrete displacements, distributed dextral shear across the Coastal Sonora fault zone was accommodated by clockwise vertical-axis rotations of some fault blocks and their bounding faults. Rotations range up to 35.5° ± 3.3° in the south and up to 52.8° ± 2.1° in the north (Fig. 9).

TABLE 3. $^{40}Ar/^{39}Ar$ STEP-HEATING DATA ON MATRIX FROM THE BASALT OF PUNTA CHUECA

Step	Temp. (°C)	%^{39}Ar of total	Radiogenic yield (%)	$^{39}Ar_k$ (moles ×10^{-12})	$^{40}Ar^*$ $^{39}Ar_k$	Apparent K/Ca	Apparent K/Cl	Apparent age (Ma)		Error (Ma)
Basalt of Punta Chueca (PC-00-06)										
A	*650*	*14.9*	*24.4*	*0.4437*	*1.490*	*2.17*	*42*	*10.49*	±	*0.17*
B	*750*	*15.5*	*36.4*	*0.4608*	*1.596*	*0.91*	*48*	*11.24*	±	*0.09*
C	850	21.8	51.3	0.6476	1.632	0.26	80	11.49	±	0.07
D	900	14.3	70.3	0.4257	1.641	0.17	216	11.55	±	0.10
E	950	11.6	78.7	0.3453	1.630	0.17	444	11.47	±	0.14
F	1000	7.2	76.1	0.2148	1.621	0.16	406	11.41	±	0.10
G	1050	3.8	68.3	0.1136	1.618	0.13	295	11.39	±	0.17
H	*1150*	*4.6*	*63.9*	*0.1378*	*1.507*	*0.10*	*222*	*10.61*	±	*0.13*
I	*1300*	*3.0*	*53.0*	*0.0905*	*1.588*	*0.02*	*25*	*11.18*	±	*0.49*
J	*1450*	*3.0*	*57.3*	*0.0906*	*1.484*	*0.02*	*162*	*10.45*	±	*0.27*
Total gas		100.0	54.1	2.9702	1.593	0.59	170	11.22		
58.82% of gas on plateau in steps C through G							**Plateau age =**	**11.47**	**±**	**0.05**
J = 0.003930 ± 0.50% wt = 225.1 mg #140KD25										

Note: Analyses in gray italics were not used to calculate the plateau age. Ages were calculated assuming an initial $^{40}Ar/^{36}Ar$ = 295.5 ± 0. All precision estimates are at the 1σ level of precision. Ages of individual steps do not include error in the irradiation parameter *J*. No error is calculated for the total gas age.

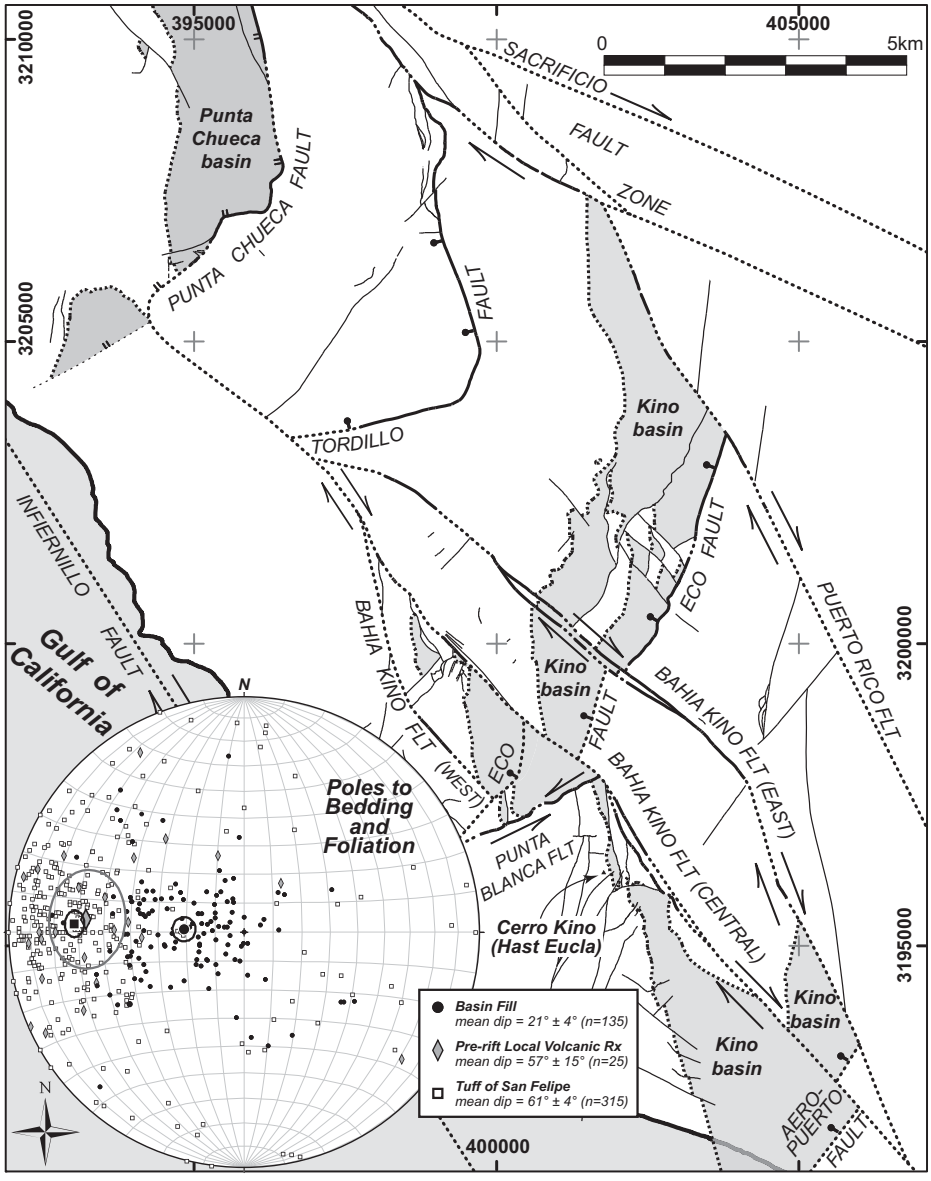

Figure 6. Simplified fault map showing major faults (thick black lines with fault decoration, dotted where concealed). Two distinct sedimentary basins (Punta Chueca and Kino) formed in the hanging wall of normal fault systems. Minor faults (thin black lines) also deform these sedimentary basins. Base of sedimentary basins (thick dotted lines) is typically a 25°–40° angular unconformity. See Figure 3 for detailed geology. Inset: Lower-hemisphere equal-area stereoplot of poles to bedding planes, measured in prerift Tuff of San Felipe (hollow black squares), prerift local volcanic rocks (gray diamonds), and synrift basin fill (black circles). Due to map scale constraints, not all of these measurements are shown on the geologic map (Fig. 3). Fisher distribution mean pole and 95% confidence cone were calculated with Stereonet software (Allmendinger et al., 2012) and are shown for each group. The occasional W-dipping measurements (poles on eastern half of stereonet) are due to either minor folding in Kino syncline or rheomorphic folding of foliation in the Tuff of San Felipe.

Total strike-slip displacement across the branches of the Bahía Kino fault is estimated as 4.2 ± 0.9 km. Here, we describe displacements on the eastern and central branches of this fault, each shown by circled numbers and arrows pointing to the displaced, correlative feature on the geologic map (Fig. 3). We report 0.8 ± 0.1 km of map-view separation of a steeply dipping basement dike on the eastern branch (circled number 1's on Fig. 3). We also observe a range of apparent dextral offsets of overlying Miocene strata: 1.4 ± 0.1 km for Kt-Tvu contact, 1.0 ± 0.1 km for Ttsf, and ~0.1 km for Ttmc. We interpret this range in offsets as evidence of pre–6.4 Ma dextral-oblique slip on the eastern branch of the Bahía Kino fault, with a component of down-to-the-SW dip slip that led to erosion of Tvu and Ttsf on its NE side. Ttmc was emplaced across this fault-controlled escarpment, which was subsequently covered by deposits of Tcg. Subsequent faulting led to the 0.1 km of apparent dextral offset of Ttmc across the southwestern fault strand. Apparent right-lateral offset of Tvu and apparent left-lateral offset of Ttmc across the northeastern strand suggest a reversal of dip-slip direction, from down-to-the-SW to down-to-the-NE.

We also report 3.4 ± 0.8 km of separation of the Ttsf-Tvls contact on the central branch (circled number 2's on Fig. 3). The relatively larger error for this estimate is due to the two possible Ttsf-Tvls contact locations on the southwestern side of the central branch that correlate to the one Ttsf-Tvls contact location northeast of this branch (Fig. 3). Distinctive epiclastic strata in Tvs, present on both sides of this central Bahía Kino fault branch, reinforce this correlation. Along strike to the northwest, two ≤6.4 Ma piercing lines are observed northeast of the central branch, formed by the angular unconformities between Ttsf and Ttmc, and between Ttmc and Tcg. Two potential candidates for correlation of this pair of piercing lines appear southwest of the fault, one offset 1.5 ± 0.1 km, and the other offset 2.9 ± 0.1 km (circled number 3's on Fig. 3). This geometry suggests that two distinct fault blocks southwest of the central branch were overlain by Ttmc. We speculate that these same two fault blocks are also present to the northeast, across the central branch of the Bahía Kino fault, but the eastern of these two blocks is concealed by Quaternary sediments in the area between the eastern and central branches. If this is the case, then the larger, post–6.4 Ma offset of 2.9 km of dextral slip would be appropriate. The alternative reconstruction of 1.5 km is also plausible, but not preferred, as reconstruction of this smaller offset would restore outcrops of Ttmc and Tcg to the southwest against outcrops of Tvu to the northeast.

The magnitude of post-Ttmc (6.4 Ma) strike-slip displacement is not constrained across the western branch due to lack of preservation of this unit to the west. Total slip on the central and western branches of the Bahía Kino fault in the central portion of the study area likely equals that found on the southern part of the central branch, with some slip transferred to the western branch in a complex manner due to sinistral slip on the NE-striking Punta Blanca

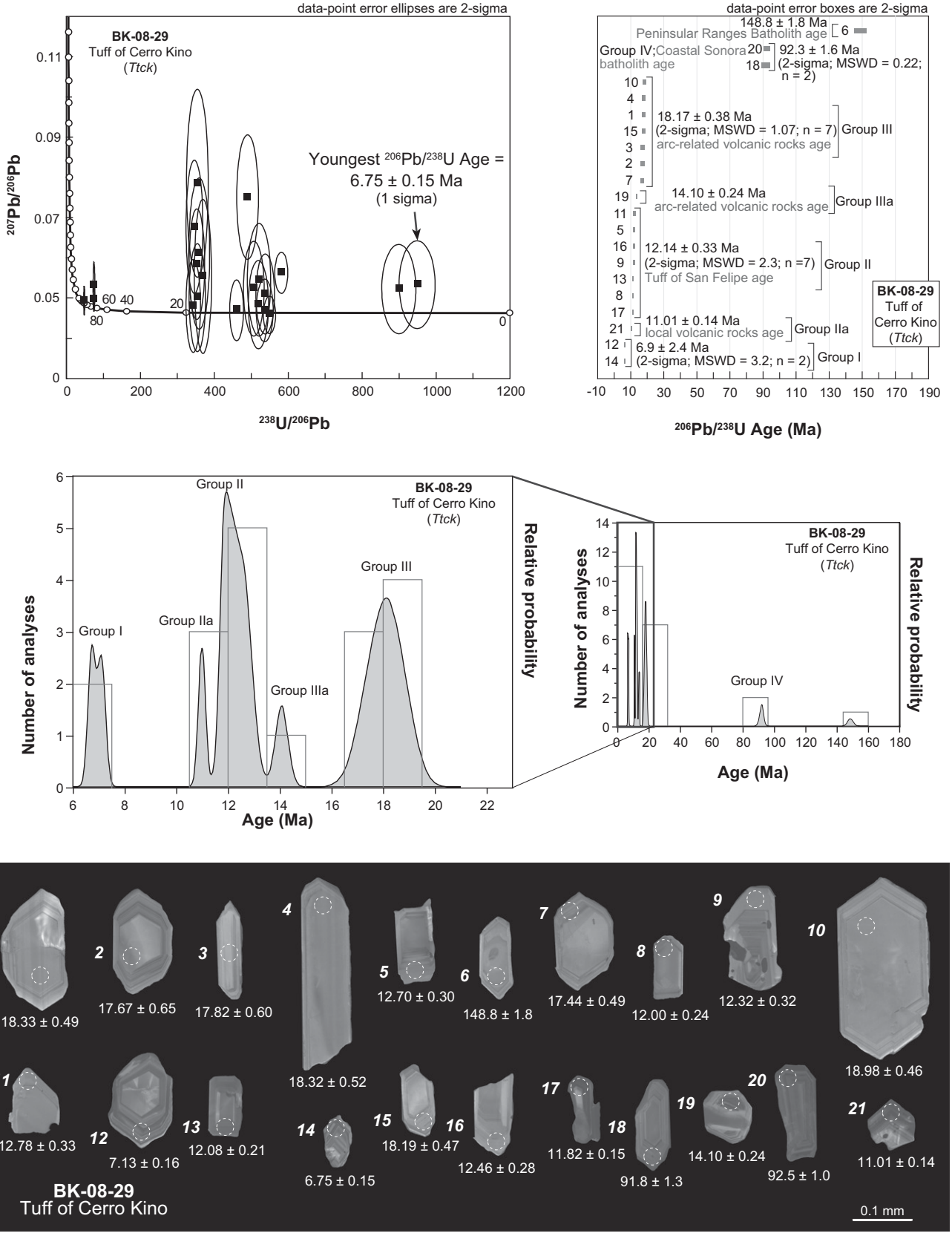

Figure 7. $^{206}Pb/^{238}U$ geochronological age calculated for the Tuff of Cerro Kino, interbedded with syntectonic sediments near the base of the Kino basin, and Tera-Wasserburg concordia diagram, age spectrum diagram, and cathodoluminescence images of analyzed zircon grains (ages in Ma). See Table 4 for data table. MSWD—mean square of weighted deviates.

TABLE 4. U-Th-Pb ANALYTICAL DATA FOR SHRIMP-RG SPOT ANALYSES ON ZIRCON GRAINS FROM TUFFS NEAR BAHIA KINO, SONORA

Spot name	Comments core/rim?	Common ^{206}Pb (%)	U (ppm)	Th (ppm)	Th/U	^{238}U/^{206}Pb*	±	Error (%)	^{207}Pb/^{206}Pb*	±	Error (%)	^{206}Pb/^{238}U†	±	Error	^{206}Pb/^{238}U† age (Ma)	±	Error (Ma)
Tuff of Cerro Tordillo (BK-08-32)																	
*BK0832-**3***	*Core*	*3.78*	*199*	*84*	*0.44*	*1058.1*	±	*3.7*	*0.0760*	±	*13.6*	*0.00091*	±	*0.00004*	*5.86*	±	*0.23*
BK0832-13	Core	1.10	149	62	0.43	1036.6	±	4.1	0.0549	±	16.9	0.00095	±	0.00004	**6.15**	**±**	**0.26**
BK0832-10	Core	4.11	79	31	0.40	1006.2	±	5.4	0.0786	±	19.7	0.00095	±	0.00005	**6.14**	**±**	**0.35**
BK0832-4	Core	2.36	210	84	0.42	1022.9	±	3.5	0.0648	±	15.8	0.00095	±	0.00004	**6.15**	**±**	**0.23**
BK0832-14	Core	2.48	86	28	0.33	990.5	±	5.3	0.0657	±	23.3	0.00098	±	0.00006	**6.34**	**±**	**0.36**
BK0832-12	Rim	2.82	161	55	0.35	981.3	±	3.8	0.0684	±	14.4	0.00099	±	0.00004	**6.38**	**±**	**0.26**
BK0832-7	Core	0.61	134	56	0.43	993.1	±	4.2	0.0509	±	19.3	0.00100	±	0.00004	**6.45**	**±**	**0.28**
BK0832-6	Core-rim	3.32	137	55	0.42	962.2	±	4.1	0.0724	±	18.2	0.00100	±	0.00004	**6.47**	**±**	**0.29**
BK0832-16	Rim	3.35	103	33	0.33	958.1	±	4.6	0.0726	±	17.8	0.00101	±	0.00005	**6.50**	**±**	**0.32**
BK0832-15	Rim	2.02	207	97	0.49	964.7	±	3.4	0.0621	±	13.1	0.00102	±	0.00004	**6.54**	**±**	**0.23**
BK0832-5	Core	0.16	145	57	0.41	961.0	±	4.3	0.0474	±	20.0	0.00104	±	0.00005	**6.69**	**±**	**0.30**
BK0832-2	Core	3.08	175	70	0.41	923.5	±	3.6	0.0705	±	16.9	0.00105	±	0.00004	**6.76**	**±**	**0.27**
BK0832-9	Core-rim	1.97	156	53	0.35	914.7	±	3.7	0.0618	±	14.9	0.00107	±	0.00004	**6.91**	**±**	**0.27**
BK0832-8	Rim	1.53	123	36	0.30	907.9	±	4.2	0.0583	±	17.0	0.00108	±	0.00005	**6.99**	**±**	**0.31**
BK0832-11	Core-rim	–0.67	113	35	0.32	898.8	±	4.3	0.0409	±	21.3	0.00112	±	0.00005	**7.22**	**±**	**0.32**
*BK0832-**1***	*Xenocrystal; core*	*0.43*	*197*	*108*	*0.57*	*65.7*	±	*2.0*	*0.0513*	±	*4.3*	*0.01516*	±	*0.00031*	*97.0*	±	*2.0*
Mount Aldo-5						(2σ; MSWD = 1.3; *n* = 14)						**Mean ^{206}Pb/^{238}U age =**			**6.53**	**±**	**0.18**
Tuff of Cerro Kino (BK-08-29)																	
BK0829-14	Rim	0.95	602	315	0.54	945.4	±	2.1	0.0537	±	8.2	0.00105	±	0.00002	**6.75**	**±**	**0.15**
BK0829-12	Rim	0.81	556	312	0.58	896.1	±	2.1	0.0526	±	8.6	0.00111	±	0.00002	**7.13**	**±**	**0.16**
BK0829-21	*Rim*	*1.31*	*1754*	*738*	*0.43*	*577.1*	±	*1.3*	*0.0566*	±	*3.6*	*0.00171*	±	*0.00002*	*11.01*	±	*0.14*
BK0829-17	*Core-rim*	*0.00*	*1841*	*652*	*0.37*	*544.8*	±	*1.3*	*0.0463*	±	*4.0*	*0.00184*	±	*0.00002*	*11.82*	±	*0.15*
BK0829-8	*Core-rim*	*0.65*	*421*	*209*	*0.51*	*533.3*	±	*2.0*	*0.0514*	±	*7.8*	*0.00186*	±	*0.00004*	*12.00*	±	*0.24*
BK0829-13	*Core-rim*	*0.13*	*556*	*228*	*0.42*	*532.3*	±	*1.7*	*0.0473*	±	*6.7*	*0.00188*	±	*0.00003*	*12.08*	±	*0.21*
BK0829-9	*Rim*	*1.09*	*221*	*76*	*0.36*	*516.9*	±	*2.5*	*0.0549*	±	*10.3*	*0.00191*	±	*0.00005*	*12.32*	±	*0.32*
BK0829-16	*Rim*	*0.32*	*298*	*118*	*0.41*	*515.0*	±	*2.2*	*0.0488*	±	*9.2*	*0.00194*	±	*0.00004*	*12.46*	±	*0.28*
BK0829-5	*Rim*	*0.82*	*276*	*111*	*0.42*	*502.8*	±	*2.3*	*0.0527*	±	*9.0*	*0.00197*	±	*0.00005*	*12.70*	±	*0.30*
BK0829-11	*Rim*	*3.67*	*201*	*76*	*0.39*	*485.6*	±	*2.5*	*0.0753*	±	*8.3*	*0.00198*	±	*0.00005*	*12.78*	±	*0.33*
BK0829-19	*Core*	*0.14*	*544*	*376*	*0.71*	*456.2*	±	*1.7*	*0.0474*	±	*6.5*	*0.00219*	±	*0.00004*	*14.10*	±	*0.24*
BK0829-7	*Rim*	*1.19*	*147*	*34*	*0.24*	*364.8*	±	*2.6*	*0.0558*	±	*14.0*	*0.00271*	±	*0.00008*	*17.44*	±	*0.49*
BK0829-2	*Core*	*4.10*	*72*	*24*	*0.34*	*349.3*	±	*3.5*	*0.0788*	±	*12.0*	*0.00275*	±	*0.00010*	*17.67*	±	*0.65*
BK0829-3	*Core*	*1.90*	*85*	*34*	*0.42*	*354.3*	±	*3.2*	*0.0614*	±	*12.4*	*0.00277*	±	*0.00009*	*17.82*	±	*0.60*
BK0829-15	*Rim*	*1.57*	*153*	*26*	*0.17*	*348.4*	±	*2.5*	*0.0588*	±	*9.5*	*0.00283*	±	*0.00007*	*18.19*	±	*0.47*
BK0829-1	*Core*	*0.52*	*139*	*17*	*0.13*	*349.3*	±	*2.6*	*0.0505*	±	*10.8*	*0.00285*	±	*0.00008*	*18.33*	±	*0.49*
BK0829-4	*Core*	*2.73*	*130*	*12*	*0.09*	*341.7*	±	*2.7*	*0.0680*	±	*9.9*	*0.00285*	±	*0.00008*	*18.32*	±	*0.52*
BK0829-10	*Core*	*0.25*	*166*	*26*	*0.16*	*338.2*	±	*2.4*	*0.0484*	±	*9.7*	*0.00295*	±	*0.00007*	*18.98*	±	*0.46*
BK0829-18	*Rim*	*0.72*	*170*	*48*	*0.29*	*69.3*	±	*1.4*	*0.0536*	±	*4.3*	*0.01434*	±	*0.00021*	*91.8*	±	*1.3*
BK0829-20	*Core-rim*	*0.27*	*571*	*118*	*0.21*	*69.0*	±	*1.1*	*0.0500*	±	*2.3*	*0.01446*	±	*0.00016*	*92.5*	±	*1.0*
BK0829-6	*Core*	*0.09*	*237*	*146*	*0.63*	*42.8*	±	*1.2*	*0.0497*	±	*2.9*	*0.02335*	±	*0.00029*	*148.8*	±	*1.8*
Mount Aldo-5						(2σ; MSWD = 3.2; *n* = 2)						**Mean ^{206}Pb/^{238}U age =**			**6.90**	**±**	**2.40**

Note: Analyses in italics were not used to calculate the weighted average ^{206}Pb/^{238}U age and its mean square of weighted deviates (MSWD). All errors given are at the 1σ level except for the weighted average ^{206}Pb/^{238}U age, which is reported at 2σ.

*Uncorrected atomic ratios.

†Atomic ratios and ages corrected for initial Pb using the amount of ^{207}Pb.

fault. Map-view outcrop patterns suggest that the Punta Blanca fault has ~1.5 km of sinistral separation of the base of the Tuff of San Felipe. No direct observation of separation was made for the Puerto Rico fault due to poor exposure and lack of matching units across this structure.

Clockwise vertical-axis block rotations contribute additional dextral deformation to the Coastal Sonora fault zone. Paleomagnetic analysis of the Tuff of San Felipe identified 35.5° ± 3.3° of clockwise vertical-axis rotation immediately west of the Bahía Kino fault (site BK of Oskin et al., 2001). Block rotation of this magnitude of this ~5-km-long strike ridge contributes an additional 1.0 ± 0.1 km of dextral deformation. If calculated clockwise vertical-axis block rotations are removed from the modern-day mean orientation of strike ridges (Fig. 13), we estimate that most incipient tilt blocks restore to NNW-striking ridges. Similar magnitudes of block rotation likely also occurred between the Bahía Kino fault and Sacrificio fault, also contributing another 1.0 ± 0.1 km to the budget of distributed deformation. Thus, including the strike-slip displacements described earlier herein, we resolve a total of 6.2 ± 1.1 km of dextral shear internal to the Coastal Sonora fault zone.

An estimate for total dextral shear across the entire Coastal Sonora fault zone largely depends on the combined dextral displacement along the Sacrificio and Infiernillo faults, the primary, bounding structures of the fault zone. Offset across the Infiernillo fault is estimated to be 20 ± 10 km from matching exposures of the Tuff of San Felipe to exposures on northeastern Isla Tiburón (Fig. 1; Oskin and Stock, 2003a). Slip on the Sacrificio fault is not well constrained due to the lack of correlative rocks and unknown, though probably minor, dip-slip motion; Miocene volcanic cover strata are exposed on both sides of the fault (Gastil and Krummenacher, 1977a). A minimum estimate of dextral displacement for the Sacrificio fault may be 15 km, the length of the fault through the Sierra Seri, across which no rocks match. A coarse upper estimate of total dextral slip across the entire Coastal Sonora fault zone can be made from exposures of a pre–15 Ma conglomerate that bears unique fusulinid-rich limestone clasts (F on Fig. 1), which outcrop east of the Sacrificio fault in coastal Sonora and at the base of the Santa Rosa basin of northeastern Baja California (Gastil et al., 1973). After restoration of the post–6.1 Ma opening of the Gulf of California (Oskin et al., 2001; Oskin and Stock, 2003a), and assuming sediment transport from NE to SW, these conglomerate exposures loosely constrain total dextral slip on the Coastal Sonora fault zone to 60 ± 30 km.

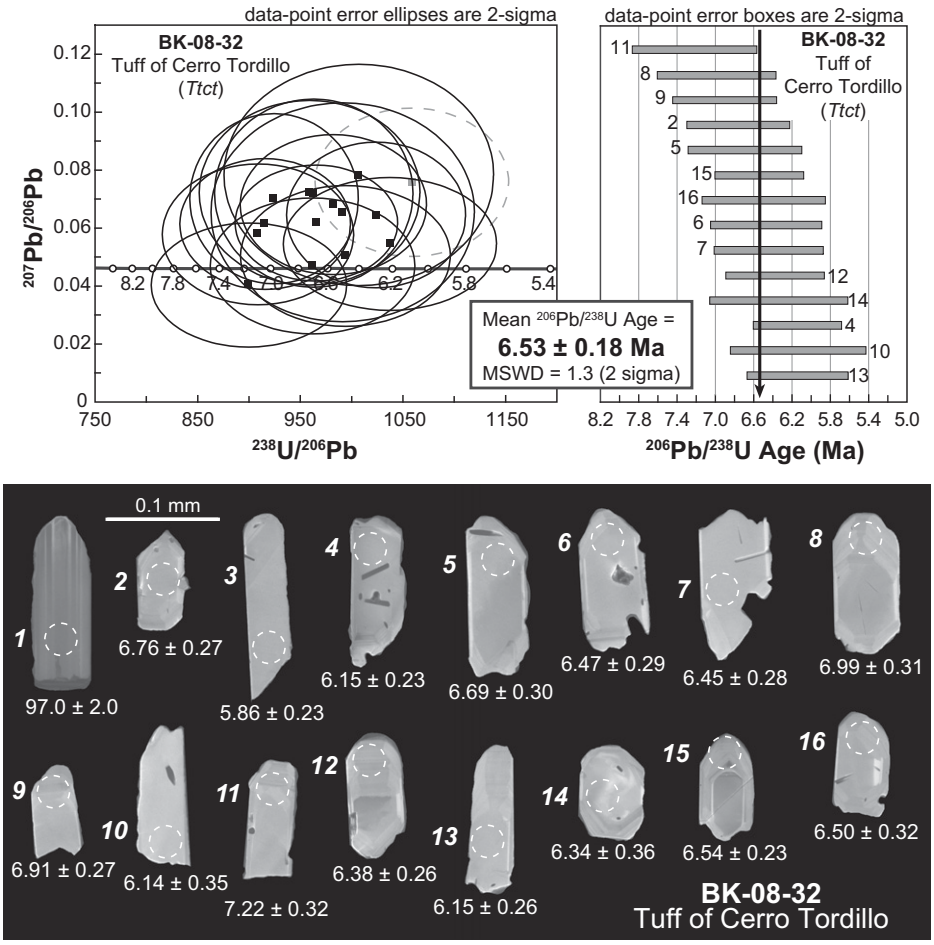

Figure 8. $^{206}Pb/^{238}U$ geochronological age calculated for the Tuff of Cerro Tordillo (Ttct), interbedded with syntectonic sediments near the base of the Punta Chueca basin, and Tera-Wasserburg concordia diagram, age spectrum diagram, and cathodoluminescence images of analyzed zircon grains (ages in Ma). See Table 4 for data table. MSWD—mean square of weighted deviates.

Coastal Sonora Fault Zone Deformation History

We describe the deformation history for the Coastal Sonora fault zone in two time periods, pre–7 Ma and post–7 Ma, because the existence of syntectonic rock units (basin conglomerate and interbedded tuffs) allows us to better define deformation rates after 7 Ma. Syntectonically emplaced sediments and volcanic rocks are sparse prior to 7 Ma, limiting our ability to place constraints on the rate at which deformation occurred. Clockwise vertical-axis rotation and strike-slip faulting may have also commenced prior to 7 Ma. After 7 Ma, coarse basin sediments and intercalated volcanic rocks accumulated above an extensive angular unconformity cut across older units. We argue that this later deformation period, which probably ended by 5–6 Ma, was characterized by rapid tilting, rapid basin sedimentation, the majority of vertical-axis clockwise rotations, and the majority of dextral fault offsets within the core of the Coastal Sonora fault zone.

Pre–7 Ma Deformation

The early period of deformation within the Coastal Sonora fault zone tilted rocks 25°–40° down to the ENE, the dip discordance between prerift rocks and the oldest exposed synrift rocks. The onset of this early deformation is not well constrained but must postdate the youngest volcanic rocks beneath the Punta Chueca and Kino basins: the 11.47 ± 0.05 Ma Basalt of Punta Chueca and the 12.50 ± 0.08 Ma Tuff of San Felipe. During this early period, accumulation of basin conglomerate (Tcg) either did not occur, due to sediment bypass, or was minimal and is now hidden at deeper structural levels. In the Punta Chueca basin, stratal dips decrease from 71°–75° in these volcanic units to 50° in the 6.53 ± 0.18 Ma Tuff of Cerro Tordillo, observed 80 m above the base of the thickest exposed section of Tcg. This indicates that the initial ~25° of tilting, ~33% of the total observed, occurred prior to 6.53 ± 0.18 Ma. In the Kino basin, the initial ~40° of tilting, ~50% of the total observed, postdates the undated southern local volcanic rocks and occurred prior to the emplacement of the 7.05 ± 0.03 Ma Tuff of Cerro Kino.

Dextral shear likely also initiated during this early period of deformation. Subtle clockwise vertical-axis rotation is suggested by discordance of Ttsf and Ttmc strike ridges near the base of the Punta Chueca basin, where these units are separated by a wedge of Tcg up to 225 m thick (Fig. 3). Based on our paleomagnetic results at the PC paleomagnetic site, Ttmc (this study; Fig. 9) and Ttsf (Oskin et al., 2001) display clockwise vertical-axis rotations of 46.1° ± 11.7° and 52.8° ± 2.1°, respectively (Fig. 14), indicating that 6.7° ± 11.9° (0%–35%) of the total post–12.5 Ma rotation occurred prior to 6.4 Ma. The majority (~90%) of ~1 km of strike slip along the eastern branch of the Bahía Kino fault may also have occurred coincident with this minor vertical-axis rotation of the Punta Chueca basin, as evidenced by erosion of Ttsf and Tvu along the northeast side of the fault, onlapped by Ttmc, as well as by the smaller magnitude of apparent dextral offset of Ttmc compared to older units.

Altogether, by ca. 7 Ma, the study area within the core of the Coastal Sonora fault zone consisted of fault blocks of early to middle Miocene volcanic rocks, which had been tilted 25°–40° down-to-the-ENE (33%–50% of the total tilting) along normal faults, rotated clockwise about a vertical-axis 0°–20° (0%–35% of the total rotation), and cut by minor strike-slip faulting (~1 km), all coincident with minor accumulation of basin conglomerate deposits in the incipient Punta Chueca and Kino half-graben basins. The NW-striking Sacrificio and Infiernillo strike-slip faults and the NNW-striking, WSW-dipping Aeropuerto and Punta Chueca normal faults were likely active and bounded the observed region of tilting and minor clockwise vertical-axis block rotation. However, the magnitude of pre–7 Ma dextral displacement on these first-order, bounding strike-slip faults is unknown. A similar style of modest ENE-WSW extension and minor dextral deformation occurred between 10.4 Ma and 6.4 Ma in the Sierra Bacha coastal mountains, located ~60 km to the NNW (Darin, 2011). Without more detailed knowledge for the onset of deforma-

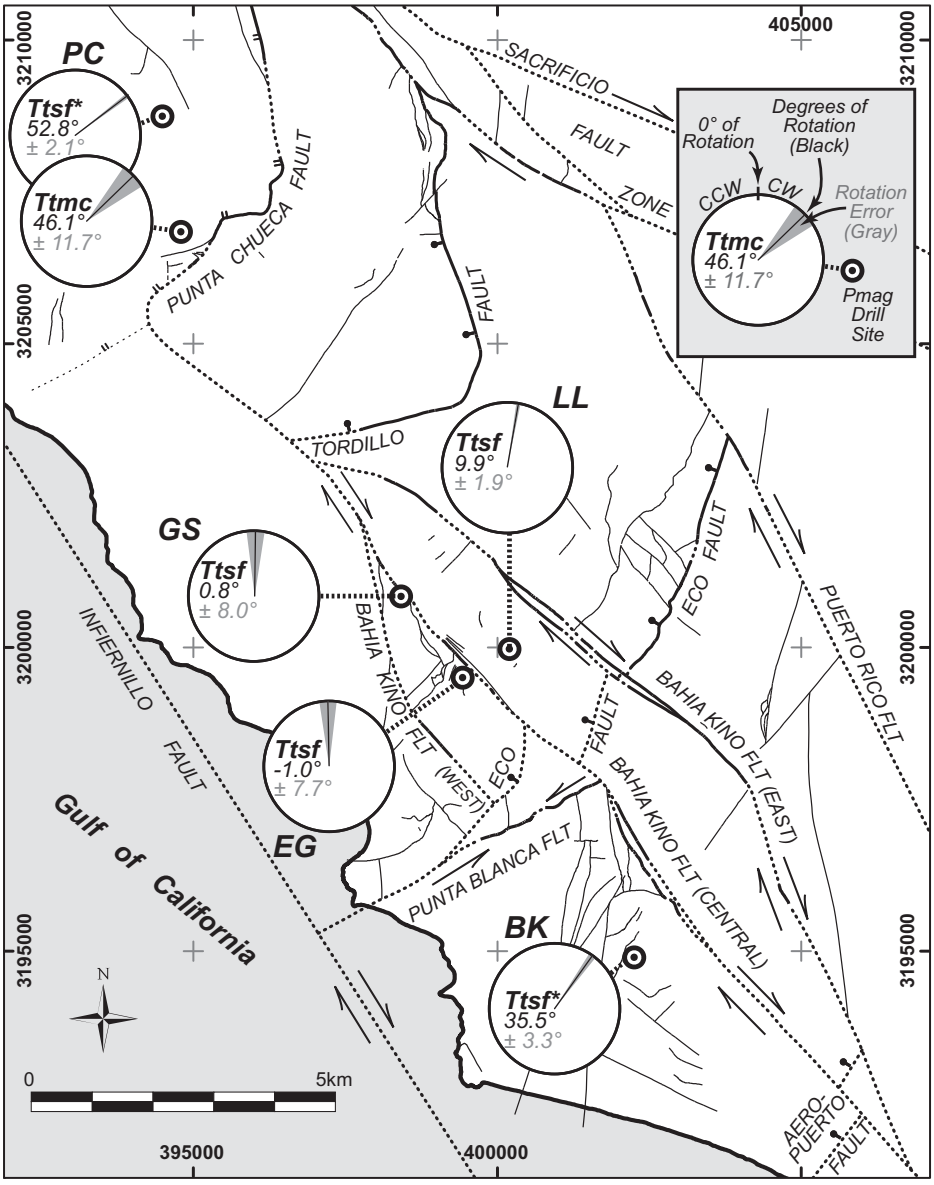

Figure 9. Simplified fault map (as Fig. 6), showing paleomagnetic drill site locations from this study and from Oskin et al. (2001) for the Tuff of San Felipe (Ttsf) and the Tuffs of Mesa Cuadrada (Ttmc). The two sites by Oskin et al. (2001) are indicated with an asterisk. Plots for each site show the calculated rotation value (black line) and error value (gray pie slice), plotted arbitrarily relative to north. See Figure 3 for detailed geology. Paleomagnetic drill sites are shown as bull's-eyes. Paleomagnetic sites: PC—Punta Chueca, LL—La Luna, GS—Guadalupe Shrine, EG—East Guadalupe, BK—Bahía Kino. CCW—counterclockwise; CW—clockwise.

tion in the Coastal Sonora fault zone, tilting and sedimentation rates prior to ca. 7.0 Ma remain poorly constrained.

Post–7 Ma Deformation

By 7 Ma, tilting, clockwise vertical-axis rotation of several fault-bounded blocks, and dextral slip along the Bahía Kino fault system had commenced. Isotopically dated tuffs interbedded within the basin conglomerate indicate rapid rates of post–7 Ma tilting and sedimentation in the Punta Chueca basin. The 6.53 ± 0.18 Ma Tuff of Cerro Tordillo, inclined 50°, and the 6.39 ± 0.02 Ma Tuff of Mesa Cuadrada, inclined 34°, bracket a section of sediment 170 m thick (Dorsey et al., 2008). These constraints yield a very high rate of tilting (at least 47°/m.y.) and also a rapid sedimentation rate of 1.2 ± 0.2 mm/yr. These high rates likely continued during deposition of the remaining ≥225 m basin conglomerate, with dips that shallow up section from 34° to ~5° adjacent to the Punta Chueca fault. We infer a similar history for the Kino basin, where the basin conglomerate contains the 7.05 ± 0.03 Ma Tuff of Cerro Kino and the 6.39 ± 0.02 Ma Tuffs of Mesa Cuadrada near its base. Unfortunately, these interbedded tuffs are not exposed in the same fault block or stratigraphic section, preventing the determination of tilting and sedimentation rates for the Kino basin. However, throughout the study area, the basin conglomerate transgressed across an angular unconformity cut across middle Miocene volcanic rocks (Figs. 3 and 11), consistent with either a widespread increase in sedimentation rate, or the development of closed sedimentary basin conditions. We note that proximal to the basin-bounding Punta Chueca normal fault, basin conglomerate clast size increases from cross-bedded sandstone and cobble conglomerate to cobble to boulder conglomerate. Such coarse, fault scarp–derived detritus is consistent with formation of steep footwall topography during the period of rapid tilting we document here. The rapid sedimentation rate for the Punta Chueca basin falls within the range of rates from a global catalogue of strike-slip basins (Xie and Heller, 2009) and is also similar to subsidence rates observed in basins related to oblique rifting in the Salton Trough (Dorsey et al., 2011).

Based on paleomagnetism and strike-slip offset of the 6.4 Ma Tuffs of Mesa Cuadrada, we interpret that the majority of dextral shear observed internal to the Coastal Sonora fault zone occurred after 7 Ma. Paleomagnetic results from the Punta Chueca basin (detailed herein) indicate that 65%–100% of clockwise vertical-axis rotation of the hanging wall of the Punta Chueca fault occurred after 6.4 Ma (Fig. 14). Paleomagnetic results from the Kino basin exist from Ttsf in four fault blocks adjacent to the central Bahía Kino fault. Two larger and more coherent structural blocks are rotated clockwise 10° and 36° (Fig. 9). Two smaller and structurally complex fault blocks immediately southwest of the central Bahía Kino fault show no net rotation. Differential block rotation is not constrained for any of these sites because Ttmc is not exposed, or it did not yield stable paleomagnetic remanence directions. Thus, these rotations are constrained only to postdate deposition of the 12.5 Ma Tuff of San Felipe. Based on offset of ≤6.4 Ma piercing lines across the central branch of the Bahía Kino fault, we interpret that the majority of its 3.4 ± 0.8 km of dextral slip postdates 6.4 Ma. Further evidence for this timing is that post–7 Ma conglomerates are folded in the Kino syncline and truncated

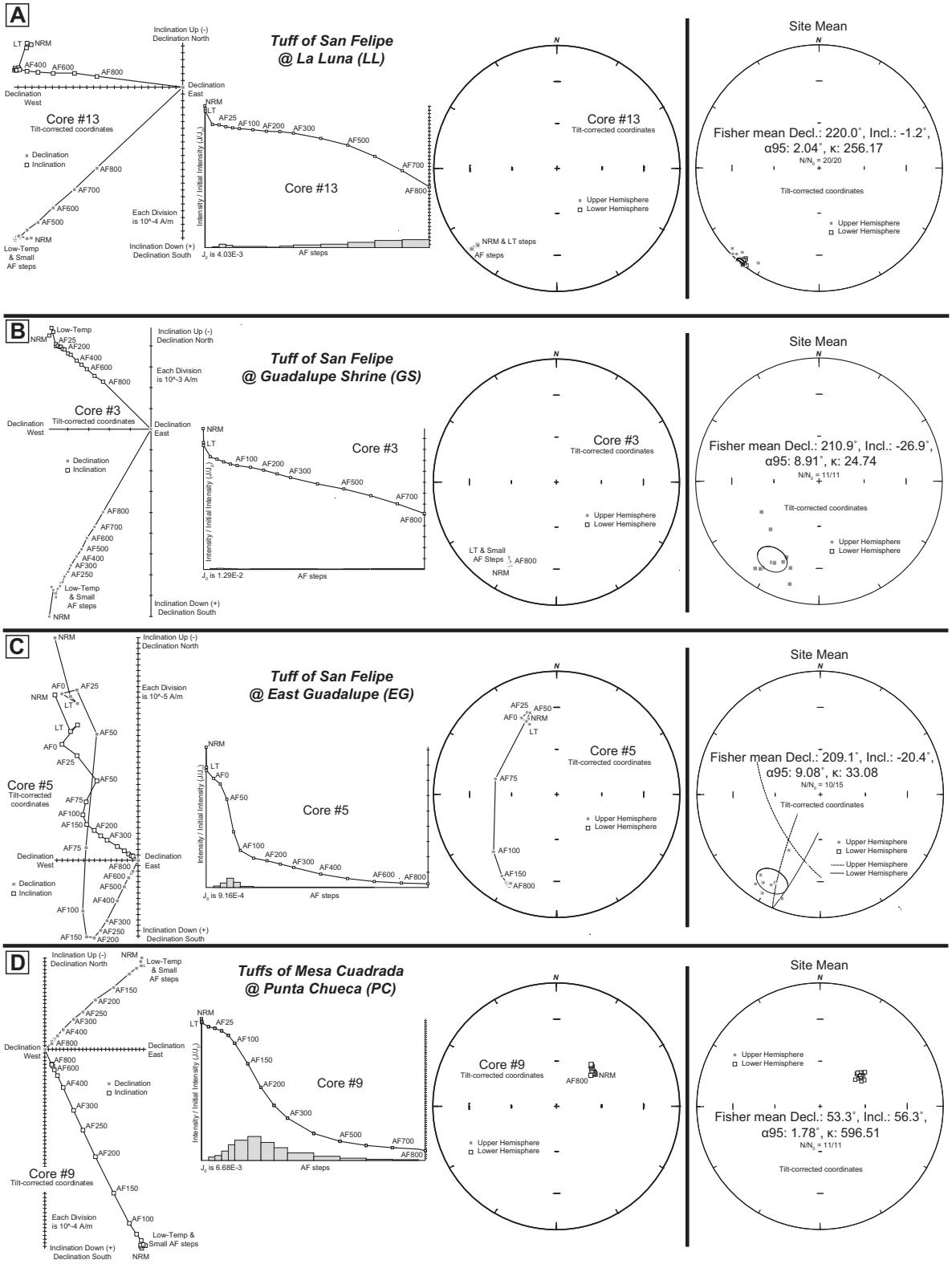

Figure 10. Paleomagnetic results from the four coastal Sonora paleomagnetic drill sites collected in this study from the 12.5 Ma Tuff of San Felipe (A–C) and the 6.4 Ma Tuffs of Mesa Cuadrada (D). For each site, vector-component Zijderveld diagram (left) and equal area stereonet (left-center) display vector orientations for all natural remanent magnetization (NRM), low-temperature (LT), and alternating field (AF) partial demagnetization steps conducted. Partial demagnetization steps are shown for only one example core at each paleomagnetic site. *J*/*J*0 plot is shown for same example core (right-center). Site mean (right) was calculated using *N* of the *N*0 cores collected. α95 confidence ellipse is shown. All analyses were conducted with PaleoMag v3.1b1 (Jones, 2002). See Table 5 for data table.

TABLE 5. PALEOMAGNETIC MEASUREMENTS AND RELATIVE DECLINATION AND INCLINATION ANOMALIES FOR THE TUFFS OF MESA CUADRADA AND TUFF OF SAN FELIPE DRILL SITES IN COASTAL SONORA, MEXICO

Drill site/unit*	Latitude (°N)	Longitude (°W)	Bedding†		N/N_0	Corr. factor	Geographic		Tilt corrected		Fisher statistics		Bingham statistics				R§ (°)	ΔR# (°)	F** (°)	ΔF# (°)
			Strike (°)	Dip (°)			Dec (°)	Inc (°)	Dec (°)	Inc (°)	α95 (°)	κ	κ1	α95 (°)	κ2	α95 (°)				
PC—Punta Chueca																				
Ttmc	28.98549	112.07985	342	37	11/11	0.79	332	71.9	53.3	56.3	1.78	596.5	–449	1.41	–302.2	1.72	46.1	11.7	–2.4	6.8
EG—East Guadalupe																				
Ttsf	28.91927	112.03152	340	76	10/15	0.79	157	–38.9	209	–20.4	9.08	33.08	–11.10	10.93	–3.85	20.06	–1.0	7.7	17.4	7.3
LL—La Luna																				
Ttsf	28.92361	112.02373	354	65	20/20	0.79	198	–40.4	220	–1.2	2.04	256.2	–227.1	1.48	–97.19	2.26	9.9	1.9	–1.8	1.9
GS—Guadalupe Shrine																				
Ttsf	28.93141	112.04202	355	72	11/11	0.79	157	–37.4	211	–26.9	8.91	24.74	–34.09	5.33	–11.17	9.5	0.8	8.0	23.9	7.1

Note: N/N_0—number of samples used to determine site mean vector/number of samples collected. Correction factor for various values of *N* (Demarest, 1983). Dec.—declination in degrees; Inc.—inclination in degrees; α95—cone of 95% confidence about mean direction; κ—the precision parameter (Fisher, 1953). Values for declination have been corrected to geographic north using an 11° magnetic declination for the study area.

*Ttmc—Tuffs of Mesa Cuadrada; Ttsf—Tuff of San Felipe.

†Structural orientation of unit used for structural correction.

§R—Rotation in degrees. Ttsf relative to Ttsf reference site of Bennett and Oskin (2008). Ttmc relative to Tmr3b reference site at Mesa Cuadrada in Baja California (Lewis and Stock, 1998). For Sonora sites, 2.3° has been added to R to account for finite rotation of reference locality due to Pacific–North America plate displacement.

#ΔR—95% confidence limits on rotation; ΔF—95% confidence limits on flattening, both calculated according to Beck (1980) and Demarest (1983).

**F—Flattening in degrees. Ttsf relative to Ttsf reference site of Bennett and Oskin (2008). Ttmc relative to Tmr3b reference site at Mesa Cuadrada in Baja California (Lewis and Stock, 1998).

by the main, central branch of the Bahía Kino fault (Fig. 3).

The timing for the cessation of transtensional deformation is poorly constrained, as no capping rock units overlie basin conglomerate deposits and major transtensional structures. Normal faulting, a component of this transtension, likely terminated near the end of conglomerate deposition. If the high deposition and tilting rates that are observed following the emplacement of the 6.53 ± 0.18 Ma Tuff of Cerro Tordillo continued throughout deposition of the remaining basin conglomerate, a maximum age for the youngest basin deposits can be estimated from their thickness (≥225 m) above the Tuffs of Mesa Cuadrada in the Punta Chueca basin. Using the 1.2 ± 0.2 mm/yr deposition rate, normal faulting on the Punta Chueca fault and associated deposition of basin conglomerate in the Punta Chueca basin may have ceased ca. 6.2 ± 0.1 Ma (Dorsey et al., 2008). This estimate is a maximum because the sedimentation rate may have decreased, and the top of Tcg may have been removed by erosion. However, because the youngest basin deposits adjacent to the Punta Chueca fault are subhorizontal (dipping 4°–5°; Fig. 3), very little of these deposits may be missing. Regionally, strike-slip motion across the Coastal Sonora fault zone is likely to have diminished when rifting localized into the Upper Tiburón basin, west of Isla Tiburón (Fig. 1). Opening of this pull-apart basin would have shunted deformation away from the Coastal Sonora fault zone by forming a new link between the De Mar fault, located along strike northwest of the Coastal Sonora fault zone, and the La Cruz fault and Tiburón fracture zone, located southwest of Isla Tiburón. Oskin and Stock (2003a) estimated that the latest this could have occurred was 5.5 ± 0.4 Ma.

Transtensional Models for the Coastal Sonora Fault Zone

Altogether, the results from geologic mapping, geochronology, and paleomagnetism suggest that transtensional deformation within the Coastal Sonora fault zone initiated sometime between 11.5 Ma and 7 Ma and waned by 5–6 Ma. Such a tectonic history improves earlier estimates for coastal Sonora, where NW-striking dextral faulting was previously thought to be complete by 8 Ma (Gastil and Krummenacher, 1977b). Because the timing of the onset of deformation is poorly constrained to between 11.5 and 7 Ma, we present two models for the deformation history of the Coastal Sonora fault zone:

Model 1: Deformation within the Coastal Sonora fault zone started shortly after 11.5 Ma at a slow rate, followed by accelerated deforma-

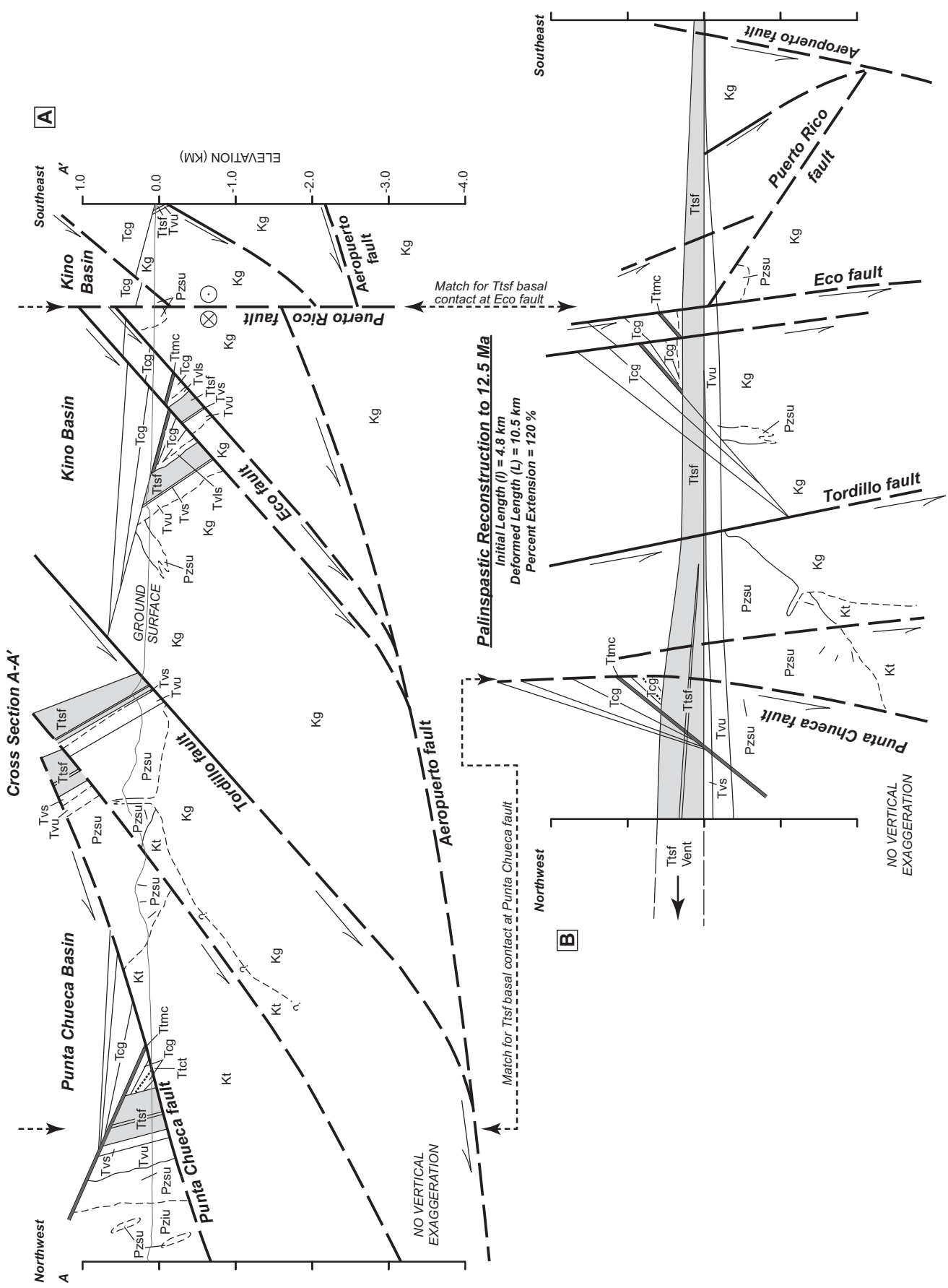

Figure 11 (*on this and following page*). (A) Cross-section A-A′ is drawn across multiple normal faults of the northern part of the study area. Tuff of San Felipe (Ttsf) is shaded light gray. Tuff of Cerro Tordillo (Ttct) and Tuffs of Mesa Cuadrada (Ttmc) are shaded dark gray. (B) Palinspastic reconstruction of cross-section A-A′ restoring the base of the 12.5 Ma Tuff of San Felipe.

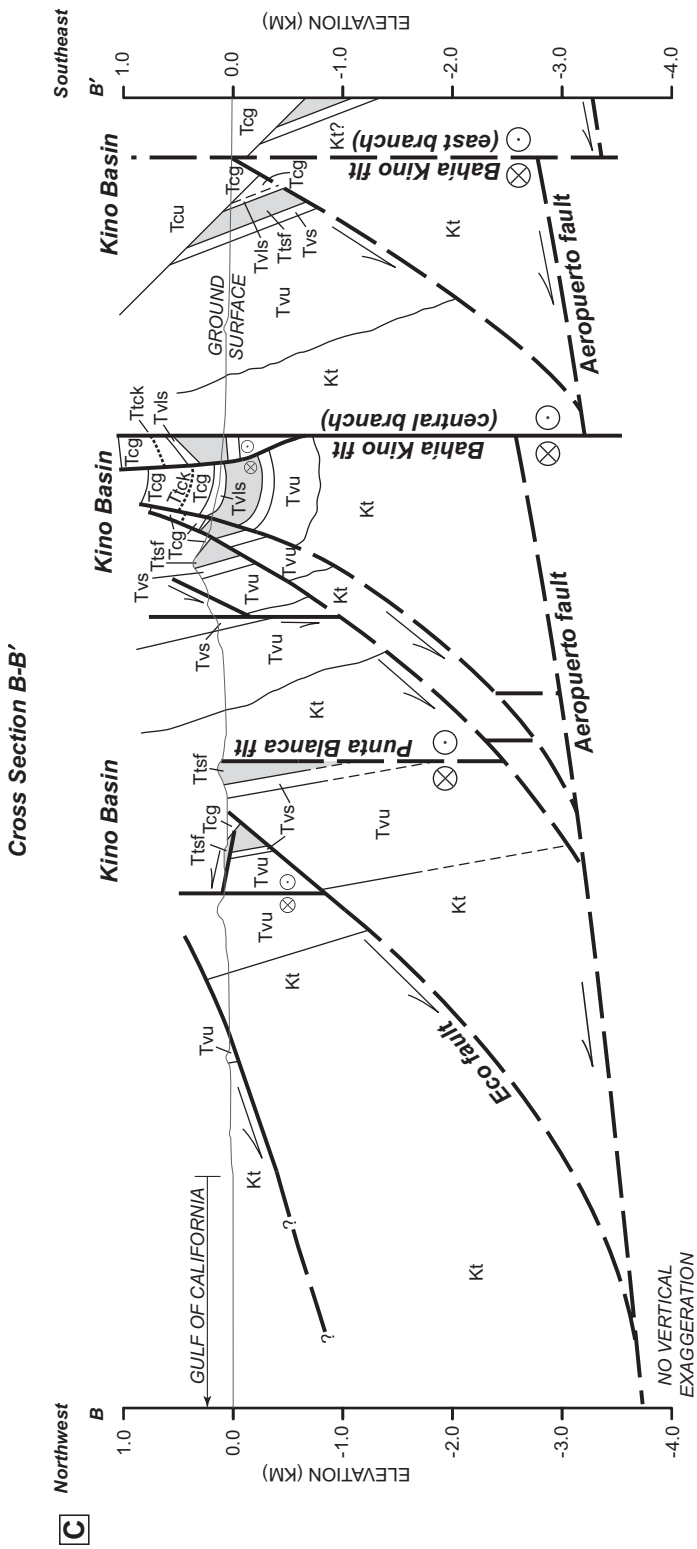

Figure 11 (*continued*). (C) Cross-section B-B′ is drawn across multiple normal and strike-slip faults of the southern part of the study area. See Figure 3 for cross section locations. See text for unit descriptions.

tion and basin deposition after 7 Ma, ending by 5–6 Ma.

Model 2: Deformation within the Coastal Sonora fault zone initiated ca. 8 Ma at a rapid rate, and remained rapid throughout its life span, ending by 5–6 Ma.

Specifically, these models only refer to the deformation history within the core Coastal Sonora fault zone, where timing constraints exist. We cannot directly constrain the timing of slip on the Sacrificio and Infiernillo faults, which accommodated at least 80% of the dextral shear across the Coastal Sonora fault zone. Our preferred interpretation is that these faults, which are kinematically linked across the study area, share a similar history of slip encapsulated by these models. However, it is also possible that the Sacrificio and Infiernillo faults could have accumulated most of their slip prior to the rapid, post–7 Ma deformation documented within the core of the Coastal Sonora fault zone. Further constraints on the slip history of these bounding faults are required to understand their role in the evolving plate boundary.

In either model 1 or model 2, rapid transtensional deformation began by 7–8 Ma and ended by 5–6 Ma, coincident with the critical time window when the Pacific–North America plate boundary localized in the Gulf of California. A zone of rotating normal-fault–bounded tilt blocks became well developed within the Coastal Sonora fault zone and subsequently was partially dissected by branches of the Bahía Kino fault system. Together, clockwise vertical-axis block rotation and dextral faulting accommodated 6.2 ± 1.1 km of dextral displacement across the ~13-km-wide core of the Coastal Sonora fault zone. The majority of this deformation occurred over a span of ~1.5 m.y., between ca. 7 Ma and 5.5 ± 0.4 Ma, yielding an average internal slip rate of 2–4 mm/yr and a strain rate that approaches $10^{-14}\,s^{-1}$. If we assume that much of the dextral slip on the Infiernillo and Sacrificio faults also primarily occurred during this same period, it is conceivable that the Coastal Sonora fault zone, with several tens of kilometers of dextral slip, may have briefly acted as a principal structure of the Pacific–North America plate boundary system in latest Miocene time.

Honoring the available timing and kinematic constraints, we present a schematic tectonic block model that illustrates the development of the Coastal Sonora fault zone (Fig. 15). Initiation of transtension occurred sometime between 11.5 Ma and 7 Ma, associated with either slow (model 1) or fast (model 2) block tilting of 25°–40°, and the onset of clockwise vertical-axis block rotation and strike-slip faulting (Fig. 15A). After 7 Ma, transtensional deformation included a greater component of dextral shear,

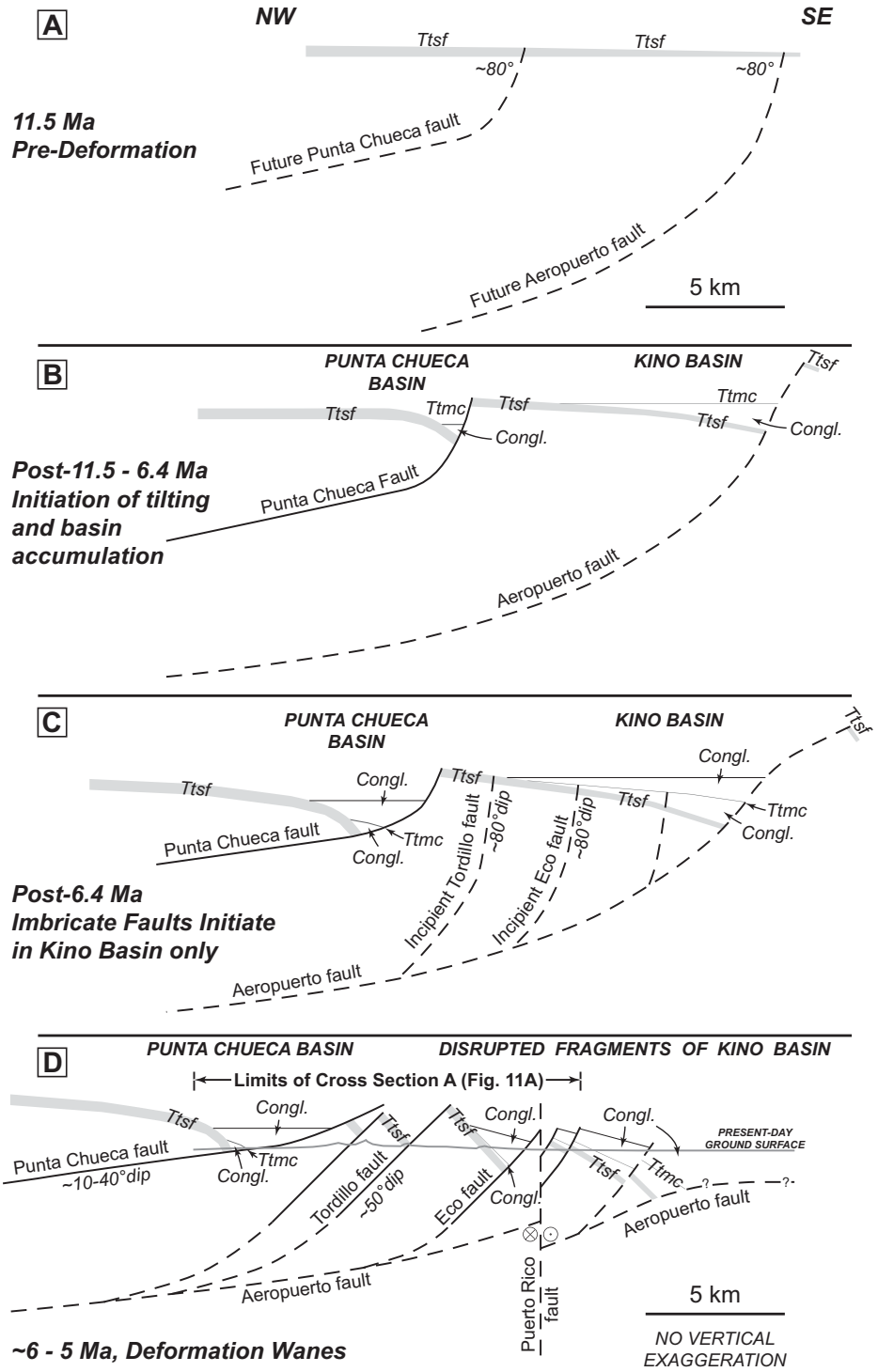

Figure 12. Schematic incremental restoration of extensional fault systems along cross section A-A′ and beyond the study area (see Fig. 3 for location). (A) By 11.5 Ma, coastal Sonora was blanketed by the Tuff of San Felipe and younger, local, discontinuous volcanic rocks (light gray). (B) After 11.5 Ma, moderate tilting (25°–40°) of all volcanic strata occurred due to slip on the Punta Chueca and Aeropuerto normal faults. Punta Chueca and Kino sedimentary basins accumulated nonmarine basin conglomerate deposits and the 6.4 Ma Tuffs of Mesa Cuadrada (dark gray) in the hanging wall of half grabens. (C) After 7 Ma, rapid transtensional deformation occurred. The footwall of the Punta Chueca fault was dissected by the high-angle imbricate Eco and Tordillo normal faults. Rapid accumulation of nonmarine basin conglomerate deposits occurred in both basins above an extensive angular unconformity. (D) Further slip on the low-angle Punta Chueca fault, moderate slip on the high-angle Tordillo and Eco faults, and late-stage strike-slip faulting characterize the final period of transtensional deformation along this profile. See text for unit descriptions.

expressed as strike-slip faulting that crosscut the Kino basin and the majority of clockwise vertical-axis block rotation of the Punta Chueca basin (Fig. 15B). Here, while similar amounts of tilting (20°–40°) occurred post–6.4 Ma as did prior, at least two times more block rotation occurred after 6.4 Ma. The post–7 Ma period is also marked by rapid sedimentation rates, resulting in progradation of basin conglomerate across an extensive angular unconformity. In the central and southern parts of the study area, a younger generation of normal faults initiated, breaking up the fault block that served as the hanging wall of the Aeropuerto fault and the footwall of the Punta Chueca fault. By 5–6 Ma, we interpret that transtensional deformation in the Coastal Sonora fault zone was complete (Fig. 15C).

Tradeoffs in deformation style between the northern (Punta Chueca basin) and southern (Kino basin) parts of the study area demonstrate that normal faulting, strike-slip faulting, and vertical-axis block rotation were intimately linked as transtensional strain accumulated across the Coastal Sonora fault zone. In the southern part of the study area, distributed deformation had tilted (up to 80°) and rotated several fault blocks clockwise (up to 36°) while sediments accumulated in the subsiding Kino basin. NW-striking branches of the dextral Bahía Kino fault were active concurrently with normal faulting, and eventually cut these normal faults and the related Kino basin. This contrasts with the Punta Chueca basin, which appears to have remained a structurally coherent hanging-wall block above the Punta Chueca low-angle normal fault. Compared to the southern part of the study area, this block accommodated larger clockwise vertical-axis rotation (53° vs. 36°), and the Punta Chueca fault displays greater amounts of total extension (~4 km vs. ~2 km) than other mapped normal faults (note that the Aeropuerto fault is an inferred structure buried southeast of our study area, and thus extension across it is not known). Dextral slip on the Bahía Kino fault of 4.2 ± 0.9 km appears to have been transferred northeastward to the Sacrificio fault via a similar amount of extension across the Punta Chueca normal fault, likely driving the

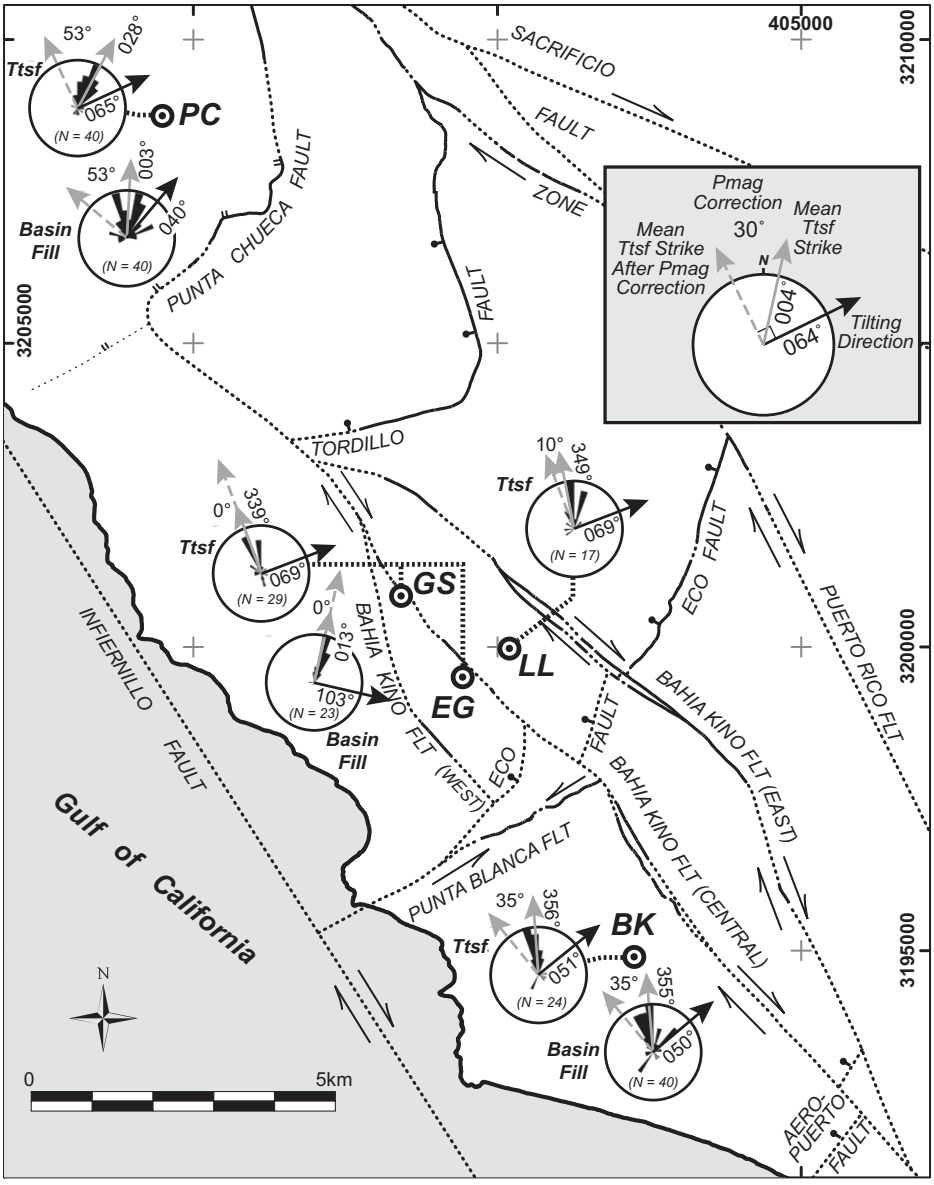

Figure 13. Simplified fault map (as Fig. 6), showing rose diagrams of modern-day structural strike for the Tuff of San Felipe (Ttsf) and basin fill (gray arrows) grouped by fault block (azimuth ~339°–028°). These mean structural strikes were corrected for variable amounts of clockwise vertical-axis block rotations where determined from paleomagnetism (dashed gray arrows). Restoration of these blocks suggests that a consistent set of NNW-striking ridges of Ttsf (azimuth ~310°–340°), initially formed as fault blocks, were tilted down to the ENE (azimuth ~050°–070°; black arrows). Tilt directions for basin fill are similar to that of Ttsf. One exception is observed in the fault block with the GS and EG drill sites, where this part of the Kino basin may have been tilted down to the ESE direction (azimuth ~100°). Paleomagnetic drill sites (Ttsf only) are shown as bull's-eyes, as in Figure 9. Paleomagnetic sites: PC—Punta Chueca, LL—La Luna, GS—Guadalupe Shrine, EG—East Guadalupe, BK—Bahía Kino.

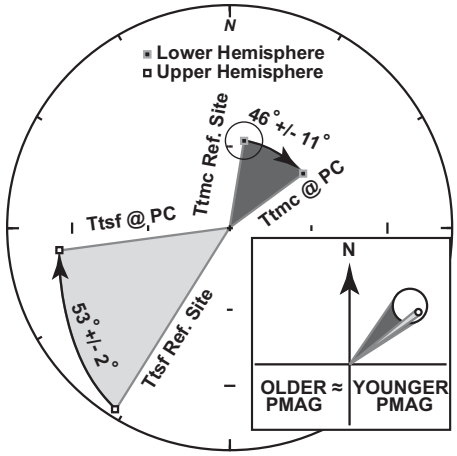

Figure 14. Chronologic comparison of calculated vertical-axis block rotations from the Punta Chueca (PC) paleomagnetic drill site. Both the 12.5 Ma Tuff of San Felipe (Ttsf) and the 6.4 Ma Tuffs of Mesa Cuadrada (Ttmc) display large magnitudes of clockwise vertical-axis rotation in the same fault block. Within uncertainty (lower right inset), these sites have been rotated the same amount. However, also within uncertainty, 6.7° ± 11.9° of this total 53° of rotation could have occurred prior to 6.4 Ma. Fisher statistic (α95) error cones for the Ttmc reference site are shown as black circles. For the Ttmc site at PC, and both the Ttsf reference site in Baja California (Bennett and Oskin, 2008) and the Ttsf site at PC, the error cones are <2.5° and are not shown for scale purposes. These results suggest that either the majority of or all block rotation in the Punta Chueca block due to dextral shearing postdates the eruption of the 6.4 Ma Tuffs of Mesa Cuadrada. Ttsf at PC is from Oskin et al. (2001).

larger amount of clockwise vertical-axis rotation of its hanging wall.

We analyzed our transtensional block model, and synthesized this information with constraints from the bounding Sacrificio and Infiernillo faults to quantify total dextral strain across the Coastal Sonora fault zone (Fig. 16). Dextral deformation across the Coastal Sonora fault zone consists of dextral offset on the bounding Sacrificio and Infiernillo faults, as well as deformation internal to the Coastal Sonora fault zone along strike-slip faults and via clockwise block rotation. As summarized previously, dextral displacement across the Infiernillo and Sacrificio faults is estimated to be 20 ± 10 km and >15 km, respectively. Geologic mapping (Fig. 3) and paleomagnetism identified a total of 6.2 ± 1.1 km of dextral displacement internal to the Coastal Sonora fault zone. These components of the Coastal Sonora fault zone sum to a minimum of 41 ± 11 km of dextral displacement. This value is consistent with the 60 ± 30 km of slip across the entire Coastal Sonora fault zone permitted from matching prerift fusulinid clast-bearing conglomerate exposures of Gastil et al. (1973) after restoration of post–6.1 Ma opening of the northern Gulf of California (see circled F locations on Fig. 1). These geologically constrained estimates of total dextral slip across of the Coastal Sonora fault zone amount to only a fraction of the ~150–250 km of slip proposed in coastal Sonora (Nicholson et al., 1994; Gans,

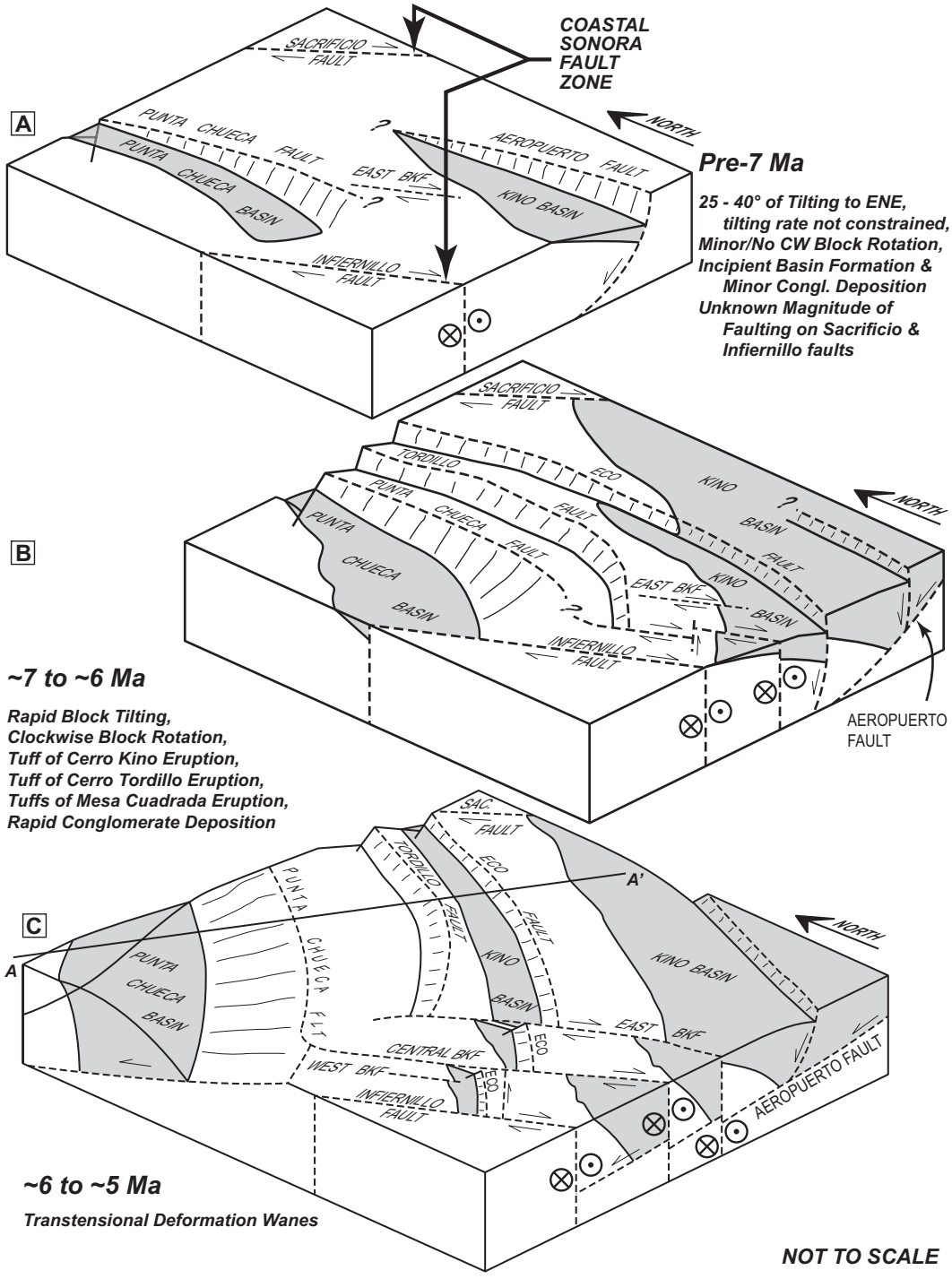

Figure 15. Oblique block diagrams showing the evolution of the transtensional Coastal Sonora fault zone. (A) Sometime after 11.5 Ma, dextral transtension initiated across the Coastal Sonora fault zone via dextral faulting on the Sacrificio and Infiernillo strike-slip faults. Associated block tilting and minor block rotations occurred in the intervening region, forming tectonic basins that began to accumulate nonmarine deposits. (B) By 7 Ma, transtensional deformation and basin sedimentation became rapid. Deformation in the south continued via block tilting and rotation, as discrete strike-slip structures began to form. First-generation normal faults slipped and rotated to lower angle (e.g., Aeropuerto fault), and new second-generation faults initiated. (C) During the final phase of transtension, dextral deformation occurred via block rotation and along discrete dextral faults in the southern and central parts of the study area, while in the north, dextral deformation continued to be accommodated entirely via clockwise rotation of the Punta Chueca basin and continued slip on the low-angle Punta Chueca normal fault. CW—clockwise; BKF—Bahía Kino fault; SAC—Sacrificio.

1997; Wilson et al., 2005; Fletcher et al., 2007; Seiler et al., 2010). It is important to note, however, that our estimate is for one major dextral fault zone, the Coastal Sonora fault zone, and does not account for distributed extension and dextral faulting within inland Sonora (Stock and Hodges, 1989; Gans, 1997), nor the component of northwestward translation of Baja California due to extension of its rifted margin (Lewis and Stock, 1998; Seiler et al., 2010).

Implications for Continental Rupture Mechanisms

This study documents large-magnitude extension hosted within a zone of strike-slip faults that project offshore, on strike with a primary transform fault between the Upper Tiburón and Adair-Tepoca marine basins in the Gulf of California (Fig. 1). The deformation documented here may exemplify the oblique rift processes that lead to strain localization and eventual continental rupture. In the Coastal Sonora fault zone, large-magnitude extension (>100%) occurred across an array of normal faults bounded by the major NW-striking dextral Sacrificio and Infiernillo faults. At the larger, rift-segment scale, a similar style of normal faulting, pinned between transform faults, may have facilitated strain localization into the axis of the Gulf of California. Sustained, large-magnitude oblique

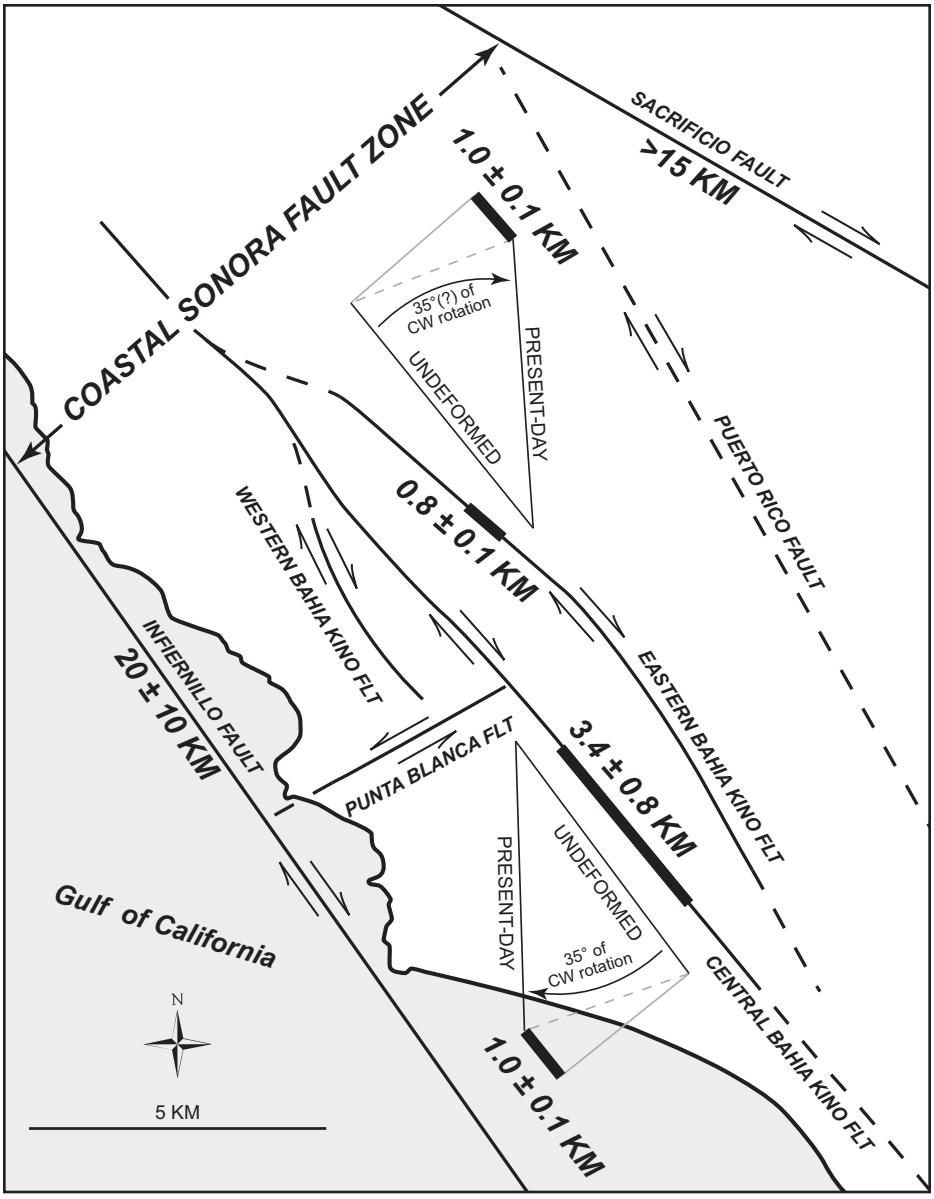

Figure 16. Simplified transtensional model summarizing the dextral displacement via clockwise block rotation and on strike-slip faults within the Coastal Sonora fault zone. CW—clockwise.

extension across such a kinematically linked transform-normal fault array may more readily localize crustal thinning than orthogonal rifting.

Evidence of such a style of oblique rift localization is preserved along several segments of the rifted margins of the northern Gulf of California (e.g., Axen and Fletcher, 1998; Pacheco et al., 2006; González-Fernández et al., 2005; Martín-Barajas et al., 2010; Seiler et al., 2010). Together, these zones should define a linked, en-echelon belt of transtension along the restored, nascent axis of Gulf of California. For example, Herman (2013) identified a zone of focused extension and block rotation in southwest coastal Sonora, near Guaymas (Fig. 1), that was active by 9 Ma and may be a southeastward continuation of the Coastal Sonora fault zone. Upon restoration of opening of the northern Gulf of California (Oskin et al., 2001), this Coastal Sonora fault zone aligns with strike-slip faults on northeast Isla Tiburón (Gastil and Krummenacher, 1977b; Bennett et al., 2012) and further to the northwest into a zone of post–9 Ma dextral strike-slip faulting that projects into the Sierra San Felipe of coastal northeastern Baja California (Seiler et al., 2010). Reconstructed, this system represents a proto–Gulf of California transform fault at least 200 km in length. Another candidate for a major proto–Gulf of California transform fault is the La Cruz fault, which transects southern Isla Tiburón west of the study area (Fig. 1; Oskin and Stock, 2003b; Bennett et al., 2012) and continues >150 km southeastward into a zone of high-angle (strike-slip?) faulting along the edge of the continental shelf offshore southern Sonora (Aragón-Arreola et al., 2005).

We hypothesize that during the latter half of proto–Gulf of California time (ca. 9–6 Ma), dextral strain became focused into an ~50–100-km-wide, NNW-trending belt of transtensional deformation embedded within the western Mexican Basin and Range Province. Other major transtensional basins along the nascent Pacific–North America plate boundary also initiated during this period, including the ca. 7 Ma development of the Guaymas basin ~350 km to the southeast of the study area (Miller and Lizarralde, 2013) and the 8.0 ± 0.4 Ma development of the Fish Creek–Vallecito basin ~350 km to the northwest of the study area (Dorsey et al., 2011). Prior to this, transtensional deformation was likely more distributed, on faults both west of Baja California (e.g., the Tosco-Abreojos fault) and east of the Coastal Sonora fault zone within Sonora. This localization process may have been enhanced by an increase in rift obliquity at ca. 8 Ma, when Pacific–North America relative plate motion became ~12° more northerly at the latitude of Isla Tiburón (Atwater and Stock, 1998). This increase in rift obliquity could have promoted the formation of lengthy strike-slip faults (Withjack and Jamison, 1986). Locally, in coastal Sonora, rapid transtensional deformation was active across the Coastal Sonora fault zone at 7 Ma, and extension here exceeds 100% across embedded normal faults. By ca. 5–6 Ma, linkage of the De Mar fault—the northwestern projection of the Coastal Sonora fault zone—with the La Cruz fault and Tiburón fracture zone (Fig. 1) was established across the Upper Tiburón basin, setting the stage for extreme crustal thinning here (Oskin and Stock, 2003a; González-Fernández et al., 2005). Once extensional strain migrated from coastal Sonora to the western side of Isla Tiburón, activity within the Coastal Sonora fault zone must have greatly diminished or became inactive, broadly similar to the way in which oceanic transform faults become inactive when they cease to connect active spreading centers. This example shows how major NW-striking dextral fault zones of proto–Gulf of California age were inherited as transform faults during subsequent development of the Gulf of California (Fig. 1), connecting intervening pull-apart basins that accomplished localized necking, and eventual rupture, of the continental lithosphere.

CONCLUSIONS

This study documents focused transtensional deformation within the Coastal Sonora fault zone that preceded regional-scale localization of the Pacific–North America plate boundary into the Gulf of California. The results from detailed geologic mapping, geochronology, and paleomagnetism constrain the timing, location, and magnitude of both normal and strike-slip faulting related to the oblique opening of the Gulf of California. In part, this study also addresses the unidentified and undocumented nature of the dextral component of Pacific–North America plate boundary motion during proto–Gulf of California time.

In coastal Sonora, transtension initiated sometime after deposition of the 12.5 Ma Tuff of San Felipe and 11.5 Ma local volcanic rocks. This deformation consisted of down-to-the-ENE block tilting (25°–40°), minor clockwise vertical-axis block rotation (6.7° ± 11.9° in the Punta Chueca basin), and the onset of dextral strike-slip faulting, with little to no sediment accumulation in the Punta Chueca and Kino half-graben basins. After 7 Ma, deformation within the core of the Coastal Sonora fault zone constituted the majority of the observed clockwise vertical-axis block rotation and dextral faulting, synchronous with rapid sedimentation rates. Syntectonic transtensional basins in coastal Sonora contain three 6.4–7.0 Ma volcanic tuffs interbedded near the base of ≥480 m of nonmarine conglomerate. Deformation must have largely ceased by 5.5 ± 0.4 Ma, when strain localized to the west of Isla Tiburón. Palinspastic reconstructions in both cross section and map view constrain a tectonic model of transtensional deformation across the Coastal Sonora fault zone over its lifetime. During this period, this region experienced 120% extension and distributed dextral deformation via clockwise block rotations up to 53°. Toward the end of this period, deformation was dominated by dextral slip along NW-striking branches of the dextral Bahía Kino fault in the south, while in the north, shear continued via clockwise vertical-axis rotation of fault blocks and ~6 km of total slip on the low-angle Punta Chueca fault. Based on these results, we present two models for the deformation history of the Coastal Sonora fault zone. Either deformation started near 11.5 Ma at a slow rate, followed by acceleration after 7 Ma (model 1), or deformation initiated ca. 8 Ma, at a rapid rate, and remained so throughout the life span of the Coastal Sonora fault zone (model 2). During late Miocene time, the entire Coastal Sonora fault zone accommodated at least 41 ± 11 km of dextral displacement. Though direct timing constraints are lacking for the Sacrificio and Infiernillo faults that bound the Coastal Sonora fault zone, we suggest that their activity also peaked with the transtensional deformation we document within the core of this fault zone.

The activity of the Coastal Sonora fault zone during latest proto–Gulf of California time demonstrates the focusing of dextral strain within an ~50–100-km-wide, NNW-trending belt of transtensional deformation embedded within the western Mexican Basin and Range Province. The onset of significant and focused dextral shear broadly coincides with a clockwise azimuthal change in Pacific–North America relative plate motion at ca. 8 Ma. Such an increase in rift obliquity likely promoted the formation of strike-slip faults. Co-location of extension and dextral shear at lithospheric scale may have helped to focus deformation within the nascent axis of the Gulf of California. Focused transtensional deformation in the Coastal Sonora fault zone and its northwestward continuation (De Mar fault) were followed shortly thereafter by the onset of rapid crustal thinning along kinematically linked N-striking extensional faults in the Upper Tiburón pull-apart basin. This result supports the hypothesis that an increase in rift obliquity and the focusing of dextral shear into the western Mexican Basin and Range extensional province may have been the catalyst for Pacific–North America plate boundary localization in the northern Gulf of California. We suggest that in highly oblique rifts (<30°), strike-slip faults that accommodate a significant component of plate boundary deformation also enhance the efficiency of adjacent crustal thinning, increasing the potential for lithospheric rupture.

ACKNOWLEDGMENTS

Funding from the National Science Foundation Tectonics and MARGINS programs, awards 0739017 and 0904337, a UC MEXUS grant, a Geological Society of America Graduate Research Grant, and the University of North Carolina–Chapel Hill Geological Sciences Department Martin Fund made this research possible. Reviews by Joann Stock, Phil Gans, and John Fletcher and discussions with Rebecca Dorsey and Arturo Martín-Barajas helped to greatly improve this manuscript. We thank Mick Kunk and Joe Wooden for assistance with our Ar/Ar and U/Pb geochronology data, respectively. Michael Tappa, Monica Iglecia, Dhelia Tucker, and Jordan Ford all provided great company, safety, and support while conducting field work in Sonora. Joe Kirschvink and the Caltech Paleomagnetics Laboratory assisted with paleomagnetic analysis. Tadeo Pfister, Tom Donovan, and the Prescott College Kino Bay Center for Cultural and Ecological Studies staff provided comfortable accommodations while mapping in Sonora. We thank Ernesto Molina Villa-Lobos and the native Comcáac tribe who granted access to their lands.

REFERENCES CITED

Abbott, P.L., and Smith, T.E., 1989, Sonora, Mexico, source for the Eocene Poway Conglomerate of southern California: Geology, v. 17, p. 329–332, doi:10.1130/0091-7613(1989)017<0329:SMSFTE>2.3.CO;2.

Allmendinger, R.W., Cardozo, N., and Fisher, D., 2012, Structural Geology Algorithms: Vectors and Tensors in Structural Geology: Cambridge, UK, Cambridge University Press, 289 p.

Al-Zoubi, A., and ten Brink, U., 2002, Lower crustal flow and the role of shear in basin subsidence: An example from the Dead Sea basin: Earth and Planetary Science Letters, v. 199, p. 67–79, doi:10.1016/S0012-821X(02)00540-X.

Angelier, J., Colletta, B., Chorowicz, J., Ortlieb, L., and Rangin, C., 1981, Fault tectonics of the Baja California Peninsula and the opening of the Sea of Cortez, Mexico: Journal of Structural Geology, v. 3, no. 4, p. 347–357, doi:10.1016/0191-8141(81)90035-3.

Applegate, B., and Shor, A. N., 1994, The northern Mid-Atlantic and Reykjanes Ridges: Spreading center morphology between 55°50′N and 63°00′N: Journal of Geophysical Research, v. 99, no. B9, p. 17,935–17,956.

Aragón-Arreola, M., and Martín-Barajas, A., 2007, Westward migration of extension in the northern Gulf of California, Mexico: Geology, v. 35, p. 571–574, doi:10.1130/G23360A.1.

Aragón-Arreola, M., Morandi, M., Martín-Barajas, A., Deldago-Argote, L., and González-Fernández, A., 2005, Structure of the rift basins in the central Gulf of California: Kinematic implications for oblique rifting: Tectonophysics, v. 409, p. 19–38, doi:10.1016/j.tecto.2005.08.002.

Atwater, T., 1989, Plate tectonic history of the northeast Pacific and western North America, *in* Winterer, E.L., Hussong, D.M., and Decker, R.W., eds., The Eastern Pacific Ocean and Hawaii: Boulder, Colorado, Geological Society of America, The Geology of North America, v. N, p. 21–72.

Atwater, T., and Stock, J.M., 1998, Pacific North America plate tectonics of the Neogene southwestern United States: An update: International Geology Review, v. 40, no. 5, p. 375–402, doi:10.1080/00206819809465216.

Axen, G.J., and Fletcher, J.M., 1998, Late Miocene–Pliocene extensional faulting, northern Gulf of California and Salton Trough, California: International Geology Review, v. 40, no. 3, p. 217–244, doi:10.1080/00206819809465207.

Bassi, G., 1995, Relative importance of strain rate and rheology for the mode of continental extension: Geophysical Journal International, v. 122, p. 195–210, doi:10.1111/j.1365-246X.1995.tb03547.x.

Beck, M.E., 1980, Paleomagnetic record of plate-margin tectonic processes along the western edge of North America: Journal of Geophysical Research, v. 85, p. 7115–7131, doi:10.1029/JB085iB12p07115.

Bellahsen, N., Fournier, M., d'Acremont, E., Leroy, S., and Daniel, J.M., 2006, Fault reactivation and rift localization: Northeastern Gulf of Aden margin: Tectonics, v. 25, TC1007, doi:10.1029/2004TC001626.

Bennett, S.E.K., 2009, Transtensional Rifting in the Late Proto–Gulf of California near Bahía Kino, Sonora, México [M.S. thesis]: Chapel Hill, North Carolina, University of North Carolina, 122 p.

Bennett, S.E.K., and Oskin, M.E., 2008, A new high-precision paleomagnetic reference vector from Mesa El Burro, Mesa Cartabón, and Mesa El Pinole, Baja California, for the Tuff of San Felipe, a Miocene ignimbrite marker bed exposed in Baja California and Sonora, México: San Francisco, American Geophysical Union, Fall Meeting, abstract T11A-1852.

Bennett, S.E.K., Oskin, M.E., and Iriondo, A., 2012, Progressive localization of dextral shear in the late proto–Gulf of California: Geological Society of America Abstracts with Programs, v. 44, no. 3, p. 5.

Bialas, R.W., and Buck, W.R., 2009, How sediment promotes narrow rifting: Application to the Gulf of California: Tectonics, v. 28, TC4014, doi:10.1029/2008TC002394.

Brady, R., Wernicke, B., and Fryxell, J., 2000, Kinematic evolution of a large-offset continental normal fault system, South Virgin Mountains, Nevada: Geological Society of America Bulletin, v. 112, p. 1375–1397, doi:10.1130/0016-7606(2000)112<1375:KEOALO>2.0.CO;2.

Brune, S., Popov, A., and Sobolev, S.V., 2012, Modeling suggests that oblique extension facilitates rifting and continental break-up: Journal of Geophysical Research, v. 117, B08402, doi:10.1029/2011JB008860.

Bryant, B.A., 1986, Geology of the Sierra Santa Rosa Basin, Baja California, Mexico [M.S. thesis]: San Diego, California, San Diego State University, 75 p.

Buck, R.W., 1991, Modes of continental extension: Journal of Geophysical Research, v. 96, p. 20,161–20,178, doi:10.1029/91JB01485.

Buck, W.R., Lavier, L.L., Poliakov, A.N.B., Rohr, K., Jackson, J., Chadwick, A., Osmaston, M., Kusznir, N., Brun, J.-P., Roberts, A., and Geli, L., 1999, How to make a rift wide: Philosophical Transactions: Mathematical, Physical and Engineering Sciences, v. 357, no. 1753, p. 671–693.

Butler, R.L., 1992, Paleomagnetism: Cambridge, Massachusetts, Blackwell Scientific Publications, 319 p.

Choi, E., and Buck, W.R., 2011, 3D numerical models for faulting patterns in oblique rifts: San Francisco, American Geophysical Union, Fall Meeting, abstract T21A-2318.

Chorowicz, J., and Sorlien, C., 1992, Oblique extension tectonics in the Malawi Rift, Africa: Geological Society of America Bulletin, v. 104, p. 1015–1023, doi:10.1130/0016-7606(1992)104<1015:OETITM>2.3.CO;2.

Darin, M.H., 2011, Late Miocene Extensional Deformation in the Sierra Bacha, Coastal Sonora, México: Implications for the Kinematic Evolution of the Proto–Gulf of California [M.S. thesis]: Eugene, Oregon, University of Oregon, 95 p.

Dauteuil, O., and Brun, J.-P., 1996, Deformation partitioning in a slow spreading ridge undergoing oblique extension: Mohns Ridge, Norwegian Sea: Tectonics, v. 15, p. 870–884, doi:10.1029/95TC03682.

deBoer, J.Z., and Clifton, A.E., 1988, Mesozoic tectogenesis: Development and deformation of 'Newark' rift zones in the Appalachians (with special emphasis on the Hartford basin, Connecticut), *in* Manspeizer, W., ed., Triassic-Jurassic Rifting, Continental Breakup and the Origin of the Atlantic and Passive Margins, Part A: Developments in Geotectonics, Volume 22: Amsterdam, Netherlands, Elsevier, p. 275–302.

Demarest, H.H., 1983, Error analysis for the determination of tectonic rotation from paleomagnetic data: Journal of Geophysical Research, v. 88, p. 4321–4328, doi:10.1029/JB088iB05p04321.

Dorsey, R.J., 2010, Sedimentation and crustal recycling along an active oblique-rift margin: Salton Trough and northern Gulf of California: Geology, v. 38, p. 443–446, doi:10.1130/G30698.1.

Dorsey, R.J., Peryam, T.C., Bennett, S., Oskin, M.E., and Iriondo, A., 2008, Preliminary basin analysis of latest Miocene conglomerate near Bahía Kino, coastal Sonora: A new record of crustal deformation during initial opening of the northern Gulf of California: San Francisco, American Geophysical Union, Fall Meeting, abstract T11A–1851.

Dorsey, R.J., Housen, B.A., Janecke, S.U., Fanning, C.M., and Spears, A.L.F., 2011, Stratigraphic record of basin development within the San Andreas fault system: Late Cenozoic Fish Creek–Vallecito basin, southern California: Geological Society of America Bulletin, v. 123, p. 771–793, doi:10.1130/B30168.1.

Edwards, R.A., Whitmarsh, R.B., and Scrutton, R.A., 1997, The crustal structure across the transform continental margin off Ghana, eastern equatorial Atlantic: Journal of Geophysical Research, v. 102, p. 747–772, doi:10.1029/96JB02098.

El Kochri, A., and Chorowicz, J., 1996, Oblique extension in the Jurassic trough of the central and eastern High Atlas (Morocco): Canadian Journal of Earth Sciences, v. 33, p. 84–92, doi:10.1139/e96-009.

England, P., 1983, Constraints on extension of continental lithosphere: Journal of Geophysical Research, v. 88, p. 1145–1152, doi:10.1029/JB088iB02p01145.

Fenby, S.S., and Gastil, R.G., 1991, Geologic-tectonic map of the Gulf of California and surrounding areas, *in* Dauphin, J.P., and Simoneit, B.R.T., eds., The Gulf and Peninsular Province of the Californias: American Association of Petroleum Geologists Memoir 47, p. 79–83.

Ferrari, L., Valencia-Moreno, M., and Bryan, S., 2007, Magmatism and tectonics of the Sierra Madre Occidental and its relation with the evolution of the western margin of North America, *in* Alaniz-Álvarez, S.A., and Nieto-Samaniego, Á.F., eds., Geology of México: Celebrating the Centenary of the Geological Society of México: Geological Society of America Special Paper 422, p. 1–39.

Ferrari, L., Orozco-Esquivel, T., Lopez-Martinez, M., Duque, J., Bryan, S., and Cerca, M., 2012, 25 million years to break a continent: Early to middle Miocene rifting and syn-extensional magmatism in the southern Gulf of California: Geological Society of America Abstracts with Programs, v. 44, no. 3, p. 6.

Fisher, S.R., 1953, Dispersion on a sphere: Proceedings of the Royal Society of London, ser. A, Mathematical and Physical Sciences, v. 217, no. 1130, p. 295–305, doi:10.1098/rspa.1953.0064.

Fletcher, J.M., and Munguía, L., 2000, Active continental rifting in southern Baja California, Mexico: Implications for plate motion partitioning and the transition to seafloor spreading in the Gulf of California: Tectonics, v. 19, p. 1107–1123, doi:10.1029/1999TC001131.

Fletcher, J.M., Grove, M., Kimbrough, D., Lovera, O., and Gehrels, G.E., 2007, Ridge-trench interactions and the Neogene tectonic evolution of the Magdalena shelf and southern Gulf of California: Insights from detrital zircon U-Pb ages from the Magdalena fan and adjacent areas: Geological Society of America Bulletin, v. 119, p. 1313–1336, doi:10.1130/B26067.1.

Forsyth, D.W., 1992, Finite extension and low-angle normal faulting: Geology, v. 20, p. 27–30, doi:10.1130/0091-7613(1992)020<0027:FEALAN>2.3.CO;2.

Gans, P., Wong, M., Macmillan, I., Blair, K., Roldan, J., Till, C., and Herman, S., 2006, Cenozoic structural and magmatic evolution of the Sonoran basin-range and Gulf of California rift system: Geological Society of America Abstracts with Programs, Specialty Meeting No. 2, p. 94.

Gans, P.B., 1997, Large-magnitude Oligo-Miocene extension in southern Sonora: Implications for the tectonic evolution of northwest Mexico: Tectonics, v. 16, no. 3, p. 388–408, doi:10.1029/97TC00496.

Gastil, R.G., 1993, Prebatholithic history of peninsular California, *in* Gastil, R.G., and Miller, R.H., eds., The Prebatholithic Stratigraphy of Peninsular California: Geological Society of America Special Paper 279, p. 145–156.

Gastil, R.G., and Krummenacher, D., 1977a, Reconnaissance geology of coastal Sonora between Puerto Lobos and Bahia Kino: Geological Society of America Bulletin, v. 88, p. 189–198, doi:10.1130/0016-7606(1977)88<189:RGOCSB>2.0.CO;2.

Gastil, R.G., and Krummenacher, D., 1977b, Reconnaissance Geologic Map of Coastal Sonora between Puerto Lobos and Bahia Kino: Geological Society of America Map and Chart Series MC-16, scale 1:150,000.

Gastil, R.G., Lemone, D.V., and Stewart, W.J., 1973, Permian fusulinids from near San Felipe, Baja California: American Association of Petroleum Geologists Bulletin, v. 57, no. 4, p. 746–747.

Gastil, R.G., Phillips, R.P., and Allison, E.C., 1975, Reconnaissance Geology of the State of Baja California: Geological Society of America Memoir 140, 170 p.

Gastil, R.G., Krummenacher, D., and Minch, J.A., 1979, The record of Cenozoic volcanism around the Gulf of California: Geological Society of America Bulletin, v. 90, p. 839–857, doi:10.1130/0016-7606(1979)90<839:TROCVA>2.0.CO;2.

González-Fernández, A., Danobeitia, J.J., Deldago-Argote, L., Michaud, F., Cordoba, D., and Bartolome, R., 2005, Mode of extension and rifting history of upper Tiburon and upper Delfin basins, northern Gulf of California: Journal of Geophysical Research, v. 110, p. 1–17, doi:10.1029/2003JB002941.

Hamilton, W., 1961, Origin of the Gulf of California: Geological Society of America Bulletin, v. 72, p. 1307–1318, doi:10.1130/0016-7606(1961)72[1307:OOTGOC]2.0.CO;2.

Hausback, B.P., 1984, Cenozoic volcanic and tectonic evolution of Baja California Sur, Mexico, *in* Frizzell, V.A., Jr., ed., Geology of the Baja California Peninsula, Volume 39: Los Angeles, California, Pacific Section of the Economic Paleontologists and Mineralogists, p. 219–236.

Henry, C.D., 1989, Late Cenozoic Basin and Range structure in western Mexico adjacent to the Gulf of California: Geological Society of America Bulletin, v. 101, p. 1147–1156, doi:10.1130/0016-7606(1989)101<1147:LCBARS>2.3.CO;2.

Henry, C.D., and Aranda Gomez, J.J., 1992, The real southern basin and range: Mid Cenozoic to late Cenozoic extension in Mexico: Geology, v. 20, p. 701–704, doi:10.1130/0091-7613(1992)020<0701:TRSBAR>2.3.CO;2.

Henry, C.D., and Faulds, J., 2006, The Walker Lane and Gulf of California: Related expressions of Pacific–North America plate boundary development, *in* Proceedings RCL-Cortez Workshop: Lithospheric Rupture in the Gulf of California–Salton Trough Region: Ensenada, Mexico, 9–13 January 2006, p. 37 (http://rcl-cortez.nsf-margins.org/Workshop_Abstracts.pdf).

Herman, S.W., 2013, A Paleomagnetic Investigation of Vertical-Axis Rotations in Coastal Sonora, Mexico: Evidence for Distributed Transtensional Deformation during the Proto-Gulf Shift from a Subduction-Dominated to Transform-Dominated Plate Boundary in the Gulf of California [M.S. thesis]: Santa Barbara, California, University of California, 39 p.

Herman, S.W., and Gans, P., 2006, A paleomagnetic investigation of large scale vertical axis rotations in coastal Sonora: Evidence for transtensional proto-Gulf deformation: Geological Society of America Abstracts with Programs, v. 38, no. 7, p. 311.

Hopper, J.R., and Buck, W.R., 1996, The effect of lower crustal flow on continental extension and passive margin formation: Journal of Geophysical Research, v. 101, p. 20,175–20,194.

Huismans, R.S., and Beaumont, C., 2003, Symmetric and asymmetric lithospheric extension: Relative effects of frictional-plastic and viscous strain softening: Journal of Geophysical Research, v. 108, 2496, doi:10.1029/2002JB002026.

Jones, C.H., 2002, User-driven integrated software lives: "PaleoMag: Paleomagnetics analysis on the Macintosh: Computers and Geosciences, v. 28, no. 10, p. 1145–1151, doi:10.1016/S0098-3004(02)00032-8.

Karig, D.E., and Jensky, W., 1972, The Proto–Gulf of California: Earth and Planetary Science Letters, v. 17, p. 169–174, doi:10.1016/0012-821X(72)90272-5.

Kirschvink, J.L., 1980, The least-squares line and plane and the analysis of paleomagnetic data: Geophysical Journal of the Royal Astronomical Society, v. 62, p. 699–718, doi:10.1111/j.1365-246X.1980.tb02601.x.

Kirschvink, J.L., Kopp, R.E., Raub, T.D., Baumgartner, C.T., and Holt, J.W., 2008, Rapid, precise, and high-sensitivity acquisition of paleomagnetic and rock-magnetic data: Development of a low-noise automatic sample changing system for superconducting rock magnetometers: Geochemistry Geophysics Geosystems, v. 9, Q05Y01, doi:10.1029/2007GC001856.

Kusznir, N.J., and Park, R.G., 1987, The extensional strength of the continental lithosphere: Its dependence on geothermal gradient, and crustal composition and thickness, *in* Coward, M.P., Dewey, J.F., and Hancock, P.L., eds., Continental Extension Tectonics: Geological Society of London Special Publication 28, p. 35–52.

Lavier, L.L., and Manatschal, G., 2006, A mechanism to thin the continental lithosphere at magma-poor margins: Nature, v. 440, p. 324–328, doi:10.1038/nature04608.

Lavier, L.L., and Steckler, M.S., 1997, The effect of sedimentary cover on flexural strength of continental lithosphere: Nature, v. 389, p. 476–479, doi:10.1038/39004.

Lavier, L.L., Buck, W.R., and Poliakov, A.N.B., 1999, Self-consistent rolling-hinge model for the evolution of large-offset low-angle normal faults: Geology, v. 27, p. 1127–1130, doi:10.1130/0091-7613(1999)027<1127:SCRHMF>2.3.CO;2.

Lewis, C.J., 1996, Stratigraphy and geochronology of Miocene and Pliocene volcanic rocks in the Sierra San Fermín and southern Sierra San Felipe, Baja California, Mexico: Geofísica Internacional, v. 35, p. 1–31.

Lewis, C.J., and Stock, J.M., 1998, Paleomagnetic evidence of localized vertical-axis rotation during Neogene extension of the Sierra San Fermín, northeastern Baja California, Mexico: Journal of Geophysical Research, v. 103, p. 2455–2470, doi:10.1029/97JB02673.

Lonsdale, P., 1989, Geology and tectonic history of the Gulf of California, *in* Winterer, E.L., Hussong, D.M., and Decker, R.W., eds., The Eastern Pacific Ocean and

Hawaii: Boulder, Colorado, Geological Society of America, Geology of North America, v. N, p. 499–521.
Lourens, L., Hilgen, F., Shackleton, N.J., Laskar, J., and Wilson, D., 2004, The Neogene Period, *in* Gradstein, F.M., Ogg, J.G., and Smith, A.G., eds., A Geologic Time Scale 2004: Cambridge University Press, p. 409–440.
Mar-Hernández, E., González-Escobar, M., and Martín-Barajas, A., 2012, Tectonic framework of Tiburon Basin, Gulf of California, from seismic reflection evidence: International Geology Review, v. 54, p. 1271–1283, doi:10.1080/00206814.2011.636988.
Martín-Barajas, A., González-Escobar, M., Fletcher, J.M., Pacheco, M., and Mar-Hernández, E., 2010, Continental rupture controlled by low-angle normal faults in the northern Gulf of California: Analysis of seismic reflection profiles: San Francisco, American Geophysical Union, Fall Meeting, abstract T32C-03.
McDowell, F.W., Roldan-Quintana, J., and Amaya-Martinez, R., 1997, Interrelationship of sedimentary and volcanic deposits associated with Tertiary extension in Sonora, Mexico: Geological Society of America Bulletin, v. 109, p. 1349–1360, doi:10.1130/0016-7606(1997)109<1349:IOSAVD>2.3.CO;2.
McKenzie, D., 1978, Some remarks on the development of sedimentary basins: Earth and Planetary Science Letters, v. 40, p. 25–32, doi:10.1016/0012-821X(78)90071-7.
Michaud, F., Sosson, M., Royer, J.-Y., Chabert, A., Bourgois, J., Calmus, T., Mortera, C., Bigot-Cormier, F., Bandy, W., Dyment, J., Pontoise, B., and Sichler, B., 2004, Motion partitioning between the Pacific plate, Baja California and the North America plate: The Tosco-Abreojos fault revisited: Geophysical Research Letters, v. 31, p. 4, doi:10.1029/2004GL019665.
Miller, N.C., and Lizarralde, D., 2013, Thick evaporites and early rifting in the Guaymas Basin, Gulf of California: Geology, v. 41, p. 283–286, doi:10.1130/G33747.1.
Moore, D.G., and Buffington, E.C., 1968, Transform faulting and growth of the Gulf of California since the late Pliocene: Science, v. 161, p. 1238–1241, doi:10.1126/science.161.3847.1238.
Nagy, E.A., 2000, Extensional deformation and paleomagnetism at the western margin of the Gulf Extensional Province, Puertecitos Volcanic Province, northeastern Baja California, Mexico: Geological Society of America Bulletin, v. 112, p. 857–870, doi:10.1130/0016-7606(2000)112<857:EDAPAT>2.0.CO;2.
Nagy, E.A., Grove, M., and Stock, J.M., 1999, Age and stratigraphic relationships of pre- and syn-rift volcanic deposits in the northern Puertecitos Volcanic Province, Baja California, Mexico: Journal of Volcanology and Geothermal Research, v. 93, p. 1–30, doi:10.1016/S0377-0273(99)00080-3.
Nicholson, C., Sorlien, C.C., Atwater, T., Crowell, J.C., and Luyendyk, B.P., 1994, Microplate capture, rotation of the western Transverse Ranges, and initiation of the San Andreas transform as a low-angle fault system: Geology, v. 22, p. 491–495, doi:10.1130/0091-7613(1994)022<0491:MCROTW>2.3.CO;2.
Oskin, M., 2002, Tectonic Evolution of the Northern Gulf of California, Mexico, Deduced from Conjugate Rifted Margins of the Upper Delfín Basin [Ph.D. thesis]: Pasadena, California, California Institute of Technology, 481 p.
Oskin, M., and Martín-Barajas, A., 2003, Continental edge tectonics of Isla Tiburón, Sonora Mexico, *in* Alcayde, M., and Caballero, A.G., eds., Geological Transects across Cordilleran Mexico, Volume 1: Mexico, D.F., Universidad Nacional Autónoma de México, p. 53–70.
Oskin, M., and Stock, J.M., 2003a, Pacific–North America plate motion and opening of the Upper Delfín basin, northern Gulf of California: Geological Society of America Bulletin, v. 115, p. 1173–1190, doi:10.1130/B25154.1.
Oskin, M., and Stock, J.M., 2003b, Marine incursion synchronous with plate-boundary localization in the Gulf of California: Geology, v. 31, p. 23–26, doi:10.1130/0091-7613(2003)031<0023:MISWPB>2.0.CO;2.
Oskin, M., Stock, J., and Martín-Barajas, A., 2001, Rapid localization of Pacific–North America plate motion in the Gulf of California: Geology, v. 29, p. 459–462, doi:10.1130/0091-7613(2001)029<0459:RLOPNA>2.0.CO;2.
Pacheco, M., Martín-Barajas, A., Elders, W., Espinosa-Cardena, J.M., Helenes, J., and Segura, A., 2006, Stratigraphy and structure of the Altar basin of NW Sonora: Implications for the history of the Colorado River delta and the Salton trough: Revista Mexicana de Ciencias Geologicas, v. 23, no. 1, p. 22.
Page, W.R., Harris, A.G., Poole, F.G., and Repetski, J.E., 2003, Reinterpretation of the stratigraphy and structure of the Rancho Las Norias area, central Sonora, Mexico: Journal of South American Earth Sciences, v. 16, p. 523–540, doi:10.1016/S0895-9811(03)00135-4.
Paz-Moreno, F.A., 1992, Le Volcanisme Mio-Plio-Quaternaire de l'Etat du Sonora (Nord-Ouest du Mexique): Évolution Spatiale et Chronologique; Implications Pétrogénétiques [thèse de Doctorat]: Aix-Marseille, France, Université Aix-Marseille, 220 p.
Paz-Moreno, F.A., Demant, A., and Ornelas-Solís, R., 2000, Las ignimbritas hiperalcalinas neogenas de la region de Hermosillo, Sonora, Mexico: Mineralogia y geoquimica, *in* Calmus, T., and Pérez-Segura, E., eds., Cuarta Reunion Sobre la Geologia del Noroeste de Mexico y Areas Adyacentes, Volume 2: Hermosillo, Sonora, Mexico, National Autonomous University of Mexico and the University of Sonora, p. 90–91.
Pezzopane, S.K., and Weldon, R.J., 1993, Tectonic role of active faulting in central Oregon: Tectonics, v. 12, p. 1140–1169, doi:10.1029/92TC02950.
Plattner, C., Malservisi, R., Dixon, T.H., LaFemina, P., Sella, G.F., Fletcher, J.M., and Suarez-Vidal, F., 2007, New constraints on relative motion between the Pacific plate and Baja California microplate (Mexico) from GPS measurements: Geophysical Journal International, v. 170, p. 1373–1380, doi:10.1111/j.1365-246X.2007.03494.x.
Proffett, J.M., 1977, Cenozoic geology of the Yerington district, Nevada, and implications for the nature and origin of Basin and Range faulting: Geological Society of America Bulletin, v. 88, p. 247–266, doi:10.1130/0016-7606(1977)88<247:CGOTYD>2.0.CO;2.
Ramos-Velázquez, E., Calmus, T., Valencia, V., Iriondo, A., Valencia-Moreno, M., and Bellon, H., 2008, U-Pb and $^{40}Ar/^{39}Ar$ geochronology of the coastal Sonora batholith: New insights on Laramide continental arc magmatism: Revista Mexicana de Ciencias Geológicas, v. 25, no. 2, p. 314–333.
Seiler, C., Fletcher, J.M., Quigley, M.C., Gleadow, A.J.W., and Kohn, B.P., 2010, Neogene structural evolution of the Sierra San Felipe, Baja California: Evidence for proto-Gulf transtension in the Gulf Extensional Province?: Tectonophysics, v. 488, p. 87–109, doi:10.1016/j.tecto.2009.09.026.
Seiler, C., Fletcher, J., Kohn, B.P., Gleadow, A.J.W., and Raza, A., 2011, Low-temperature thermochronology of northern Baja California, Mexico: Decoupled slip-exhumation gradients and delayed onset of oblique rifting across the Gulf of California: Tectonics, v. 30, TC3004, doi:10.1029/2009TC002649.
Spencer, J.E., and Normark, W.R., 1979, Tosco-Abreojos fault zone: A Neogene transform plate boundary within the Pacific margin of southern Baja California: Geology, v. 7, p. 554–557, doi:10.1130/0091-7613(1979)7<554:TFZANT>2.0.CO;2.
Stock, J.M., 1989, Sequence and geochronology of Miocene rocks adjacent to the main gulf escarpment: Southern Valle Chico, Baja California Norte, Mexico: Geofísica Internacional, v. 28, no. 5, p. 851–896.
Stock, J.M., and Hodges, K.V., 1989, Pre-Pliocene extension around the Gulf of California and the transfer of Baja California to the Pacific plate: Tectonics, v. 8, p. 99–115, doi:10.1029/TC008i001p00099.
Stock, J.M., Lewis, C.J., and Nagy, E.A., 1999, The Tuff of San Felipe: An extensive middle Miocene pyroclastic flow deposit in Baja California, Mexico: Journal of Volcanology and Geothermal Research, v. 93, p. 53–74, doi:10.1016/S0377-0273(99)00079-7.
Stock, J.M., Paz-Moreno, F.A., Martin, K., and Lin, D., 2006, The 12.5 Ma Tuff of San Felipe: A major structural marker horizon in northwestern Mexico, *in* Proceedings, RCL-Cortez Workshop: Lithospheric Rupture in the Gulf of California–Salton Trough Region: Ensenada, Mexico, 9–13 January 2006, p. 72 (http://rcl-cortez.nsf-margins.org/Workshop_Abstracts.pdf).
Stock, J.M., Martín-Barajas, A., Martinez-Lopez, M., and Chapman, A., 2008, Net slip across the Ballenas transform fault measured from offset ignimbrite deposits: San Francisco, American Geophysical Union, Fall Meeting, abstract T11A–1853.
Sutherland, F.H., Kent, G.M., Harding, A.J., Umhoefer, P.J., Driscoll, N.W., Lizarralde, D., Fletcher, J.M., Axen, G.J., Holbrook, W.S., González-Fernández, A., and Lonsdale, P., 2012, Middle Miocene to early Pliocene oblique extension in the southern Gulf of California: Geosphere, v. 8, p. 752–770, doi:10.1130/GES00770.1.
Tron, V., and Brun, J.-P., 1991, Experiments on oblique rifting in brittle-ductile systems: Tectonophysics, v. 188, p. 71–84, doi:10.1016/0040-1951(91)90315-J.
Umhoefer, P.J., 2011, Why did the southern Gulf of California rupture so rapidly?—Oblique divergence across hot, weak lithosphere along a tectonically active margin: GSA Today, v. 21, no. 11, p. 4–10, doi:10.1130/G133A.1.
Umhoefer, P.J., and Stone, K.A., 1996, Description and kinematics of the SE Loreto basin fault array, Baja California Sur, Mexico: A positive field test of oblique-rift models: Journal of Structural Geology, v. 18, p. 595, doi:10.1016/S0191-8141(96)80027-7.
Unruh, J., Humphrey, J., and Barron, A., 2003, Transtensional model for the Sierra Nevada frontal fault system, eastern California: Geology, v. 31, p. 327–330, doi:10.1130/0091-7613(2003)031<0327:TMFTSN>2.0.CO;2.
Van Wijk, J., Adams, D.A., and Murphy, M.A., 2011, Pull-apart basin evolution: Insights from numerical models: San Francisco, American Geophysical Union, Fall Meeting, abstract T23F-05.
Vidal-Solano, J., Moreno, F.A.P., Alexander Iriondo, C.D., Demant, A., and Cochemé, J.-J., 2005, Middle Miocene peralkaline ignimbrites in the Hermosillo region (Sonora, Mexico): Geodynamic implications: Comptes Rendus Geoscience, v. 337, p. 1421–1430, doi:10.1016/j.crte.2005.08.007.
Vidal-Solano, J.R., Paz-Moreno, F.A., Demant, A., and Lopez-Martinez, M., 2007, Ignimbritas hiperalcalinas del Mioceno medio en Sonora Central: Revaluacion de la estratigrafia y significado del volcanismo terciario: Revista Mexicana de Ciencias Geologicas, v. 24, no. 1, p. 47–67.
Wernicke, B., and Burchfiel, B.C., 1982, Modes of extensional tectonics: Journal of Structural Geology, v. 4, p. 105–115, doi:10.1016/0191-8141(82)90021-9.
Wilson, D., McCrory, P., and Stanley, R., 2005, Implications of volcanism in coastal California for the Neogene deformation history of western North America: Tectonics, v. 24, TC3008, doi:10.1029/2003TC001621.
Withjack, M.O., and Jamison, W.R., 1986, Deformation produced by oblique rifting: Tectonophysics, v. 126, p. 99–124, doi:10.1016/0040-1951(86)90222-2.
Xie, X., and Heller, P.L., 2009, Plate tectonics and basin subsidence history: Geological Society of America Bulletin, v. 121, no. 1–2, p. 55–64.

Science Editor: Christian Koeberl
Associate Editor: John M. Fletcher

Manuscript Received 20 January 2012
Revised Manuscript Received 11 June 2013
Manuscript Accepted 12 August 2013

Printed in the USA